# Study on Phytochemicals and Bioactivities of the Medicinal Halophyte *Tamarix gallica*

January 2017

Asma Ben Hmidene

# Study on Phytochemicals and Bioactivities of the Medicinal Halophyte *Tamarix gallica*

A Dissertation Submitted to
the Graduate School of Life and Environmental Sciences,
the University of Tsukuba
in Partial Fulfillment of the Requirements
for the Degree of Doctor of Philosophy in Biotechnology
(Doctoral Program in Bioindustrial Sciences)

Asma Ben Hmidene

# Abstract

Type 2 diabetes (T2D) and Alzheimer's disease (AD) are age-related conditions. T2D is characterized as a peripheral metabolic disorder and AD a degenerative disease of the central nervous system, respectively. The incidence of both disturbances is increasing and has become a major public health concern in many industrialized countries. Despite intense research, best strategies to treat and prevent these costly diseases are still under investigation. However, it is now widely recognized that T2D and AD share many pathophysiological features including increased oxidative stress and amyloid aggregation.

Amyloid Beta (Aβ) is the components of the amyloid deposits in the AD brain, while the component of the amyloidogenic peptide deposit in the pancreatic islets of Langerhans is identified as human islet amyloid polypeptide (hIAPP). These two proteins are originated from the amyloid precursor protein and have a high sequence similarity. Although the amino acid sequences of amyloidogenic proteins are diverse, they all adopt a similar structure in aggregates called cross-beta-spine. Add at that, extensive studies in the past years have found that like $A\beta_{1\text{-}42}$, hIAPP forms early intermediate assemblies as spherical oligomers, implicating that these oligomers possess a common folding pattern or conformation. These similarities can be used in the search for effective pharmacotherapy for T2D, since potent therapeutic agents such as antioxidants with a catechol moiety, proved to inhibit Aβ aggregation, may play a key role to inhibit the aggregation of hIAPP responsible of the β cell death in the pancreas of diabetic patients.

*Tamarix gallica* is one of the medicinal halophyte species having a powerful antioxidant system. Although it was traditionally used for the treatment of various liver metabolic disorders, there is no report about the use of this plant for the treatment or prevention of T2D and AD.

Therefore, the aim of this work is to investigate its protective effect towards T2D and AD by isolation and identification of the bioactive compounds with α-glucosidase inhibitory activity and antioxidant potential, which play a role in the regulation of glucose metabolism in diabetic patient, as well as, the polymerization of hIAPP and Aβ

aggregation inhibitors.

Dried and crushed aerial parts of *T. gallica* were extracted with 70% EtOH and then partitioned with $CHCl_3$, EtOAc, BuOH, and $H_2O$. From the $CHCl_3$ and EtOAc layers, 10 flavonoids **1**-**10** were isolated and identified using the bioassay-guided fractionation for α-glucosidase inhibition assays. And among those substances, *O*-methylated and glucuronosylated flavonoids were selected to conduct further advanced experiment.

For α-glucosidase inhibitory activity, *p*-nitrophenol-α-D-glucopyranoside (*p*-NPG) and glucose oxidase assays were performed to determine the inhibition potential of each flavonoid and to study the structure-activity relationship of flavonoids **1**-**10**. The enzyme kinetic protocol was used to study the mechanism of action. Synergistic potential of the selected substances, when applied with a very low concentration of acarbose, was also performed, suggesting that they can be used not only as α-glucosidase inhibitors but also combined with established α-glucosidase inhibitors to reduce the adverse effect.

The antioxidant potential of the purified flavonoids **1**-**10** was evaluated by DPPH (2,2-diphenylpicrylhydrazyl) and superoxide dismutase (SOD) assays. Furthermore, thioflavin T (Th-T) assay using 42-mer amyloid β-protein ($A\beta_{1\text{-}42}$) for AD and hIAPP which is a 37-residue peptide secreted by the pancreatic β cells for T2D and transmission electronic microscopy (TEM) observation were conducted to evaluate the amyloid aggregation of flavonoids **1**-**10** and to study their structure-activity relationship.

From this research, it was concluded that glucuronosylated flavonoids playing a role in the regulation of glucose metabolism as α-glucosidase inhibitors and antioxidant substances may also inhibit the amyloid aggregation, and that the flavonoids with a catechol moieties inhibiting Aβ aggregation, might be used to inhibit the aggregation of hIAPP responsible of the β cell destruction in the pancreas of diabetic patients.

# Contents

# Abbreviations

EtOAc: ethyl acetate

EtOH: ethanol

$^{1}$H NMR: proton nuclear magnetic resonance

HPLC: high performance liquid chromatography

MeOH: methanol

ODS : octadecyl silane

Si gel C.C.: silica gel column chromatography

$t_R$: retention time

TLC: thin layer chromatgraphy

δ: chemical shift

# *Chapter I*

# General introduction

Diabetes mellitus (DM) and Alzheimer's disease (AD) are age-related conditions[1,2]. Nowadays, the incidence of both Diabetes mellitus (DM) and Alzheimer's disease (AD) is increasing at an alarming rate and has become a major public health concern in many industrialized countries[3].

DM is one of the most common metabolic diseases, affecting more than 240 million people worldwide and it is projected that this number will continue to increase in the next decade because of the sedentary life style and inappropriate diet[4].

AD is the most common form of dementia and is characterized by progressive cognitive and behavioral deficits. This disease affects over 24 million people globally and the worldwide prevalence of AD is estimated to double in the next 20 years[5].

Despite many years of intense research, the field lacks consensus regarding the etiology and pathogenesis of type 2 diabetes (T2D) and AD, and therefore the best strategies for treating and preventing these costly diseases are still under investigation[6].

However, growing evidence supports the concept that AD is fundamentally a metabolic disease with substantial and progressive derangements in brain glucose utilization. And, many epidemiological studies have shown that diabetic individuals have a significantly higher risk of developing AD[7,8].

Moreover, AD is now recognized to be heterogeneous in nature, and not solely the end-product of aberrantly processed, misfolded, and aggregated oligomeric amyloid $\beta$ peptides and hyperphosphorylated tau. Other factors, including impairments in energy metabolism and increased oxidative stress should be incorporated into all equations used to develop diagnostic and therapeutic approaches to AD[6,8].

In addition, many research suggested that it is imperative for future therapeutic strategies of AD to abandon the concept of uni-modal therapy in favor of multi-modal treatments that target distinct impairments at different levels[9].

Common pathophysiological features between T2D and AD have already been reported including glucose metabolism, increased oxidative stress and amyloid aggregation[6, 10-13].

The role that glucose plays in the diabetic conditions is well known, yet, glucose was also reported to be the only required source of energy for neurons and any disruption in glucose metabolism leads to compromised neuronal functions. Adolfsson *et al.* reported that the hypoglycemic condition (low blood glucose) can ameliorate brain status in AD[14].

Amyloid β (Aβ) is the components of the amyloid deposits in the AD brain and originated from the amyloid precursor protein (APP) [15], while the component of the amyloidogenic peptide deposit in the pancreatic islets of Langerhans is identified as islet amyloid polypeptide (IAPP), a 37-amino acid peptide[16,17].

These two proteins have a high sequence similarity, where the chaperone protein pathway preventing IAPP and Aβ aggregation may be common and act on both of them. It has been suggested that the decreased capacity of this shared chaperone protein is responsible for the development of AD and T2D. This means that islet amylogenesis is increased in patients with AD, and that the density of neurite plaques and their diffusion are positively related to the duration of diabetes[17]. Although the amino acid sequences of amyloidogenic proteins are diverse, they all adopt a similar structure in aggregates called cross-beta-spine[18]. Add at that, extensive studies in the past years have found that like $A\beta_{1-42}$, IAPP forms early intermediate assemblies as spherical oligomers[19-20] that are recognized by soluble Aβ oligomers antibody[21] implicating that these oligomers possess a common folding pattern or conformation[13].

A healthy body physiology tends to maintain a balance between production of ROS and body's antioxidant defense system and the alteration of this system. It is known that diabetic patients have more oxidative cellular environment as compared to healthy ones[22].

Furthermore, Aβ aggregation and oxidative stress have both way relationships controlling each other's turnover. Oxidative stress channels regulate Aβ dynamicity from non-aggregated form to aggregated form. Furthermore, aggregated Aβ acts like a source of free radical production to drive brain towards neurodegeneration[23].

The significance of these results is that therapeutic strategies designed to treat T2D, and oxidative stress could help slow the progress or reduce the severity of AD. Correspondingly, a number of studies have already demonstrated that treatment with

hypoglycemic can be protective in reducing the incidence and severity of AD brain pathology [24].

Halophyte is a kind of plants growing in a wide variety of saline habitats. Living in extreme environment, salt tolerant plants have to deal with frequent changes in salinity level. This can be done by developing adaptive responses including the biosynthesis of several bioactive molecules. Currently, an increasing interest is granted to these species because several of their secondary metabolites are restricted to halophytic species or are found in higher concentration than in glycophytes [25].

For the present research, *Tamarix gallica* L. was selected as a plant material (Figure 1). It is a tree or shrub halophyte from coastal regions and desert. It is a relatively long-living plant that can tolerate a wide range of environmental conditions and resist to abiotic stresses. Furthermore, *T. gallica* was reported to have a higher content of polyphenols compared to some other species of halophytes[26].

The choice of this plant was made based on three main reasons:

First of all, *T. gallica* was traditionally employed for the treatment of various diseases and was reported to be used as astringent, anti-inflammatory, cicatrizing agent, antiseptic and stimulant of perspiration[27-29]. It is also known for its effectiveness in conditions associated with hepatic insufficiency and the treatment of various liver disorders. The distinguished feature of growing in harsh climatic conditions is often ascribed to their high contents in antioxidant substances. And the enhanced synthesis of secondary metabolites under stressful conditions in halophyte is believed to protect the cellular structures from oxidative effects[25].

Furthermore, this halophyte is used for the preparation of poly-herbal drugs commercially available such as Liv 52, reported for protection activity against liver paracetamol, ethanol, *tert*-butyl hydroperoxide, and $CCl_4$ inducing hepatotoxicity and other liver disease, and Livergen used for its hepatoprotective effect[27].

The third reason is that *T. gallica*, like most *Tamarix* species, is considered as an invasive plant in the country from where they are not originated. The nature conservancy nominated Tamarisks as one of America's twelve worst invaders and the control measures are often expensive and ineffective. Therefore, it would be of interest to valorize the use of this plant instead of its eradication because of the ecological problem that it causes[26].

Some compounds were already identified from *T. gallica* such as rhamnetin (**a**), kaempferide (**b**), rhamnocitrin (**c**), coniferyl alcohol 4-*O*-sulfate (**d**), 2,7-dimethyl ether ellagic acid (**e**), β-sitosterol β-D-glucoside (**f**), and 12-hentriacontanol (**g**) (Figure 2)[30-32].

But, there is little report about the bioactivity of isolated substances from this halophyte for the prevention of diseases and the main reported activity was related to the solvent extract.

Although it was traditionally used for the treatment of various liver disorders, which is closely related to the glucose metabolic regulation, there is no report about the use of this plant for the treatment or prevention of T2D or/and AD.

Therefore, the aim of this research is to investigate the contributions of polyphenols from the halophyte *T. gallica* to prevent T2D and AD by isolation and identification of antioxidant substances with α-glucosidase inhibition activity and polymerization of amyloid aggregation inhibition potential.


Figure 1. Dried aerial part of *Tamarix gallica* L.

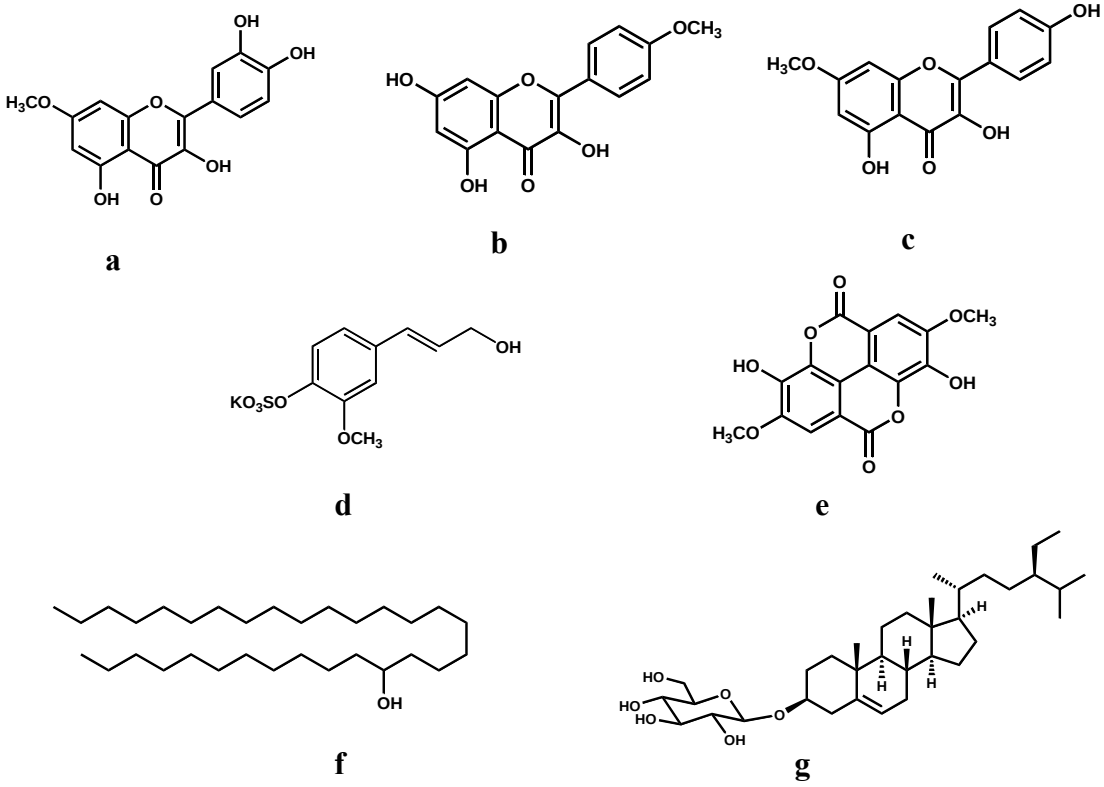


Figure 2. Example of some known substances isolated from *T. gallica*. (**a**): rhamnetin, (**b**): kaempferide, (**c**): rhamnocitrin, (**d**): coniferyl alcohol 4-*O*-sulfate, (**e**): 2,7-dimethyl ether ellagic acid, (**f**): β-sitosterol β-D-glucoside, and (**g**): 12-hentriacontanol.

# *Chapter II*

# Isolation of bioactive compounds for α-glucosidase inhibitory activity from *Tamarix gallica*

## **II-1.** Introduction

Diabetes mellitus (DM) is one of the leading and serious health concerns worldwide. Type 2 diabetes (T2D) accounts for more than 90% of all cases of diabetes globally[33]. Despite numerous pharmaceutical strategies for treatment of diabetes, its incidence continues to increase. Postprandial hyperglycemia contributes much to the overall glycemic control in T2D patients. Hence its management is considered as a major therapeutic strategy[34]. This can be achieved by delaying the release of glucose through the inhibition of carbohydrate hydrolyzing enzyme α-glucosidase (EC 3.2.1.20) in the digestive tract[35,36]. Commercial α-glucosidase inhibitors such as acarbose and voglibose have been used to treat diabetes, while they exhibit side effects including liver disorders, abdominal pain, acute hepatitis, abdominal fullness, and diarrhea[37-39]. Therefore, identifying and characterizing other inhibitors of α-glucosidase is still needed.

Hyperglycemia results also in the generation of reactive oxygen species (ROS), ultimately leading to increased oxidative stress in a variety of tissues that may partially mediate the initiation and progression of diabetes-associated complications. Hence, supplementation with antioxidant can be beneficial for diabetic patients, not only to maintain antioxidant levels in the body but also to treat the long-term complications that can arise [40].

*T. gallica* L. was mentioned as a remarkable spectrum of biochemical and pharmacological activities, especially for the treatment of liver disorders that are tightly related to the glucose regulation system in the human body. However, there is no report about the use of this plant for the treatment or prevention of T2D. Thus, the objective of this chapter is to isolate α-glucosidase inhibitory active compounds from this halophyte and to verify their antioxidant potential.

**II-2.** α-glucosidase inhibitory activity of *T. gallica* extracts

Dried and crushed aerial part (200 g) of *T. gallica* were extracted with 70% ethanol and left at room temperature for 24h. After filtration, the extract was evaporated in a rotary evaporator. The residue was partitioned among hexane (200 mL x 2), $CHCl_3$ (200 mL x 2), EtOAc (200 mL x 3), BuOH (200 mL x 3), and $H_2O$ (200 mL).

Yeast and mammalian α-glucosidase inhibition potential of different solvents extract from *T. gallica* was measured at different concentrations of 1, 10 and 100 µg/mL and their effective inhibition was displayed in Figures 3 and 4.

The results show that all extracts are dose dependent and that they are more sensitive to yeast enzyme than the mammalian α- glucosidase.

Based on the exhibited activity of each layer and by taking into consideration NMR data, $CHCl_3$ and EtOAc layers were selected to conduct further purification aiming to identify the α-glucosidase inhibitory active compounds.

**II-3.** Isolation and structure elucidation of bioactive compounds for α-glucosidase inhibitory activity

From the $CHCl_3$ layer and EtOAc layer, 10 active compounds were identified. The structures of these substances (Figure 5) were confirmed by NMR spectral analyses (Tables 1, 2, and 3) and compared with the literature[41-44].

The $^1$H NMR spectrum of compound **1** were characterized by the presence of an AMX system which is typical of a flavanone structure with resonances at $\delta_H$ 5.40 (dd, $J$ = 12.9 and 2.5 Hz, H-2), $\delta_H$ 3.12 (dd, $J$ = 17.0 and 12.9 Hz, H-3), and $\delta_H$ 2.68 (dd, $J$ = 17.0 and 2.5 Hz, H-3) and the compound was identified as naringenin (**1**).

The $^1$H NMR spectra of compounds **2**, **3**, **4**, **5**, and **6** suggested a flavanol structure presenting an AX system in ring A with two meta-protons at $\delta_H$ 6.28 (d, $J$ = 1.9 Hz, H-6) and $\delta_H$ 6.67 (d, $J$ = 1.9 Hz, H-8) for **2**; $\delta_H$ 6.23 (d, $J$ = 1.9 Hz, H-6) and $\delta_H$ 6.52 (d, $J$ = 1.9 Hz, H-8) for **3**; $\delta_H$ 6.25 (d, $J$ = 1.5 Hz, H-6) and $\delta_H$ 6.53 (d, $J$ = 1.5 Hz, H-8) for **4**; $\delta_H$ 6.27 (d, $J$ = 2.0 Hz, H-6) and $\delta_H$ 6.55 (d, $J$ = 2.0 Hz, H-8) for **5**; $\delta_H$ 6.21 (d, $J$ = 1.9 Hz, H-6) and $\delta_H$ 6.41 (d, $J$ = 1.9 Hz, H-8) for **6**.

In the B-ring, an ABX system was observed for **2**, **3**, **4**, and **5**: two aromatic protons ortho-coupled with each other and one singlet proton. Compound **2** was identified as quercetin.

Compounds **3**, **4**, and **5** are similar to quercetin with the addition of one methoxyl group for **3** and **5** ($\delta_H$ 3.89 and $\delta_H$ 3.95, respectively) and two methoxyl groups for **4** ($\delta_H$ 3.86 and $\delta_H$ 3.85). By comparing with commercially available compounds, substances **3**, **4**, and **5** were identical to rhamnetin, rhamnazin, and tamarixetin, respectively.

A characteristic resonance of AA'XX' system was observed in the B-ring of **6**, suggesting that compound **6** is kaempferol.

The $^1$H NMR spectra of compounds **7** and **8** suggest that the aglycone is similar to the structure of quercetin with the presence of anomeric proton at $\delta_H$ 5.22 (d, $J$ = 7.5, H-3). The HRESI-MS data of the two compounds suggest a monoglucuronide conjugate of quercetin. Compound **7** was identified as quercetin 3-*O*-β-D-glucuronide (MW 478) and compound **8** was identified as quercetin 3-*O*-β-D-glucuronide methyl ester (MW 492).

The $^1$H NMR spectra of compounds **9** and **10** suggest that the aglycone is similar to the structure of kaempferol with the presence of anomeric proton at $\delta_H$ 5.23 (d, $J$ = 7.4, H-3). The HRESI-MS data of the two compounds suggest a monoglucuronide conjugate of kaempferol. Compound **9** was identified as kaempferol 3-*O*-β-D-glucuronide (MW 462) and compound **10** was identified as kaempferol 3-*O*-β-D-glucuronide methyl ester (MW 478).

The purified active substances are mainly *O*-methylated and glucuronosylated flavonoids. These kinds of substances are usually reported as being less toxic than their aglycone. Add at that, glucuronosylated flavonoids are reported as substrates for human L-glucuronidase and they play an important role in the metabolic system of the human body [45)].

Therefore, it will be of interest to investigate their effect as a multi-modal treatment targeting the common pathophysiological features of both disturbances T2D and AD which will be the objective of Chapters III and IV.

**II-4**. Antioxidant activity

Biological effects of ROS are controlled *in vivo* by a wide spectrum of enzymatic and non-enzymatic defense mechanisms, in particular superoxide dismutases (SOD), which catalyze dismutation of superoxide anions to hydrogen peroxide and catalase, which then converts $H_2O_2$ into molecular oxygen and water. The role of those enzymes, as protective one, is well known and has been investigated extensively[65)].

SOD activities of flavonoids **1**-**10** are represented in Figure 6 and the result shows that **4**, **5**, **7**, **8**, and **9** have the highest inhibition percentage. A similar result was also observed in case of DPPH assay (Figure 7).

*O*-methylated and glucuronosylated flavonoids showed a higher inhibition percentage than their aglycone analogs, proving that methylation decrease the activity of quercetin (**2**) and kaempferol (**6**).

**II-5.** Experimental

II-5-1. General procedure

$^1$H NMR spectra were obtained with a Bruker Avance 500 spectrometer in $CD_3OD$. The resonance at $\delta_H$ 3.35 was used as an internal reference for the $^1$H NMR spectra. ESI-MS and HRESI-MS spectra were recorded with a Waters Synapt G2 mass spectrometer.

II-5-2. Plant materials

The aerial part of T. gallica was collected at Tunisia. The voucher specimen (UT-ARENA-01097) is maintained at Alliance for Research on North Africa (ARENA), University of Tsukuba.

II-5-3. Extraction and isolation

Dried and crushed aerial part (200 g) of *T. gallica* were extracted with 70% EtOH (900 mL x 3) and left at room temperature for 24 h. After filtration, the extract was evaporated in a rotary evaporator. The residue was partitioned among hexane (200 mL x 2), $CHCl_3$ (200 mL x 2), EtOAc (200 mL x 3), BuOH (200 mL x 3), and $H_2O$ (200 mL) to give hexane (2.6 g), $CHCl_3$ (1.1 g), EtOAc (2.4 g), BuOH (26.4 g), and $H_2O$ (17.4 g) soluble materials, respectively.

The $CHCl_3$ layer (TGC, 1.1 g) was chromatographed on a silica gel column ($\phi$ 3.0 × 35 cm, Nacalai Tesque, Inc., Japan) with acetone-hexane (0:100 → 10:90 → 20:80 → 30:70 → 40:50 → 50:50 → 60:40 → 80:20 → 100:0), which yielded eight fractions, TGC-1-8 (Figure 8).

Taking into consideration the inhibitory activity of each obtained fraction towards yeast and mammalian enzymes, TGC-5 and TGC-6 were selected for further purification (Figures 9 and 10).

TGC-5 (299.4 mg) eluted with acetone-hexane (40:60) was purified by octadecyl-silane (ODS) HPLC [TSKgel ODS-80Ts ($\phi$ 4.6 × 250 mm, Tosoh Corporation, Japan), flow rate 1.0 mL/min; MeCN/$H_2O$–0.1% trifluoroacetic acid (TFA) (5:95 (5 min) → 30:70 (5 min) → 40:60 (40 min) → 40:60 (10 min) → 55:54 (2 min) → 100:0 (2 min)); detection UV (210,

254, and 280 nm)] to yield naringenin (**1**, 3.4 mg, , $t_R$ 41 min), quercetin (**2**, 1.2 mg, $t_R$ 43 min), rhamnetin (**3**, 2.9 mg, $t_R$ 46 min), and rhamnazin (**4**, 1.6 mg, $t_R$ 72 min) (Figure 11).

Tamarixetin (**5**, 2.0 mg, $t_R$ 37 min) was purified from TGC-6 (100.1 mg) using ODS HPLC [TSKgel ODS-80Ts ($\phi$ 4.6 × 250 mm), flow rate 1.0 mL/min; MeCN/$H_2O$–0.1%TFA (5:95 (5 min) → 30:70 (25 min) → 40:60 (10 min) → 40:60 (10 min) → 55:54 (2 min) → 100:0 (2 min)); detection UV (210, 254, and 280 nm)] (Figure 12).

The EtOAc-soluble portion (TGE, 987 mg) was eluted on an ODS column (Cosmosil 75 C18-PREP, $\phi$ 3.0 × 35 cm, Nacalai Tesque, Inc., Japan) with MeOH/$H_2O$ (10 : 90 → 20:80 → 40:60 → 50:50 → 60:40 → 100 : 0), yielding six fractions, TGE-1-6 (Figure 13).

TGE-6 (228.3 mg), showing the strongest activity among all the fractions (Figures 14 and 15) eluted with MeOH/$H_2O$ (100: 0) was fractionated by ODS HPLC [TSKgel ODS-80Ts ($\phi$ 4.6 × 250 mm), flow rate 1.0 mL/min; MeOH/$H_2O$–0.1%TFA (5:95 (5 min) → 55:54 (55 min) → 85:15 (2 min) → 100:0 (2 min)); detection UV (280 and 320 nm)] to yield eight sub-fractions TGE-6-1-8 (Figure 16).

TGE-6-8 was identified as kaempferol (**6**, 3.3 mg, $t_R$ 37.5 min). TGE-6-3 (4.7 mg, $t_R$ 28.1 min) was purified by ODS HPLC [TSKgel ODS-80Ts ($\phi$ 4.6 × 250 mm), flow rate 1.0 mL/min; MeCN/$H_2O$ (5:95 (5 min) → 25:75 (41 min)); detection UV (210, 254, and 280 nm)] (Figure 17) to yield quercetin 3-*O*-β-D-glucuronide (QGlcA) (**7**, 6.3 mg, $t_R$ 9.3 min), and quercetin 3-*O*-β-D-glucuronide methyl ester (QGlcA-Me) (**8**, 9.0 mg, $t_R$ 17.6 min).

And then, TGE-6-5 (20 mg, $t_R$ 32.3 min) was also purified by ODS HPLC [TSKgel ODS-80Ts ($\phi$ 4.6 × 250 mm), flow rate 1.0 mL/min; MeCN/$H_2O$ (5:95 (1 min) → 30:70 (45 min)); detection UV (210 nm)] (Figure 18) to yield kaempferol 3-*O*-β-D-glucuronide (KGlcA) (**9**, 2.0 mg, $t_R$ 11.5 min), and kaempferol 3-*O*-β-D-glucuronide methyl ester (KGlcA-Me) (**10**, 5.0 mg, $t_R$ 12.3 min).

### II-5-4. *p*-NPG assay

*p*-Nitrophenol α-D-glucopyranoside (*p*-NPG), *p*-nitrophenol, sodium phosphate, and sodium carbonate were purchased from Nacalai Tesque Inc., Kyoto, Japan. Yeast α-glucosidase and intestinal acetone powders from rats were obtained from Sigma Aldrich Chemical Co., USA and acarbose was procured from LKT laboratories, Inc., USA.

Yeast and mammalian α-glucosidase inhibitory activities were analyzed as follows: Mammalian α-glucosidase was prepared by homogenizing 100 mg of rat intestinal acetone powder in 3 mL of 0.9% NaCl solution (5,000 *g* x 30 min).

Twenty five µL of 3.5 U/100 mL stock solution of yeast enzyme were diluted into 12.5 mL of phosphate buffer to obtain the final α-glucosidase solution.

The reaction mixture comprising 50 µL of 0.1 M phosphate buffer (pH 6.8), 10 µL of 1 mM *p*-NPG, and 10 µL of the samples (in varying concentrations) was pre-incubated at 37°C for 5 min. Then, 10 µL yeast (0.07 U/mL) / mammalian α-glucosidase of was added as a substrate, followed by incubation at 37°C for 30 min. After then the reaction was stopped by adding 50 µL of $Na_2CO_3$ (0.1 M).

Acarbose was used as a positive control and MeOH as a negative control. Since MeOH was used to dissolve the samples, a negative blank without the enzyme was prepared to subtract the possible interference of MeOH with the reaction.

The enzyme activity was quantified by measuring the absorbance at 410 nm in a microtiter plate reader (Bio-TEK, USA).

All experiments were performed in triplicate and the percentage of enzyme inhibition was calculated using the following formula[46]:

$$(\%)\ \text{inhibition} = [(AC - AS) / AC] \times 100,$$

where AC is the absorbance of the control and AS is the absorbance of the tested sample.

II-5-5. SOD activity

SOD activity was determined with the use of kits obtained from Dojindo molecular technologies, Inc.

The determination principle of SOD assay was that the superoxide anion ($O^{2-}$) generated from the reaction of xanthine and xanthine oxidase and then the ($O^{2-}$) oxidized the hydroxylamine, which generated the nitrite.

Nitrite could be presented purplish red by the effect of chromogenic agent. Then the absorbance was taken at 550 nm by the spectrophotometer. When the samples are containing SOD, the superoxide anion radicals could be distinctively inhibited and as a result, the nitrite was reduced.

The SOD activity of samples can be measured according to the formula:

$$\text{SOD activity}\ (\%) = [(\text{blank 1-blank 3})-(\text{sample-blank 2})] / (\text{blank 1- blank 3});$$

with blank 1 being the coloring without sample, blank 2 sample blank and blank 3 reagent blank. Epigallocatechin gallate (EGCG) was used as a positive control.

II-5-6. Free Radical Scavenging Activity (DPPH) assay

In a 96-well micro plate, a 10 mM of test sample was dissolved in MeOH (50 mM). And 190 mL of a mixed solution, prepared of MilliQ: 400 mM MES buffer: 0.4 mM DPPH solution dissolved in EtOH (3:4:1) were added. The reaction solution was measured at a wavelength 490 nm using a spectrophotometer. The percentage of DPPH scavenging was calculated as follow:

$$\text{Antioxidant (\%)} = (1-B/A) \times 100,$$

where A represents the absorbance of the control without the test samples and B represents the absorbance in the presence of test samples.

Table 1. $^{1}$H NMR data of compounds **1**, **2**, and **6**.

| Position | Substances<br>$\delta_H$ (m, *J* $H_Z$) (500 MHz, $CD_3OD$) | | |
|---|---|---|---|
| | **1** | **2** | **6** |
| 2 | 5.40 (dd, 12.9, 2.5, 1H) | - | - |
| 3 | 3.12 (dd, 17.0, 12.9, 1H)<br>2.68 (dd, 17.0, 2.5, 1H) | - | - |
| 4 | - | - | - |
| 5 | - | - | - |
| 6 | 5.91 (s, 1H) | 6.28 (d, 1.9, 1H) | 6.21 (d, 1.9, 1H) |
| 7 | - | - | - |
| 8 | 5.91 (s, 1H) | 6.67 (d, 1.9, 1H) | 6.41 (d, 1.9, 1H) |
| 9 | - | - | - |
| 10 | - | - | - |
| 1’ | - | - | - |
| 2’ | 7.34 (d, 8.0, 1H) | 7.95 (s, 1H) | 8.05 (d, 8.6, 1H) |
| 3’ | 6.84 (d, 8.0, 1H) | - | 6.92 (d, 8.6, 1H) |
| 4’ | - | - | - |
| 5’ | 6.84 (d, 8.0, 1H) | 8.10 (d, 8.9, 1H) | 6.92 (d, 8.6, 1H) |
| 6’ | 7.34 (d, 8.0, 1H) | 7.08 (d, 8.9, 1H) | 8.05 (d, 8.6, 1H) |

Table 2. $^{1}$H NMR data of compounds **3**, **4**, and **5**.

| Position | Substances<br>$\delta_H$ (m, *J* $H_Z$) (500 MHz, $CD_3OD$) | | |
|---|---|---|---|
| | **3** | **4** | **5** |
| 2 | - | | - |
| 3 | | | - |
| 4 | - | | - |
| 5 | - | | - |
| 6 | 6.23 (d, 1.9, 1H) | 6.25 (d, 1.5, 1H) | 6.27 (d, 2.0, 1H) |
| 7 | - | - | - |
| 8 | 6.52 (d, 1.9, 1H) | 6.53 (d, 1.5, 1H) | 6.55 (d, 2.0, 1H) |
| 9 | - | - | - |
| 10 | - | - | - |
| 1’ | - | - | - |
| 2’ | 7.74 (s, 1H) | 7.81 (s, 1H) | 7.79 (s, 1H) |
| 3’ | - | - | - |
| 4’ | - | - | - |
| 5’ | 7.76 (d, 9.1, 1H) | 7.84 (d, 8.5, 1H) | 7.80 (d, 9.0, 1H) |
| 6’ | 7.08 (d, 9.1, 1H) | 7.08 (d, 8.5, 1H) | 7.13 (d, 9.0, 1H) |
| 3’- OMe | - | 3.86 (s, 3H) | - |
| 4’- OMe | - | - | 3.95 (s, 3H) |
| 7- OMe | 3.89 (s, 3H) | 3.85 (s, 3H) | - |

Table 3. $^{1}$H NMR data of substances **7**, **8**, **9**, and **10**.

| Position | Substances<br>$\delta_H$ (m, *J* $H_Z$) (500 MHz, $CD_3OD$) | | | |
|---|---|---|---|---|
| | **7** | **8** | **9** | **10** |
| 2 | - | - | - | - |
| 3 | - | - | - | - |
| 4 | - | - | - | - |
| 5 | - | - | - | - |
| 6 | 6.20 (d, 1.5, 1H) | 6.20 (d, 2.0, 1H) | 6.21 (d, 1.9, 1H) | 6.21 (d, 1.9, 1H) |
| 7 | - | - | - | - |
| 8 | 6.35 (d, 1.5, 1H) | 6.39 (d, 2.0, 1H) | 6.41 (d, 1.9, 1H) | 6.41 (d, 1.9, 1H) |
| 9 | - | - | - | - |
| 10 | - | - | - | - |
| 1’ | - | - | - | - |
| 2’ | 7.52 (s, 1H) | 7.52 (s, 1H) | 8.05 (d, 8.6, 1H) | 8.05 (d, 8.6, 1H) |
| 3’ | - | - | 6.92 (d, 8.6, 1H) | 6.93 (d, 8.6, 1H) |
| 4’ | - | - | - | - |
| 5’ | 6.98 (d, 8.5, 1H) | 6.98 (d, 8.5, 1H) | 6.92 (d, 8.6, 1H) | 6.93 (d, 8.6, 1H) |
| 6’ | 7.57 (d, 8.5, 1H) | 7.57 (d, 8.5, 1H) | 8.05 (d, 8.6, 1H) | 8.05 (d, 8.6, 1H) |
| 1’’ | 5.22 (d, 7.5, 1H) | 5.22 (d, 7.5, 1H) | 5.23 (d, 7.4, 1H) | 5.23 (d, 7.4, 1H) |
| 2’’ | 3.57 (m, 1H) | 3.57 (m, 1H) | 3.56 (m, 1H) | 3.56 (m, 1H) |
| 3’’ | 3.51 (m, 1H) | 3.51 (m, 1H) | 3.46 (m, 1H) | 3.46 (m, 1H) |
| 4’’ | 3.41 (m, 1H) | 3.41 (m, 1H) | 3.40(m, 1H) | 3.40 (m, 1H) |
| 5’’ | 3.72 (d, 9.6, 1H) | 3.68 (d, 9.4, 1H) | 3.74 (d, 9.8, 1H) | 3.74 (d, 9.8, 1H) |
| 6’’ | - | - | - | - |
| 6’’-$OCH_3$ | 3.64 (s, 3H) | - | 3.64 (s, 3H) | - |

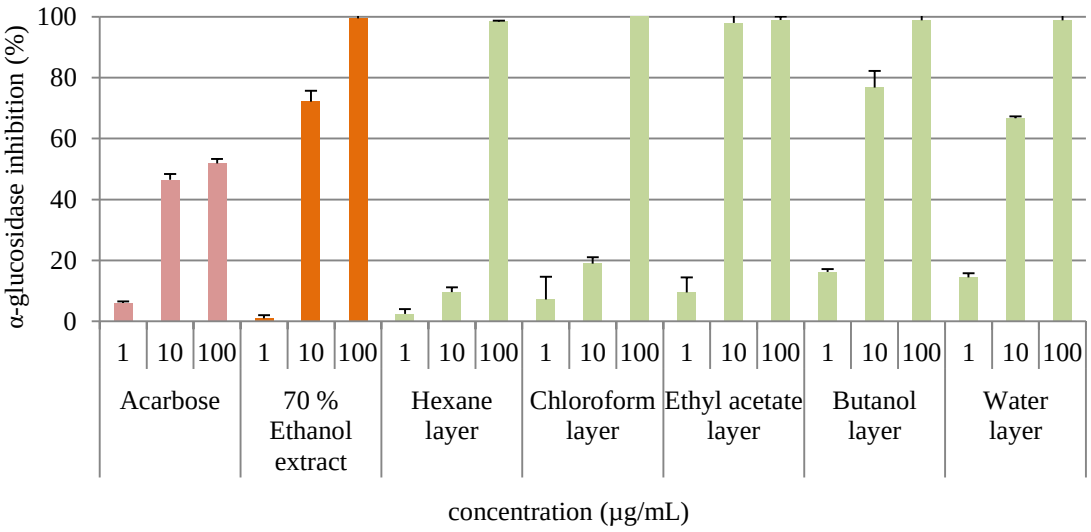


Figure 3. α-Glucosidase inhibitory activity against yeast enzyme.

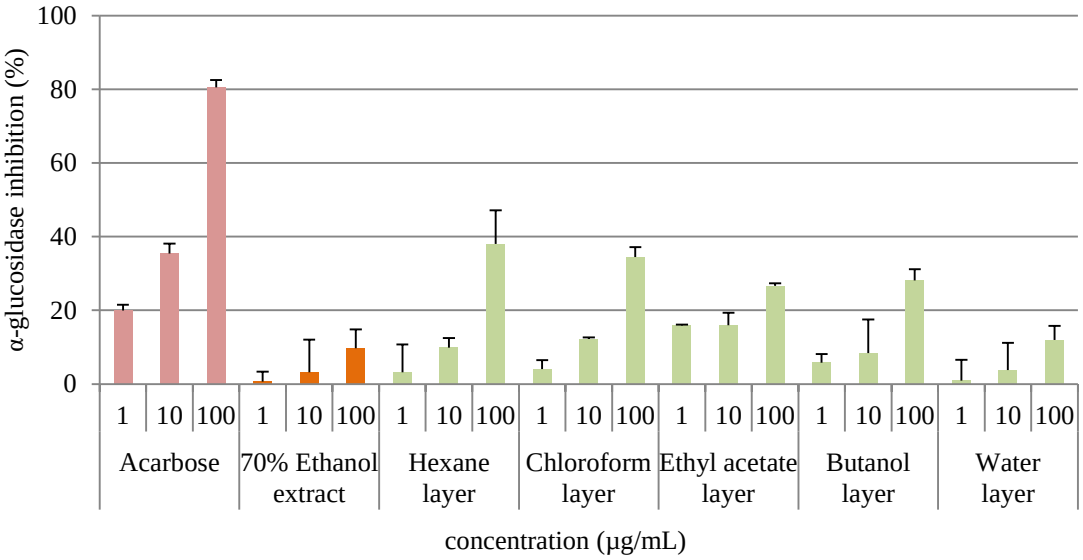


Figure 4. α-Glucosidase inhibitory activity against mammalian enzyme.

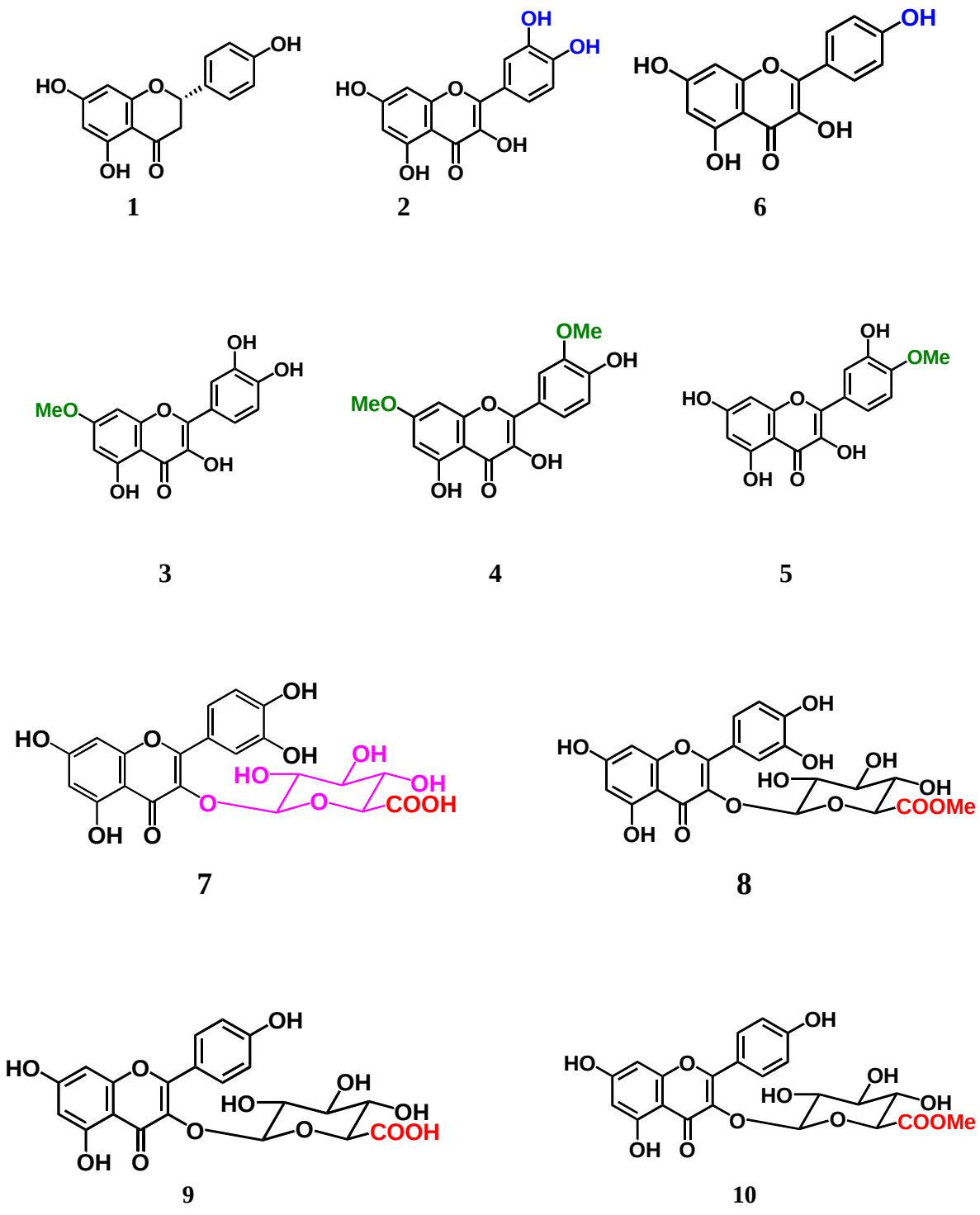


Figure 5. Structures of flavonoids **1**-**10**.

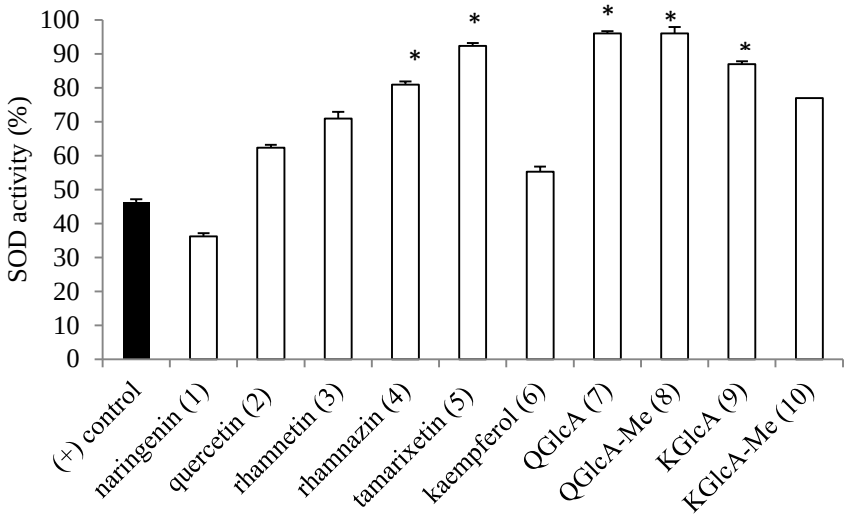


Figure 6. SOD activity of flavonoids **1**-**10**.

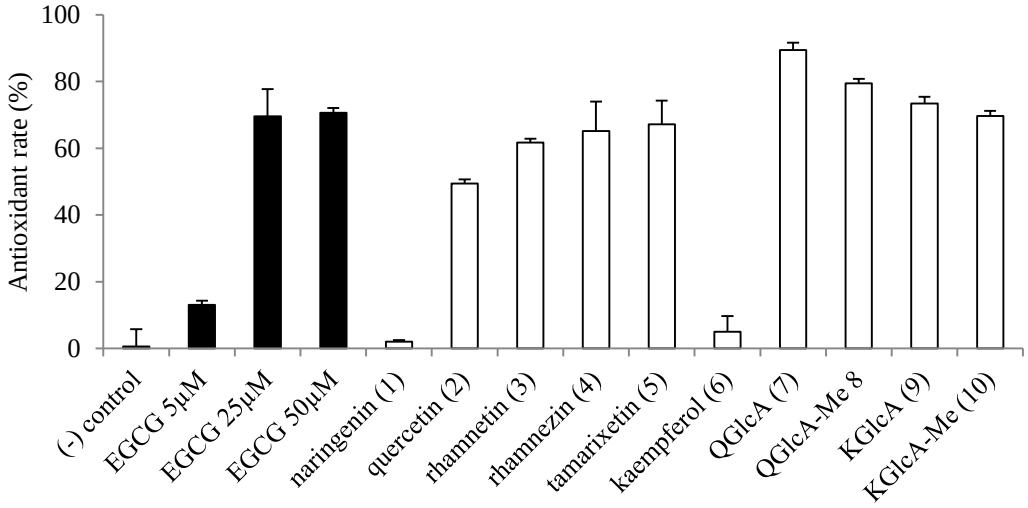


Figure 7. Antioxidant activity of flavonoids **1**-**10**

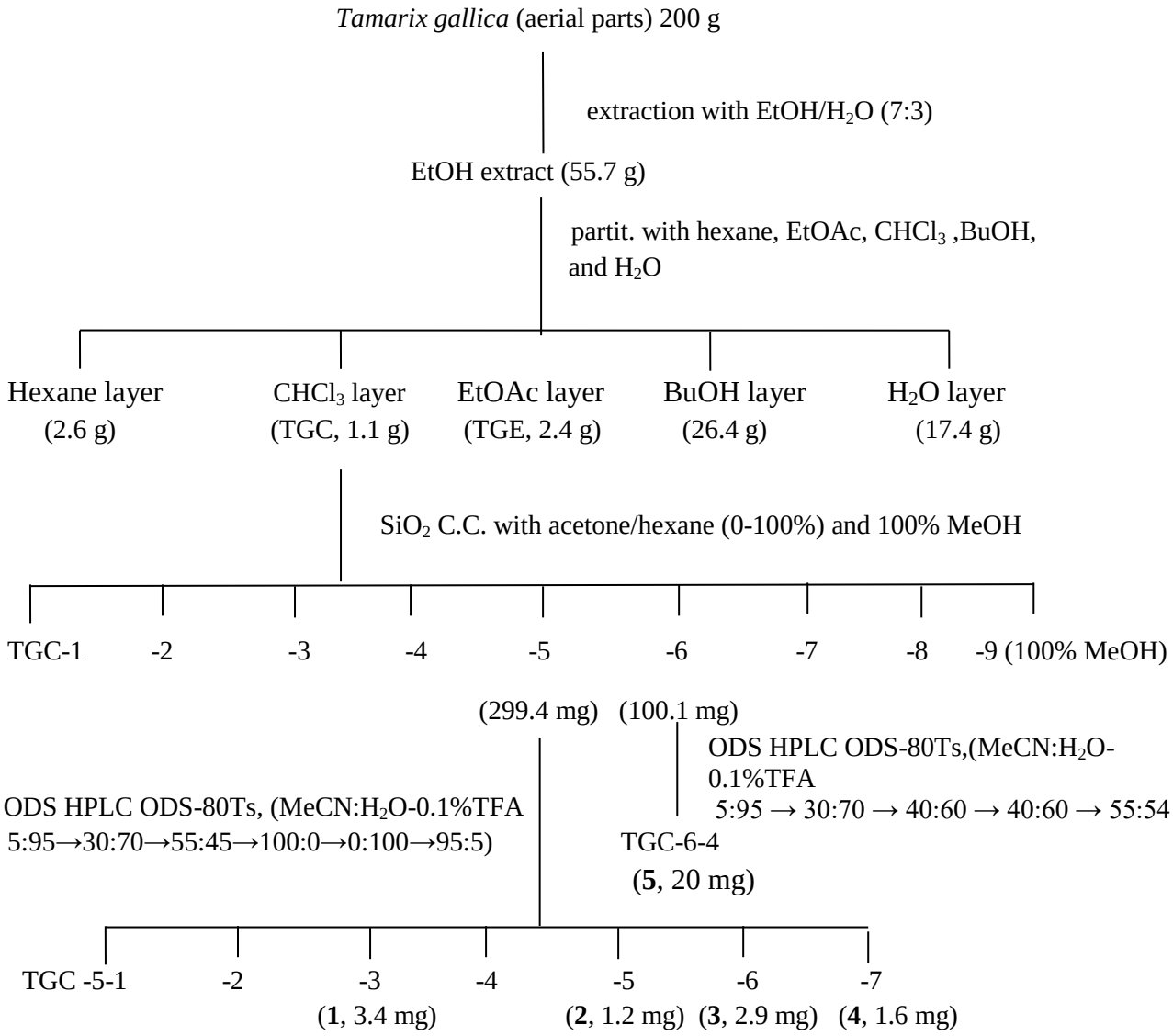


Figure 8. Isolation scheme of α-glucosidase inhibitory active compounds from TGC.

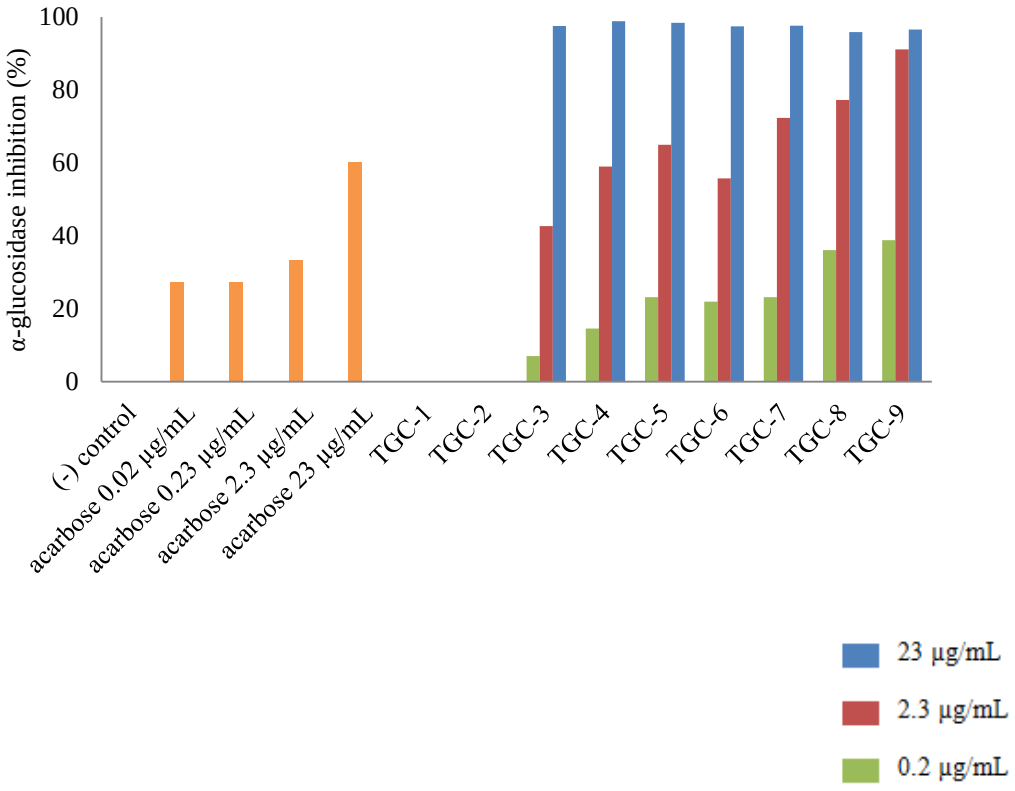


Figure 9. α-Glucosidase inhibitory activity against yeast enzyme of TGC-1─9.

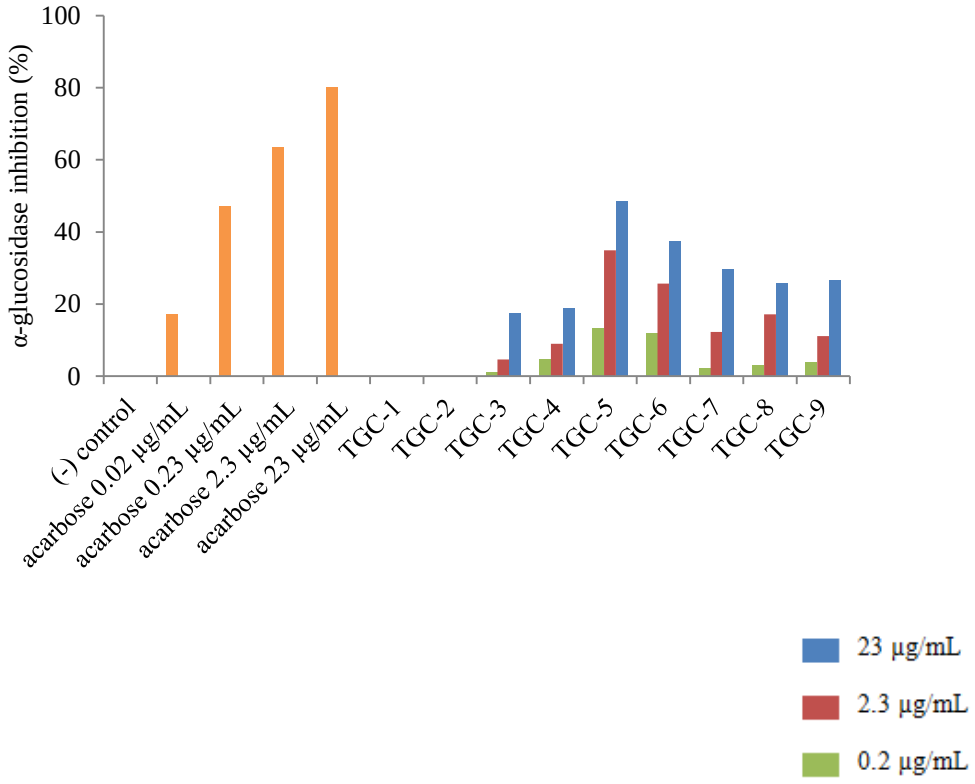


Figure 10. α-Glucosidase inhibitory activity against mammalian enzyme of TGC-1─9.

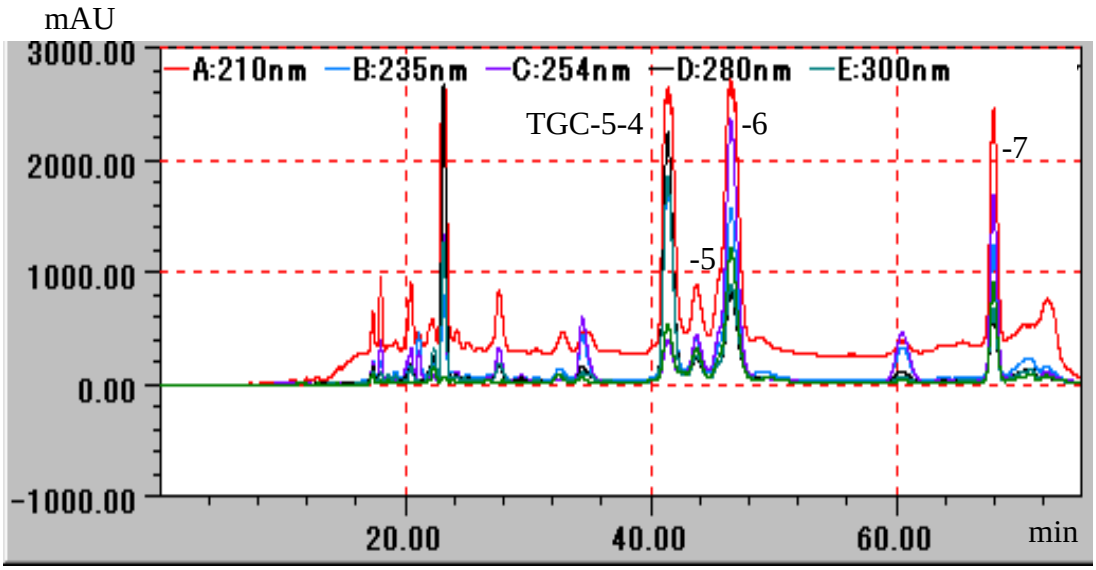


Figure 11. HPLC chromatogram of TGC-5.

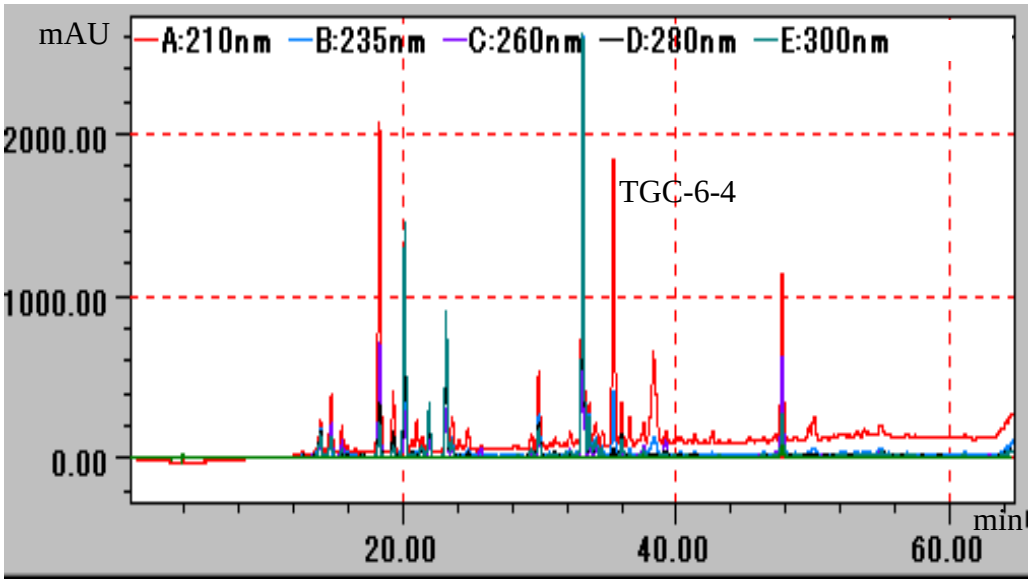


Figure 12. HPLC chromatogram of TGC-6.

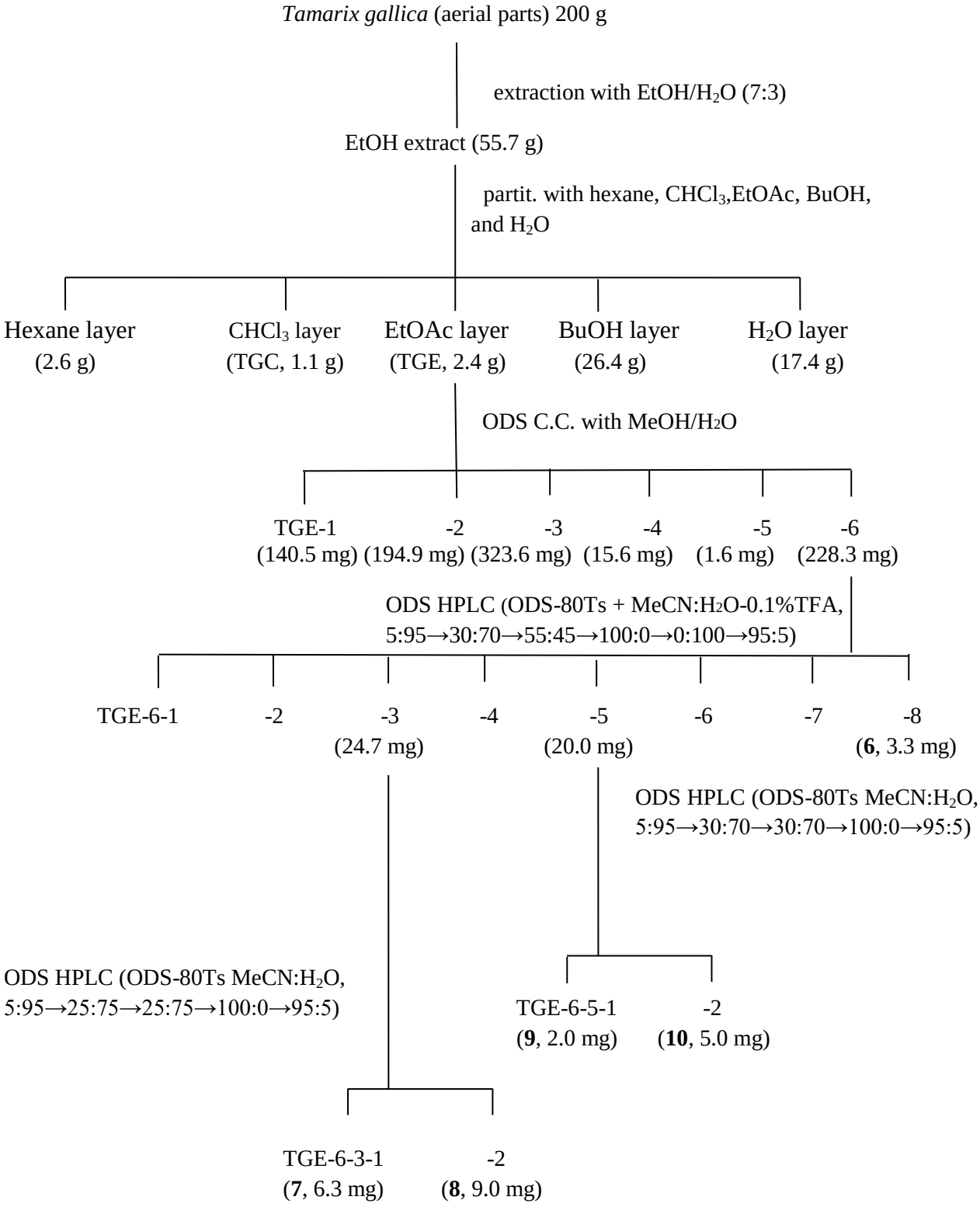


Figure 13. Isolation scheme of α-glucosidase inhibitory active compounds from TGE.

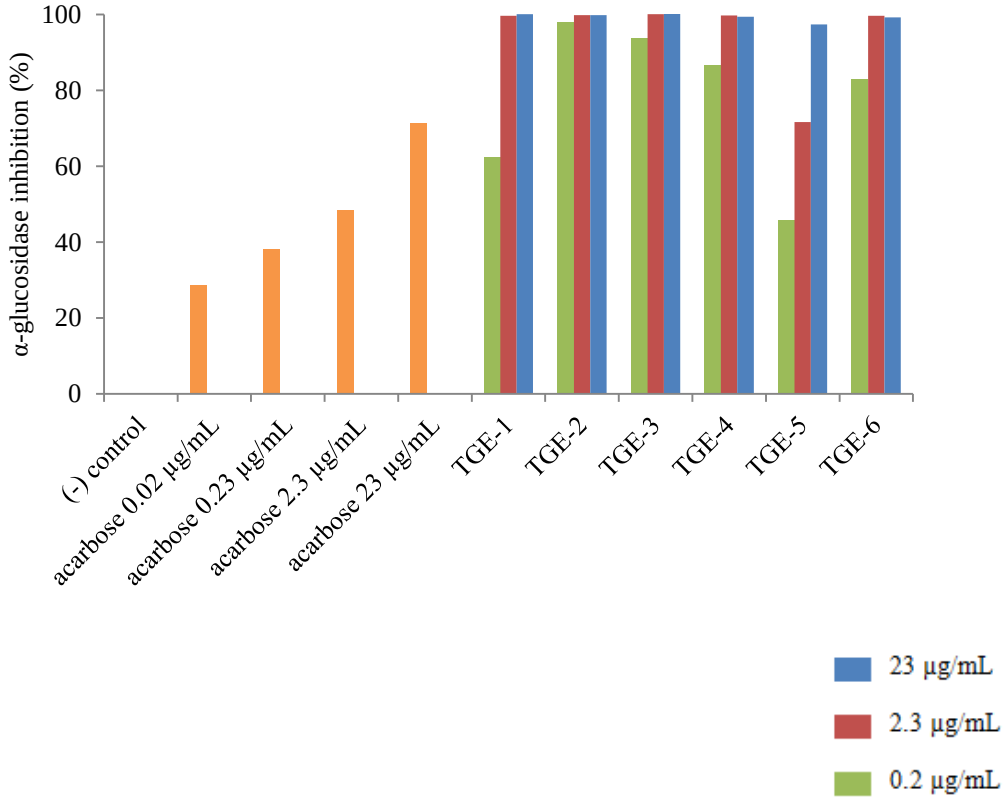


Figure 14. α-Glucosidase inhibition against yeast enzyme of TGE-1─6.

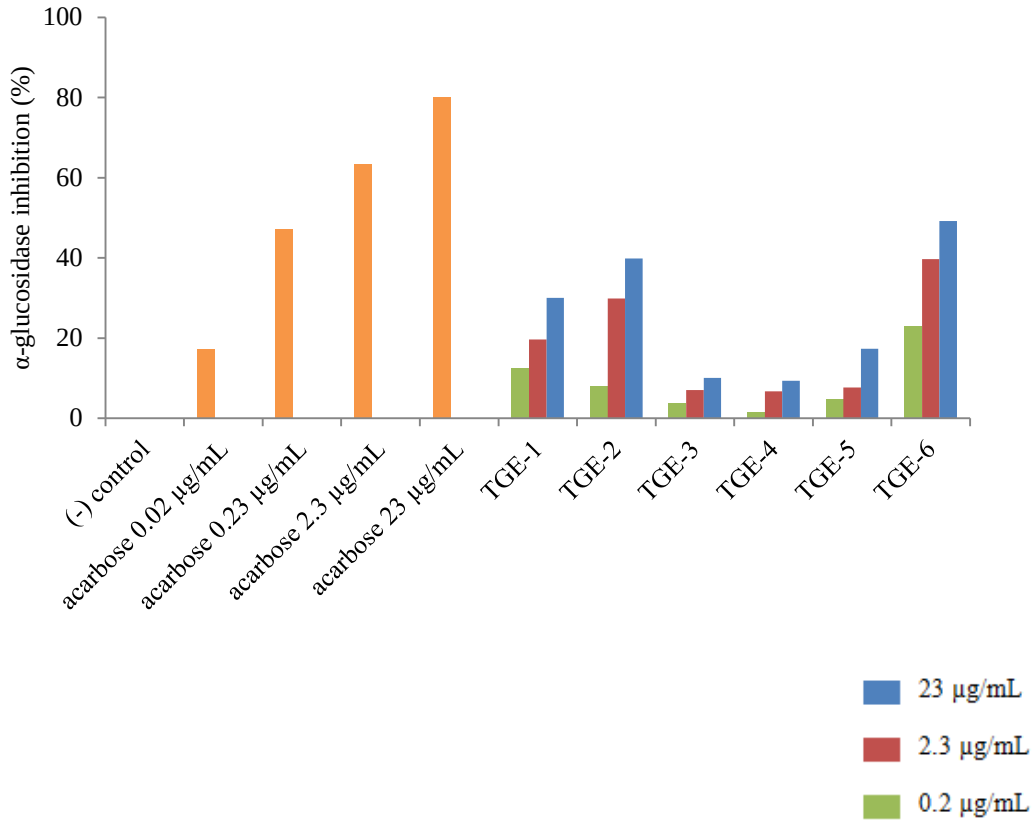


Figure 15. α-Glucosidase inhibitory activity against mammalian enzyme of TGE-1─6.

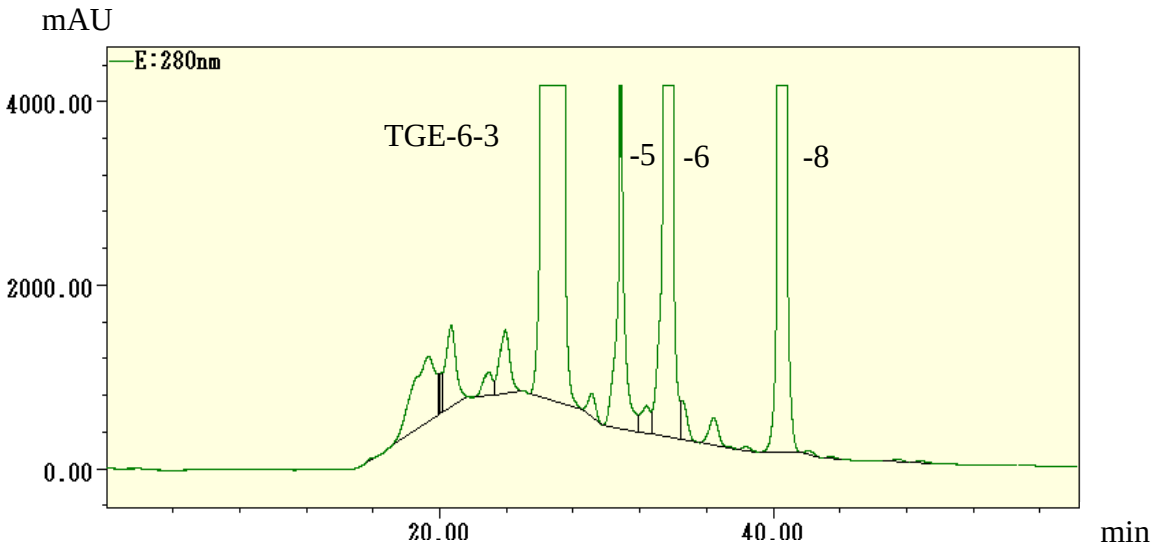


Figure 16. HPLC chromatogram of TGE-6.

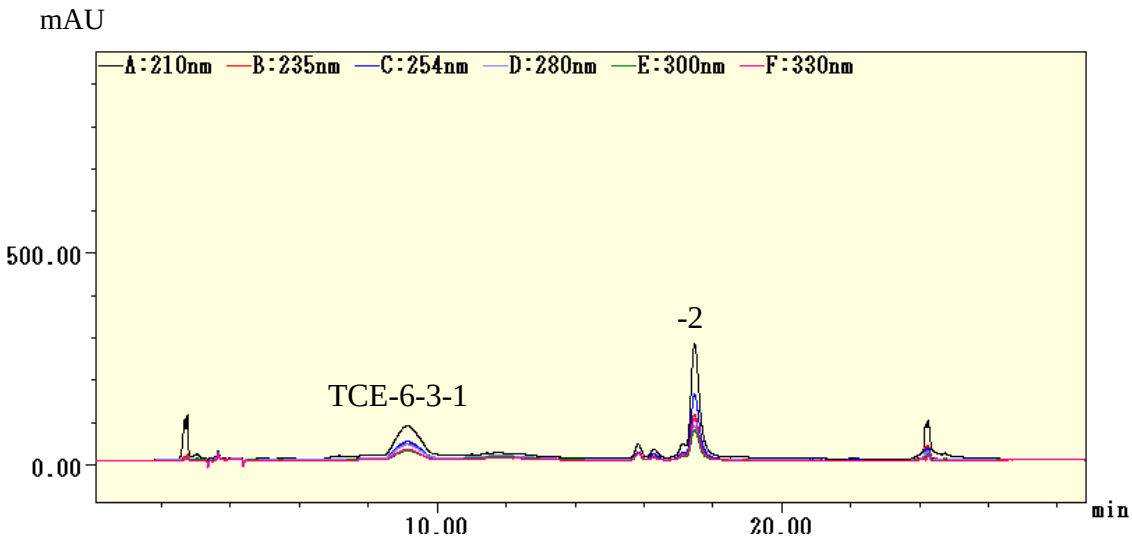


Figure 17. HPLC chromatogram of TGE-6-3.

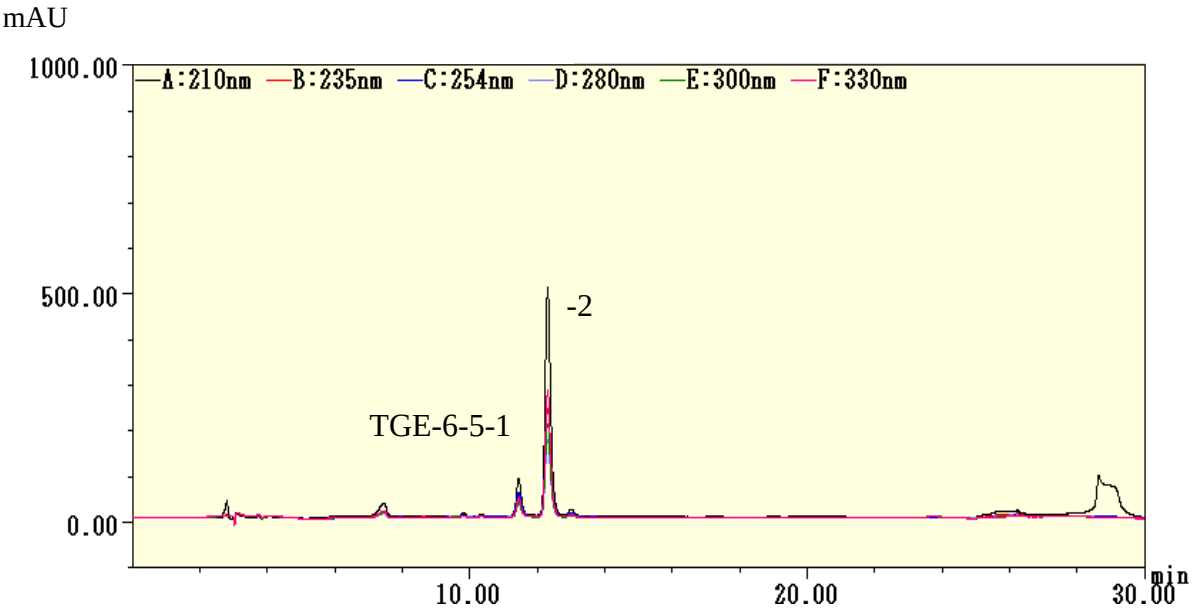


Figure 18. HPLC chromatogram of TGE-6-5.

# *Chapter III*

## Structure-activity relationship, mechanism of action and synergistic effect of the isolated flavonoids **1-10** for α-glucosidase inhibitory activity

### **III-1.** Introduction

Nowadays, it is well established that flavonoids undergo extensive metabolism after ingestion. After the release of the aglycone by hydrolysis, glucuronosylation, and methylation of the aglycones occur in the intestinal epithelial cells by the action of uridine 5′-diphospho-glucuronyltransferases (UGT) and catechol *O*-methyltransferases (COMT) before they enter the bloodstream. There is even report about some efflux of these metabolites back into the small intestine. Once in the bloodstream, the conjugates reach the liver, where they are further methylated/ glucuronosylated as part of phase II liver metabolism, and then the cells of the different organs in the human body. Metabolism can also occur in the kidney and the conjugates are recycled back to the small intestine through the bile (Figure 19)[47].

Absorption, metabolism, and bioavailability are remarkably different among the flavonoid subclasses. Indeed, the most abundant flavonoids in the human diet may not necessarily be the most bioavailable or the most biologically active. Flavonoid subclasses have different absorption kinetics and are highly metabolized, with the resulting metabolites differing in biological activity from their parent compounds and from each other. It is now recognized to be imperative to identity the flavonoid metabolites that may exert beneficial effects on health[48].

The objective of this chapter is to study the structure-activity relationship of the flavonoids **1-10** isolated from *T. gallica* compared with their aglycones, to determine their inhibition mechanism and finally, to check their synergistic effects.

### **III-2.** Inhibitory activity and structure-activity relationship of the isolated flavonoids **1-10**

Alpha-glucosidase inhibition potential of different purified flavonoids **1-10** was measured and their effectiveness was displayed in Table 4.

Rhamnetin (**3**), tamarixetin (**5**), rhamnazin (**4**), KGlcA (**9**), KGlcA-Me (**10**), QGlcA (**7**), and QGlcA-Me (**8**) are reported for the first time as α-glucosidase inhibitors.

The results revealed that among all the tested flavonoids, compound **8** showed the strongest inhibitory potential with an $IC_{50}$ 62.3 μM which is slightly lower than that of the positive control acarbose which showed an $IC_{50}$ 95.1 μM for the yeast α-glucosidase (Table 4).

The inhibitory sequence for the aglycone compounds was **2** > **6** > **1**, while, for quercetin and its *O*-methylated flavonoids was: **3** > **2** > **5** > **4**.

For the glucuronide substances, quercetin analogs **7** and **8** showed a slightly higher inhibition percentage compared to kaempferol analogs **9** and **10**.

The structure-activity relationship study of quercetin (**2**), kaempferol (**6**), and naringenin (**1**) shows that the B-ring plays an important role for the α-glucosidase activity.

Furthermore, and according to the obtained data, an unsaturated C-ring and the number of hydroxyl group in B-ring enhance the inhibitory activity.

Methoxylation of flavonoids affected also the inhibitory potential for α-glucosidase *in vitro* depending on the replaced site. In fact, the substitution of a hydroxyl group with a methoxy one in A-ring decrease significantly the α-glucosidase inhibition activity, while the same substitution in the B-ring reduced the potential of quercetin (**2**) and rhamnetin (**3**) leading to the conclusion that the catechol moiety in B-ring is a factor of activity enhancement.

Tadera *et al.* suggested that the unsaturated C-ring, 3-OH, 4-CO, and the hydroxyl substitution on the B-ring enhanced the α-glucosidase inhibitory activity[49].

Li *et al.* reported that the glycosylation of hydroxyl group on flavonoids at C-3 weakened the inhibition against α-glucosidases[50]. The larger volume and polarity of glucosides compared to their aglycone structures might play a role in their activity depending in their target.

However, according to the obtained results from the current report, the substitution of the hydroxyl group at C-3 position by a glucuronic acid and its methyl ester analog increased significantly the inhibition activity of quercetin (**2**) and kaempferol (**6**) towards α-glucosidase and so far, no publications have reported investigation of the

relation between the α-glucosidase inhibitory activity and the replacement of 3-OH on flavonoids by glucuronic acid and glucuronic acid methyl ester.

**III-3.** Mechanism of action: Inhibition mode

The mechanism of inhibition of flavonoids **1**-**10** was evaluated by Michaelis Menten saturation kinetics represented by LB plot (Figures 20─29). The kinetics of inhibition (Tables 5─14) was evaluated by varying the concentration of *p*-NPG (0.25-16 mM) in the presence or absence of flavonoids **1**-**10** at two different concentrations (16 and 64 µg/mL) and the following results were obtained:

The double-reciprocal plot displayed competitive inhibition for **1**, mixed inhibition for **2**, **3**, **4**, **5**, and **6**, and a non-competitive inhibition for **7**, **8**, **9**, and **10** (Table 15). In fact, in the case of **1**, $V_{max}$ was unchanged while $K_m$ increased when the concentration of the inhibitor was increased (Table 5) which corresponds to the competitive inhibition mode: the inhibitor binds to the same site on the enzyme that the substrate would normally do and this kind of inhibition is reversible. For **2**, **3**, **4**, **5**, and **6**, $K_m$ decreased and/or increased, while $V_{max}$ decreased in all the cases (Tables 6─10). This type of parameters is characteristic of the mixed inhibition where the inhibitor binds to the enzyme at a different site away from the active site. In this situation, the inhibitor can bind to both free enzyme or enzyme-substrate complex and the later has a residual enzyme activity. Add at that, the analysis of the glucuronosylated flavonoids showed a constant $K_m$ and a decrease in the rate of $V_{max}$ that cannot be overcome by increasing the flavonoid concentrations (Tables 11-14). This inhibition is irreversible and classified as non-competitive inhibition where the inhibitor binds to the enzyme at an allosteric site causing shape change of the enzyme's active site.

From the values of inhibition constants (*Ki*) as is seen in Table 15, the sequence of affinity ($1/K_i$) between the tested substances and α-glucosidase was deduced to be **8** > **7** > **10** > **9** > **2** > **6** for the glucuronosylated flavonoids and **3** > **2** > **5** > **4** for the *O*-methylated flavonoids, consistent with the $IC_{50}$ data.

**III-4.** Specificity of flavonoids **1-10** for α-glucosidase inhibitory activity

The activity towards mammalian α-glucosidase and their selectivity for sugar (sucrose and maltose) hydrolase inhibition were evaluated and the results are shown in Table 16. Each of the isolated flavonoids **1-10** showed a dose dependent inhibitory activity with an inhibition preference for maltose even at a very low concentration (1 µM).

A part of their structure functionality, the effectiveness of α-glucosidase inhibitors is affected by the origin of enzyme, as well as, the type of target substrate. In fact, phenolic compounds are considered as potent class of α-glucosidase inhibitors. But, most of yeast's α-glucosidase inhibitors did not show any activity against mammalian α-glucosidase (class III) due to the difference of molecular recognition in the target binding site of these enzymes. Mammalian α-glucosidases (*α*-D-glucoside glucohydrolase EC.3.2.1.20) inhibitors, which interfere with enzymatic action in the brush border of the small intestine, could slow the liberation of D-glucose from oligosaccharides and disaccharides, resulting in delaying glucose absorption and decreasing postprandial plasma glucose levels. Hence, it was also of interest to evaluate the inhibitory activity of the purified flavonoids **1-10** towards mammalian α-glucosidases, sucrase and maltase, as well as their selectivity for sugar hydrolase inhibition.

According to the obtained data, flavonoids **1-10** inhibited both yeast and mammalian enzymatic activity at a dose-dependent effect and the substrate preference where different depending on the inhibitors' chemical structures. This finding suggests that the isolated flavonoids **1-10** would have a physiological function relating to the prevention of glucose absorption at the small intestine within this experiment conditions.

**III-5.** Synergistic effect of flavonoids **1-10**

The bioassay guided isolation process revealed that the separation of some compounds from the same fraction reduced their activity. So, It was also of interest to establish whether quercetin or/and kaempferol analogs might interact synergistically on intestinal α-glucosidase inhibition.

There are reports of established α-glucosidase inhibitors such as acarbose and their effects on blood glucose levels after food uptake. Acarbose has been clinically studied in type 2 diabetes. A recent report has shown that the lowest dose of acarbose with clinical effects is 150 mg/day, with doses > 300 mg/day already exceeding the saturated binding of α-glucosidase[51, 52]. It was also reported that the most common adverse effect of acarbose is gastrointestinal disturbance which occurs in a dose-dependent manner. Thus, it is possible that the mixture of flavonoids **1**-**10** together with acarbose may lead to the development of a novel combined therapy in type 2 diabetic patients.

Data in Table 16 indicate that the *O*-methylated flavonoids **3**-**5** and glucuronosylated flavonoids **7**-**10** at very low concentration (1 μM) had a very low or no inhibitory activity in case of using sucrose as a substrate and moderate to low inhibition percentage in case of maltose. Therefore, it was of interest to establish whether *O*-methylated and glucuronosylated flavonoids and acarbose might interact synergistically on intestinal α-glucosidase inhibition. Results of this experiment are represented in Figures 30 and 31 and show that when *O*-methylated flavonoids **3**-**5** and glucuronosylated flavonoids **7**-**10** were added to the assay system with acarbose (0.5 μM and 3.12 μM), the percentage intestinal maltase and sucrase inhibition, respectively, were increased compared with acarbose. The combination at a low concentration produces more synergistic inhibition than either drug alone, suggesting that they may provide a significant clinical benefit in delaying postprandial hyperglycemia. As a consequence, it will be possible to reduce dosage of acarbose. However, further investigation in diabetic patients should be conducted.

The synergestic effect might be explained in relation with the inhibition mode of each substances. In the simplest molecular case, two α-glucosidase inhibitiors targeting the same site, such as acarbose and **1**, would produce an additive effect only. However, if two different binding sites for inhibitors exist on an enzyme, two α-glucosidase inhibitors may bind simultaneously and therefore, synergy can be a necessary consequence[53]. In case of non-competitive, inhibitors have spesific and independent sites on the enzyme different from the active site. Thus, two inhibitors, for example acarbose and glucuronosylated flavonoids **7**-**10**, are able to bind simultaneously, and this state is called “mutually non-exclusive” binding (Figure 32). In case of mixed inhibition, inhibitors also can bind to a site different from the active one and their for

can cause a synergestic effect (Figure 33). However, mixed inhibitors might act as a competitive inhibitor or/and non-competitive inhibitor, which may explain the difference between the *O*-methylated flavonoids **3-5** and their aglycones **2** and **6**.

**III-6.** Experimental: general methods

III-6-1. Determination of $IC_{50}$

The concentration of the inhibitor required to inhibit 50% of the enzyme activity ($IC_{50}$) was calculated under the same *p*-NPG assay conditions, using concentrations of 25, 50, 75, 100, 125, 150, 175, and 200 µmol/L for the flavonoids **1-10** and the following obtained curve were used to determine the $IC_{50}$ (Figures 34-44).

III-6-2. Disaccharide assay

The α-glucosidase inhibition potential of the purified flavonoids **1-10** was measured at concentrations of 1, 10, and 100 µM, using the disaccharide assay as follows:

Mammalian α-glucosidase was prepared by homogenizing 100 mg of rat intestinal acetone powder in 3 mL of 0.9% NaCl solution (5,000*g* x 30 min).

The reaction mixture comprising from 50 µL of 0.1 M phosphate buffer (pH 6.8) and 10 µL of the sample at various concentrations was mixed with 35 µL of maltose solution (5 mM) for maltase inhibition test, and 20 µL of sucrose (56 mM) for sucrase inhibition test.

After pre-incubation for 5 min at 37°C, the enzyme solution was added, 20 µL in case of sucrase inhibition assay and 5 µL for maltase inhibition assay, and incubated with the mixture for 15 min at 37 °C.

To stop/suspend the reaction, Tris-HCl buffer 2 M (75 µL) was added to the reaction mixture. The concentrations of glucose released from the reaction mixtures were determined using glucose oxidase method.

The enzyme activity was quantified by measuring the absorbance at 490 nm in a microtiter plate reader (Bio-TEK, USA). Acarbose was used as a positive control.

All experiments were performed in triplicate and the percentage of enzyme inhibition was calculated using the following formula:

$$(\%)\ \text{inhibition} = [(AC - AS) / AC] \times 100,$$

where *AC* is the absorbance of the control and *AS* is the absorbance of the tested sample.

III-6-3. Enzyme kinetic assay:

To determine the inhibition mechanism of the flavonoids **1-10**, enzyme kinetic parameters should be determined.

III-6-3-1. Determination of the standard curve:

In order to correlate between the fact that *p*-NPG and different molecules absorb in different wavelengths, the absorbance of known dilutions (100-1000 µM) of *p*-nitrophenol was conducted with the spectrophotometer at 410 nm (Table 17).

From Figure 45, standard curve formula was determined as Y= 0.0123X; with Y: absorbance at 410 nm and X: *p*-nitrophenol concentration.

III-6-3-2. Calculation of $V_{max}$ and $K_m$ for enzyme and *p*-NPG

$V_{max}$ is the maximum rate of reaction for the enzyme and the substrate. $K_m$ is the specific enzyme constant of Michaelis equal to the concentration of substrate (sugar) that gives $V_{max}/2$.

These two basic kinetic parameters were obtained by conducting the following experiment: A series of tube was set up in which the enzyme amount is the same but the amount of *p*-NPG varies from 0.25 mM to 12 mM. In each tube, 3.5 mL of buffer was mixed with 0.5 mL of *p*-NPG at different concentration and 0.5 mL of enzyme stock solution.

The reaction was run for 30 min, stopped with $Na_2CO_3$ (0.1 M) and then the absorbance was measured with the spectrophotometer at 410 nm.

To obtain the velocity (*V*) of the reaction (Table 18), the approximate concentration (*S*) of the product, determined from the standard curve, was divided by the reaction duration:

$$V=S/\text{time (min)}$$

The effect of the different types of inhibitions can be graphically represented using Lineweaver-Burk plot (double reciprocal plot). This graph was obtained from the parameters (Table 19) determined by the velocity curve and it will be considered as the control for the following experiment (Figures 46 and 47).

III-6-3-3. Calculation of $V_{max}$ and $K_m$ for each sample:

From the basic kinetic parameters of enzyme/*p*-NPG reaction and following the same experimental process, the effect of the flavonoids on $V_{max}$ and $K_m$ was determined. Four possible types of inhibitions can occur:

- If $V_{max}$ decreases and $K_m$ may either be decreased or increased, the inhibition mode is classified as mixed one.
- If $V_{max}$ is unchanged and $K_m$ is increased with the increase of the substrate concentration, the inhibition is competitive.
- If $K_m$ is unchanged and $V_{max}$ decreases and cannot be overcome by increasing substrate concentration, the inhibition type is considered as a non-competitive.
- If $K_m$ and $V_{max}$ decrease both, the inhibition is uncompetitive.

Mode of inhibition was measured with increasing concentrations of *p*-NPG (0.25, 0.5, 1.0, 2.0, 4.0, 8.0, and 16.0 mM) as a substrate in the presence or absence of samples. Optimal amount of flavonoids **1**-**10** was determined based on the enzyme inhibitory activity assay. The inhibition mode was determined by Lineweaver-Burk (LB) plot analysis of the data calculated following Michaelis-Menten kinetics and Michealis equation:

$$V = V_{max}\,[S] / K_m + [S]$$

The *Ki* was calculated using Cheng Prusoff equation:

$$Ki = IC_{50} / (1 + [S] / K_m);$$

*Ki*: inhibition constant; S: concentration of substrate; $K_m$: Michaelis-Menten constant

III-6-4. Dissacharide assay

The α-glucosidase inhibition potential of the purified flavonoids **1**-**10** was measured at concentrations of 1, 10, and 100 μM, using disaccharide assay as follows: mammalian α-glucosidase was prepared by homogenizing 100 mg of rat intestinal acetone powder in 3 mL of 0.9% NaCl solution (5,000*g* x 30 min). The reaction mixture comprising from 50 μL of 0.1 M phosphate buffer (pH 6.8) and 10 μL of the sample at various concentrations was mixed with 35 μL of maltose solution (5 mM) for maltase inhibition test, and 20 μL of sucrose (56 mM) for sucrase inhibition test. After pre-incubation for 5 min at 37°C, the enzyme solution

was added, 20 µL in case of sucrase inhibition assay and 5 µL for maltase inhibition assay, and incubated with the mixture for 15 min at 37 °C. To stop/suspend the reaction, 2 M Tris-HCl buffer (75 µL) was added to the reaction mixture. The concentrations of glucose released from the reaction mixtures were determined using glucose oxidase method. The enzyme activity was quantified by measuring the absorbance at 490 nm in a microtiter plate reader (Bio-TEK, USA). Acarbose was used as a positive control. All experiments were performed in triplicate and the percentages of enzyme inhibition was calculated using the following formula:

$$(\%)\ \text{inhibition} = [(AC - AS) / AC] \times 100,$$

where *AC* is the absorbance of the control and *AS* is the absorbance of the tested sample.

III-6-5- Synergistic effect assay.

The synergistic potential of the purified flavonoids **2**-**10** was measured at concentrations of 1 µM, using disaccharide assay as follows: mammalian α-glucosidase was prepared by homogenizing 100 mg of rat intestinal acetone powder in 3 mL of 0.9% NaCl solution (5,000*g* x 30 min). Acarbose was combined with and without flavonoids **2**-**10**.

In case of maltase activity test, acarbose was added at the concentration of 0.5 µM and for the sucrase activity assay, acarbose was added at the concentration of 3.12 µM.

For this reaction, since flavonoids **2**-**10** were dissolved in MeOH, 10µL of dissolved acarbose was first of all added to appropriate wells and after that the MeOH was evaporated from each well, where the substances will be added as a following step, to obtain at the end the same volume of MeOH in all the wells.

After evaporating the solvent of acarbose, the reaction mixture comprising from 50 µL of 0.1 M phosphate buffer (pH 6.8) and 10 µL of the sample at 1 µM was mixed with 35 µL of maltose solution (5 mM) for maltase inhibition test, and 20 µL of sucrose (56 mM) for sucrase inhibition test.

Once pre-incubation for 5 min at 37°C ended, the enzyme solution was added, 20 µL in case of sucrase inhibition assay and 5 µL for maltase inhibition assay, and incubated with the mixture for 15 min at 37°C. To stop/suspend the reaction, 2 M Tris-HCl buffer (75 µL) was added to the reaction mixture.

The concentrations of glucose released from the reaction mixtures were determined using glucose oxidase method. The enzyme activity was quantified by measuring the absorbance at 490 nm in a microtiter plate reader (Bio-TEK, USA).

Acarbose was used as a positive control. All experiments were performed in triplicate and the percentage of enzyme inhibition was calculated using the following formula:

$$(\%)\ \text{inhibition} = [(AC - AS) / AC] \times 100,$$

where *AC* is the absorbance of the control and *AS* is the absorbance of the tested sample.

III-6-6. Statistical analysis.

Data were expressed as means ± S.E.M. Statistical analysis was performed by Student's t test. *p*-values were considered to be statistically significant as follow: $*p < 0.05$; $** p < 0.01$; $*** p < 0.001$ compared with acarbose.

Table 4. $IC_{50}$ values of compounds **1**-**10**.

| Substances | $IC_{50}$ (μM) |
|---|---|
| naringenin (**1**) | 180.2 ± 1.7 |
| quercetin (**2**) | 114.6 ± 1.9 |
| rhamnetin (**3**) | 94.6 ± 4.1 |
| rhamnazin (**4**) | > 200 |
| tamarixetin (**5**) | 190.0 ± 0.5 |
| kaempferol (**6**) | 122.1 ± 3.2 |
| QGlcA (**7**) | 76.1 ± 2.2 |
| QGlcA-Me (**8**) | 62.3 ± 2.9 |
| KGlcA (**9**) | 89.7 ± 3.7 |
| KGlcA-Me (**10**) | 75.3 ± 1.5 |
| Acarbose | 95.1 ± 1.4 |

Table 5. Kinetic parameter of naringenin **1**.

| | Control (without inhibitor) | Substrate concentration | |
|---|---|---|---|
| | | 64 µg/mL | 16 µg/mL |
| $K_m$ | 2.75 | 5.90 | 4.00 |
| $V_{max}$ | 5.07 | 5.07 | 5.07 |
| $K_m/V_{max}$ | 0.54 | 1.16 | 0.78 |
| $(-1/K_m)$ | -0.36 | -0.17 | -0.25 |
| $1/V_{max}$ | 0.19 | 0.19 | 0.19 |

Table 6. Kinetic parameter of quercetin **2**.

| | Control (without inhibitor) | Substrate concentration | |
|---|---|---|---|
| | | 16 µg/mL | 64 µg/mL |
| $K_m$ | 2.75 | 2.00 | 3.50 |
| $V_{max}$ | 5.07 | 1.30 | 3.00 |
| $K_m/V_{max}$ | 0.54 | 1.54 | 1.17 |
| $(-1/K_m)$ | -0.36 | -0.50 | -0.28 |
| $1/V_{max}$ | 0.19 | 0.77 | 0.33 |

Table 7. Kinetic parameter of rhamnetin **3**.

| | Control (without inhibitor) | Substrate concentration | |
|---|---|---|---|
| | | 64 µg/mL | 16 µg/mL |
| $K_m$ | 2.75 | 1.90 | 0.50 |
| $V_{max}$ | 5.07 | 5.06 | 3.00 |
| $K_m/V_{max}$ | 0.54 | 0.37 | 0.17 |
| $(-1/K_m)$ | -0.36 | -0.53 | -2.00 |
| $1/V_{max}$ | 0.19 | 0.19 | 0.33 |

Table 8. Kinetic parameter of rhamnazin **4**.

| | Control (without inhibitor) | Substrate concentration | |
|---|---|---|---|
| | | 64 µg/mL | 16 µg/mL |
| $K_m$ | 2.75 | 2.10 | 1.90 |
| $V_{max}$ | 5.07 | 4.54 | 2.71 |
| $K_m/V_{max}$ | 0.54 | 0.46 | 0.70 |
| $(-1/K_m)$ | -0.36 | -0.47 | -0.53 |
| $1/V_{max}$ | 0.19 | 0.22 | 0.37 |

Table 9. Kinetic parameter of tamarixetin **5**.

| | Control (without inhibitor) | Substrate concentration | |
|---|---|---|---|
| | | 64 µg/mL | 16 µg/mL |
| $K_m$ | 2.75 | 2.10 | 1.90 |
| $V_{max}$ | 5.07 | 3.44 | 2.71 |
| $K_m/V_{max}$ | 0.54 | 0.61 | 0.70 |
| $(-1/K_m)$ | -0.36 | -0.47 | -0.52 |
| $1/V_{max}$ | 0.19 | 0.29 | 0.36 |

Table 10. Kinetic parameter of kaempferol **6**.

| | Control (without inhibitor) | Substrate concentration | |
|---|---|---|---|
| | | 64 µg/mL | 16 µg/mL |
| $K_m$ | 2.75 | 2.10 | 1.90 |
| $V_{max}$ | 5.07 | 3.44 | 2.71 |
| $K_m/V_{max}$ | 0.54 | 0.61 | 0.70 |
| $(-1/K_m)$ | -0.36 | -0.47 | -0.53 |
| $1/V_{max}$ | 0.19 | 0.29 | 0.37 |

-

Table 11. Kinetic parameter of QGlcA **7**.

| | Control (without inhibitor) | Substrate concentration | |
|---|---|---|---|
| | | 64 µg/mL | 16 µg/mL |
| $K_m$ | 2.75 | 2.75 | 2.75 |
| $V_{max}$ | 5.07 | 4.31 | 2.46 |
| $K_m/V_{max}$ | 0.54 | 0.64 | 1.12 |
| $(-1/K_m)$ | -0.36 | -0.36 | -0.36 |
| $1/V_{max}$ | 0.19 | 0.23 | 0.41 |

-

Table 12. Kinetic parameter of QGlcA-Me **8**.

| | Control (without inhibitor) | Substrate concentration | |
|---|---|---|---|
| | | 64 µg/mL | 16 µg/mL |
| $K_m$ | 2.75 | 2.75 | 2.75 |
| $V_{max}$ | 5.07 | 4.09 | 1.31 |
| $K_m/V_{max}$ | 0.54 | 0.67 | 2.09 |
| $(-1/K_m)$ | -0.36 | -0.36 | -0.36 |
| $1/V_{max}$ | 0.19 | 0.24 | 0.76 |

Table 13. Kinetic parameter of KGlcA **9**.

| | Control (without inhibitor) | Substrate concentration | |
|---|---|---|---|
| | | 64 μg/mL | 16 μg/mL |
| $K_m$ | 2.75 | 2.75 | 2.75 |
| $V_{max}$ | 5.07 | 4.10 | 3.20 |
| $K_m/V_{max}$ | 0.54 | 0.67 | 0.85 |
| $(-1/K_m)$ | -0.36 | -0.36 | -0.36 |
| $1/V_{max}$ | 0.19 | 0.24 | 0.31 |

Table 14. Kinetic parameter of KGlcA-Me **10**.

| | Control (without inhibitor) | Substrate concentration | |
|---|---|---|---|
| | | 64 μg/mL | 16 μg/mL |
| $K_m$ | 2.75 | 2.75 | 2.75 |
| $V_{max}$ | 5.07 | 4.10 | 2.31 |
| $K_m/V_{max}$ | 0.54 | 0.67 | 1.19 |
| $(-1/K_m)$ | -0.36 | -0.36 | -0.36 |
| $1/V_{max}$ | 0.19 | 0.24 | 0.43 |

Table 15. Kinetic parameters and inhibition mode.

| Substances | *Ki* (μM) | 1/*Ki* ($\mu M^{-1}$) | Inhibition mode |
|---|---|---|---|
| naringenin (**1**) | 149 | 0.0069 | Competitive |
| quercetin (**2**) | 80.1 | 0.0125 | Mixed |
| rhamnetin (**3**) | 51.7 | 0.0193 | Mixed |
| rhamnazin (**4**) | 118.0 | 0.0084 | Mixed |
| tamarixetin (**5**) | 92.7 | 0.0107 | Mixed |
| kaempferol (**6**) | 81.4 | 0.0123 | Mixed |
| QGlcA (**7**) | 55.3 | 0.0181 | Non-competitive |
| QGlcA-Me (**8**) | 45.8 | 0.0218 | Non-competitive |
| KGlcA (**9**) | 65.9 | 0.0152 | Non-competitive |
| KGlcA-Me (**10**) | 55.4 | 0.0180 | Non-competitive |

Table 16. Specificity of flavonoids **1**-**10** for sucrase and maltase inhibitory activities.

| Substances | α-Glucosidase inhibition (%) | | | | | |
|---|---|---|---|---|---|---|
| | Sucrase activity | | | Maltase activity | | |
| | 1 μM | 10 μM | 100 μM | 1 μM | 10 μM | 100 μM |
| **1** | 0.5 ± 2.5 | 5.9 ± 1.8 | 12.8 ± 2.6 | 4.7 ± 1.6 | 46.8 ± 0.5 | 71.8 ± 1.9 |
| **2** | 0.2 ± 1.1 | 15.7 ± 1.3 | 21.8 ± 0.5 | 3.7 ± 1.1 | 16.9 ± 0.3 | 20.2 ± 1.5 |
| **3** | 0.0 ± 2.8 | 24.9 ± 1.3 | 29.5 ± 0.5 | 8.5 ± 1.5 | 16.5 ± 2.3 | 23.7 ± 1.2 |
| **4** | 0.1 ± 0.5 | 10.7 ± 1.9 | 17.5 ± 0.4 | 5.1 ± 0.2 | 17.0 ± 1.9 | 19.6 ± 1.7 |
| **5** | 0.0 ± 1.8 | 12.9 ± 2.3 | 20.9 ± 1.2 | 7.5 ± 2.3 | 13.5 ± 1.3 | 20.7 ± 0.2 |
| **6** | 1.0 ± 1.2 | 4.6 ± 2.5 | 9.2 ± 0.5 | 4.6 ± 0.3 | 12.0 ± 1.6 | 19.1 ± 0.5 |
| **7** | 2.4 ± 2.5 | 20.0 ± 2.8 | 27.8 ± 0.5 | 4.1 ± 1.0 | 1.5 ± 1.6 | 62.0 ± 0.1 |
| **8** | 2.2 ± 1.8 | 28.6 ± 0.1 | 30.9 ± 2.2 | 8.3 ± 1.5 | 18.9 ± 1.6 | 75.3 ± 0.5 |
| **9** | 1.8 ± 0.5 | 3.0 ± 2.5 | 11.2 ± 1.5 | 4.9 ± 0.4 | 21.4 ± 0.9 | 31.7 ± 1.1 |
| **10** | 2.5 ± 1.0 | 11.7 ± 2.6 | 16.7 ± 1.3 | 8.4 ± 1.3 | 15.2 ± 0.6 | 33.5 ± 1.1 |
| Acarbose | 32.8 ± 1.5 | 33.3 ± 1.8 | 56.1 ± 0.6 | 6.1 ± 1.4 | 23.9 ± 0.9 | 62.5 ± 0.5 |

Table17. *p*-Nitrophenol absorbance at different concentration.

| *p*-nitrophenol (µM) | Absorbance average | Erreur | Corrected absorbance |
|---|---|---|---|
| 0 | 0.0540 | 0.0509 | - |
| 1000 | 0.1966 | 0.1325 | 0.1420 |
| 900 | 0.1818 | 0.2045 | 0.1278 |
| 800 | 0.1676 | 0.1222 | 0.1136 |
| 700 | 0.1534 | 0.1054 | 0.0994 |
| 600 | 0.1392 | 0.0919 | 0.0852 |
| 500 | 0.1250 | 0.0708 | 0.0710 |
| 400 | 0.1108 | 0.0658 | 0.0568 |
| 300 | 0.1489 | 0.0523 | 0.0426 |
| 200 | 0.0966 | 0.0397 | 0.0284 |
| 100 | 0.0908 | 0.0226 | 0.0142 |

Table 18. Determination of the velocity (*V*).

| [*S*] (mM) | absorbance of the reaction product | concentration of the product (μM) | Velocity (*V*) (μM/min) |
|---|---|---|---|
| 0.25 | 0.0660 | 5.3672 | 0.1789 |
| 0.5 | 0.1965 | 15.9810 | 0.5327 |
| 1 | 0.3408 | 27.7073 | 0.9235 |
| 2 | 0.6622 | 53.8373 | 1.7945 |
| 4 | 1.2555 | 102.0691 | 3.4023 |
| 8 | 1.7528 | 142.5081 | 4.7502 |
| 16 | 1.7934 | 145.8081 | 4.8602 |

Table 19. Kinetic parameters determined from the velocity curve.

| | |
|---|---|
| $K_m$ | 2.75 |
| $V_{max}$ | 5.07 |
| $K_m/V_{max}$ | 0.54 |
| $(-1/K_m)$ | -0.36 |
| $1/V_{max}$ | 0.19 |

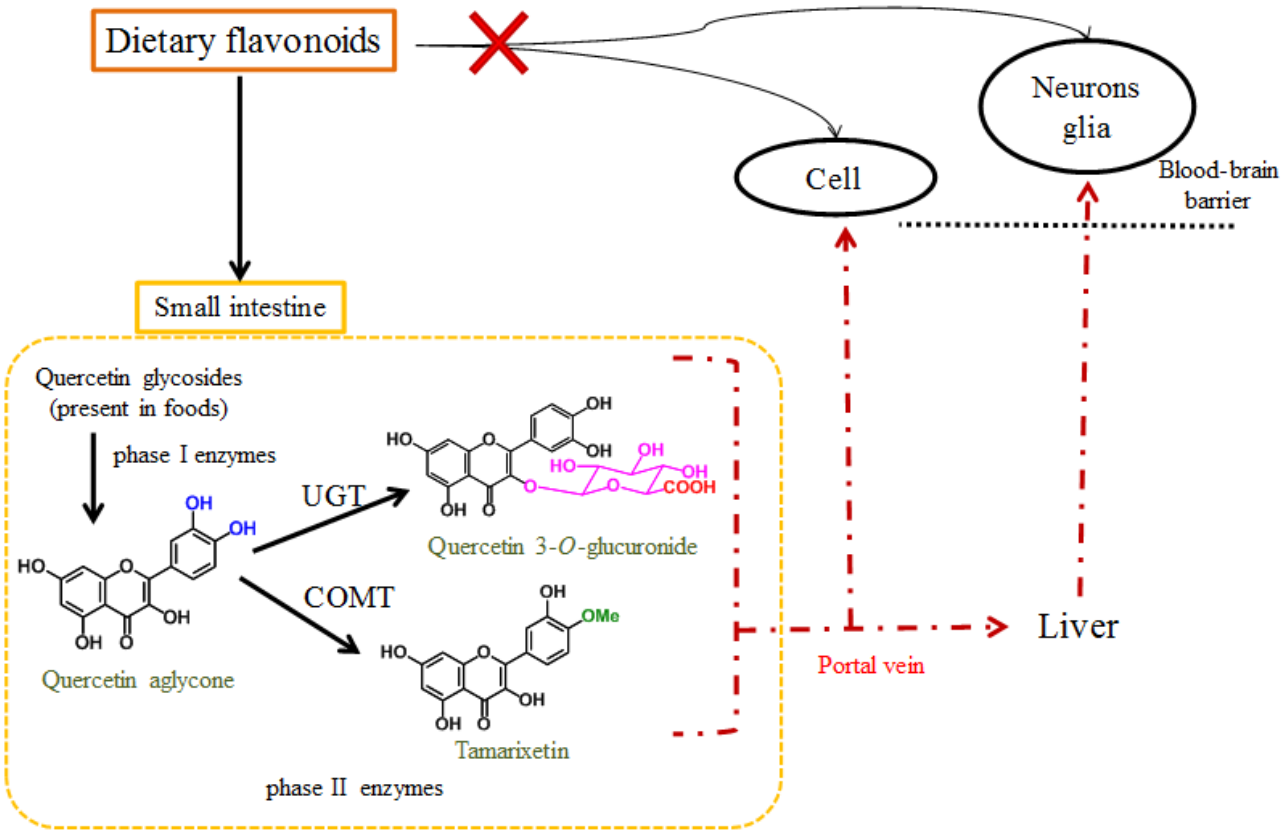


Figure 19. Simplified schematic representing one step of human flavonoid metabolism. Ingested flavonoids undergo extensive intestinal metabolism. Metabolites are then transported to the liver *via* hepatic portal vein and undergo further metabolism. The liver metabolites can be transported to targeted cells and tissues.

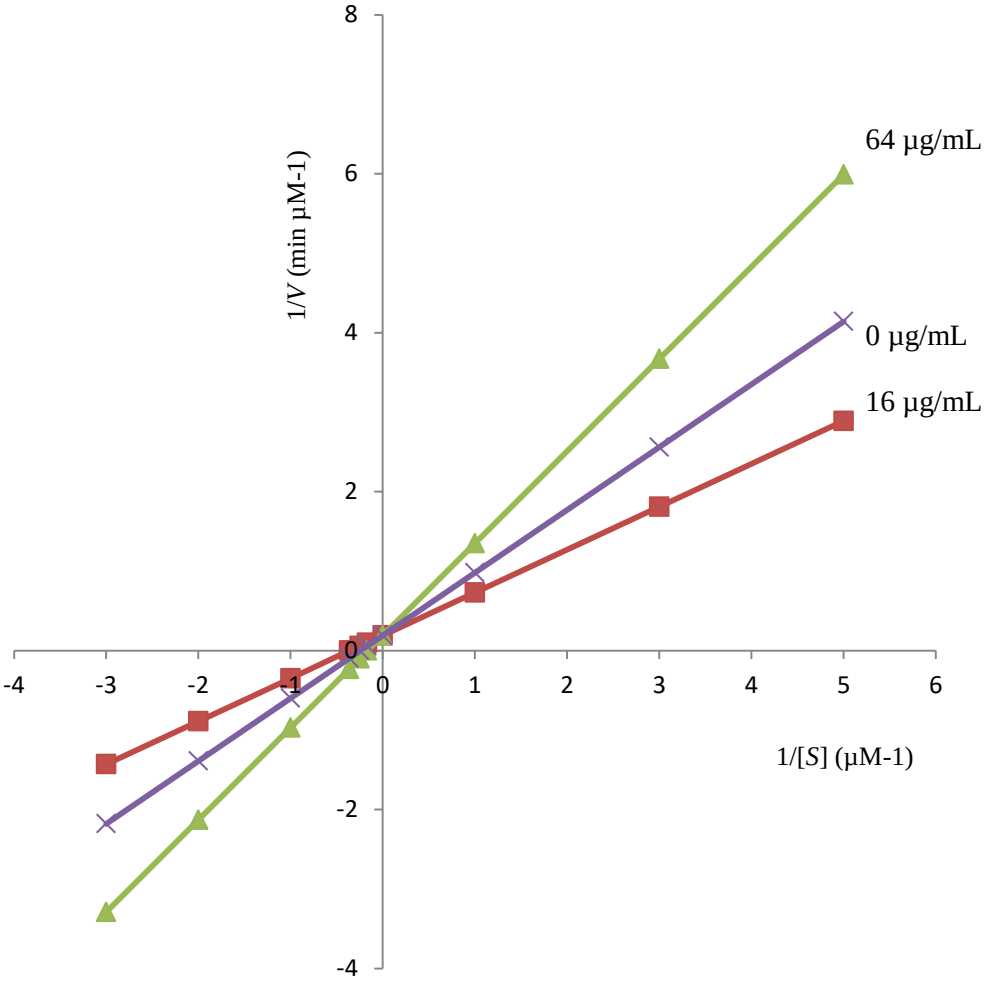


Figure 20. Lineweaver-Burk plot graph of naringenin **1**.

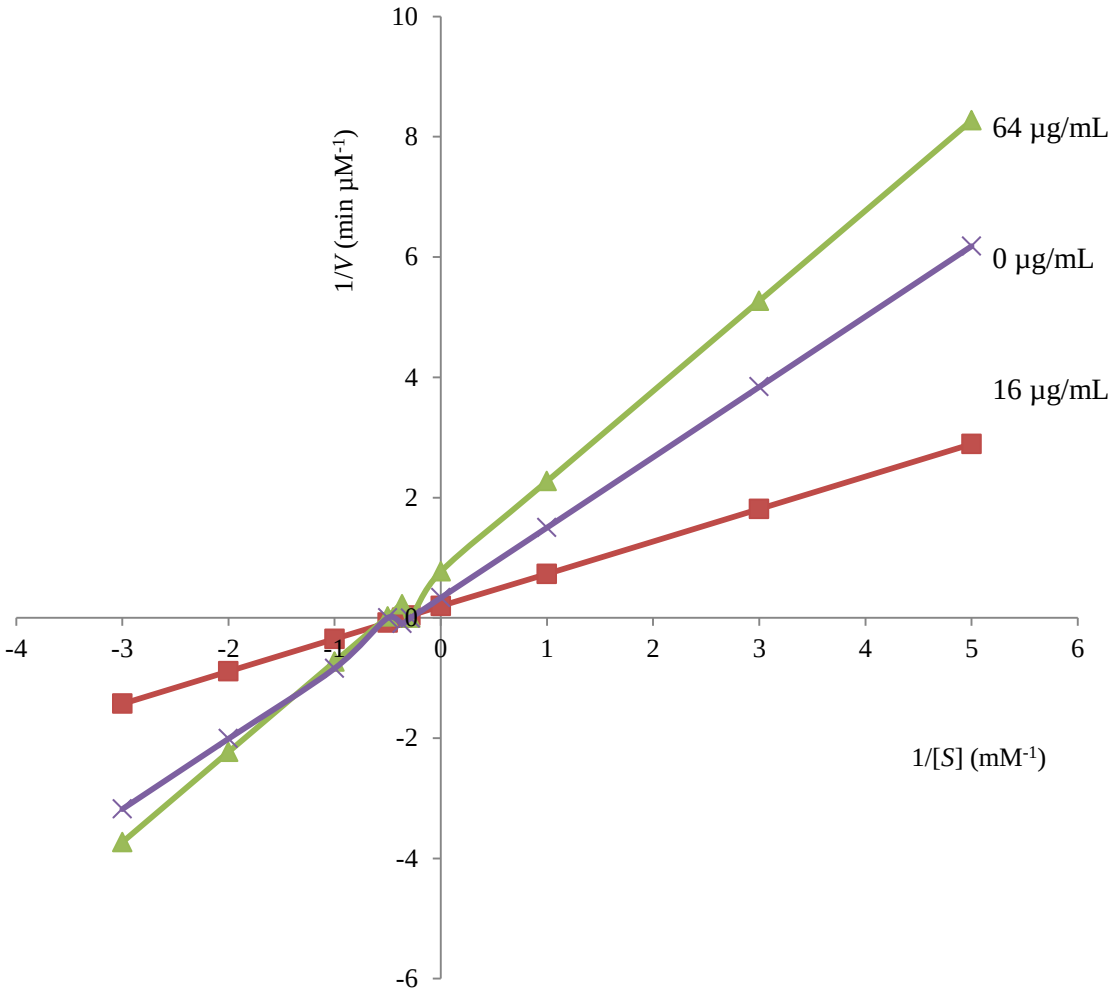


Figure 21. Lineweaver-Burk plot graph of quercetin **2**.

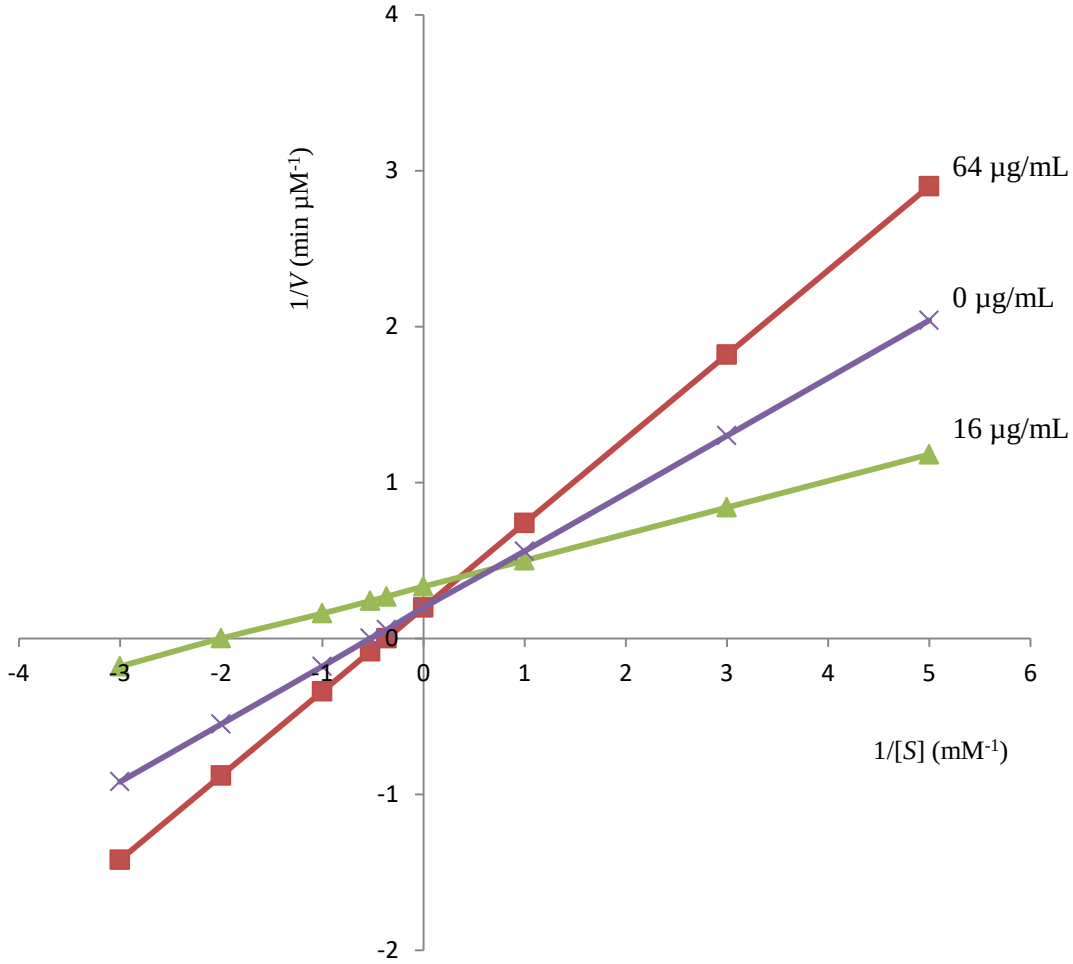


Figure 22. Lineweaver-Burk plot graph of rhamnetin **3**.

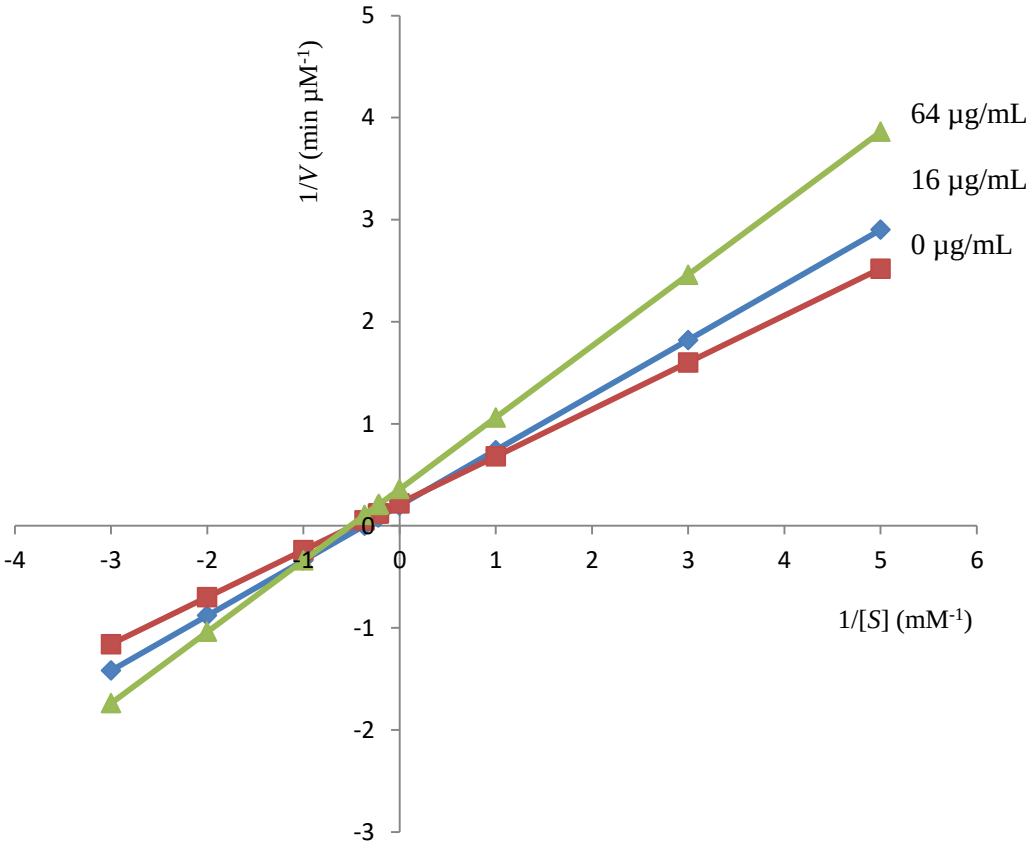


Figure 23. Lineweaver-Burk plot graph of rhamnazin **4**.

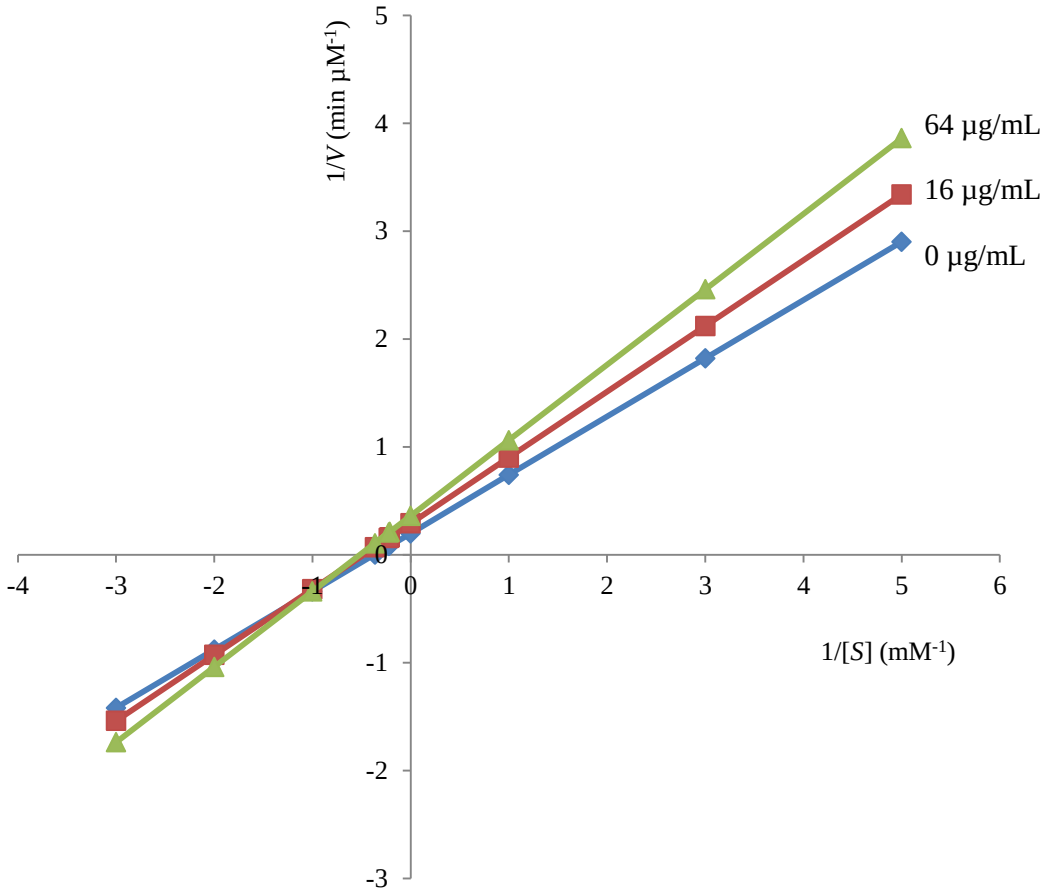


Figure 24. Lineweaver-Burk plot graph of tamarixetin **5**.

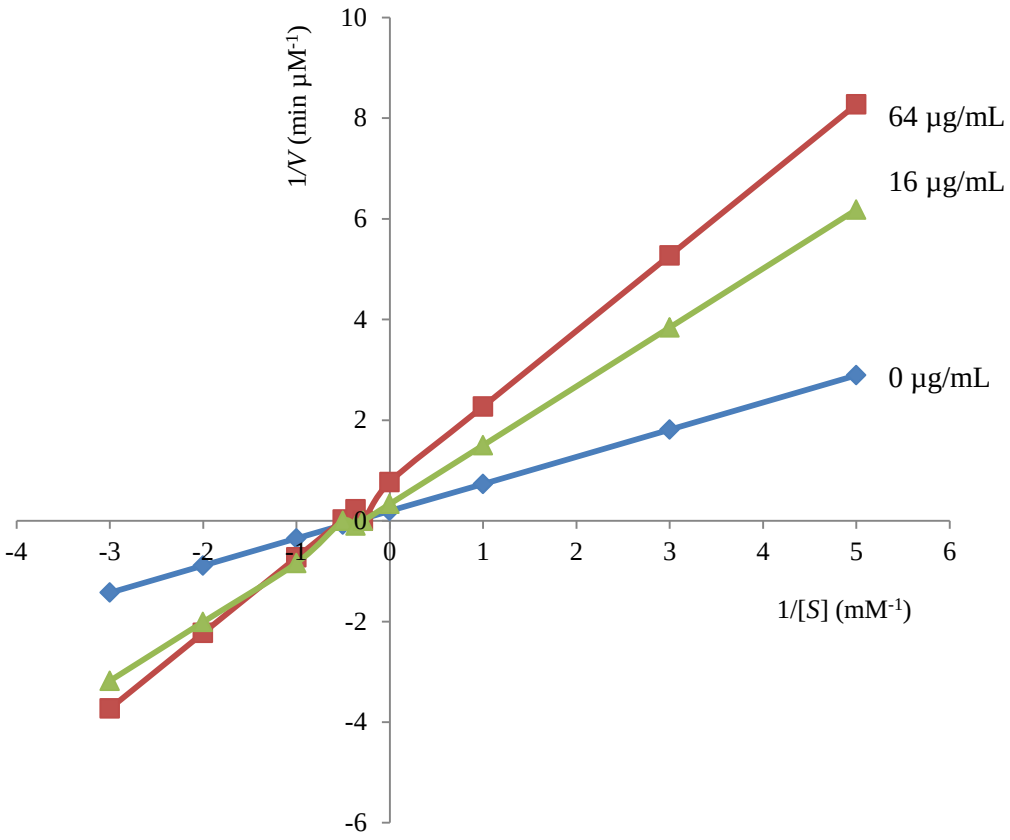


Figure 25. Lineweaver-Burk plot graph of kaempferol **6**.

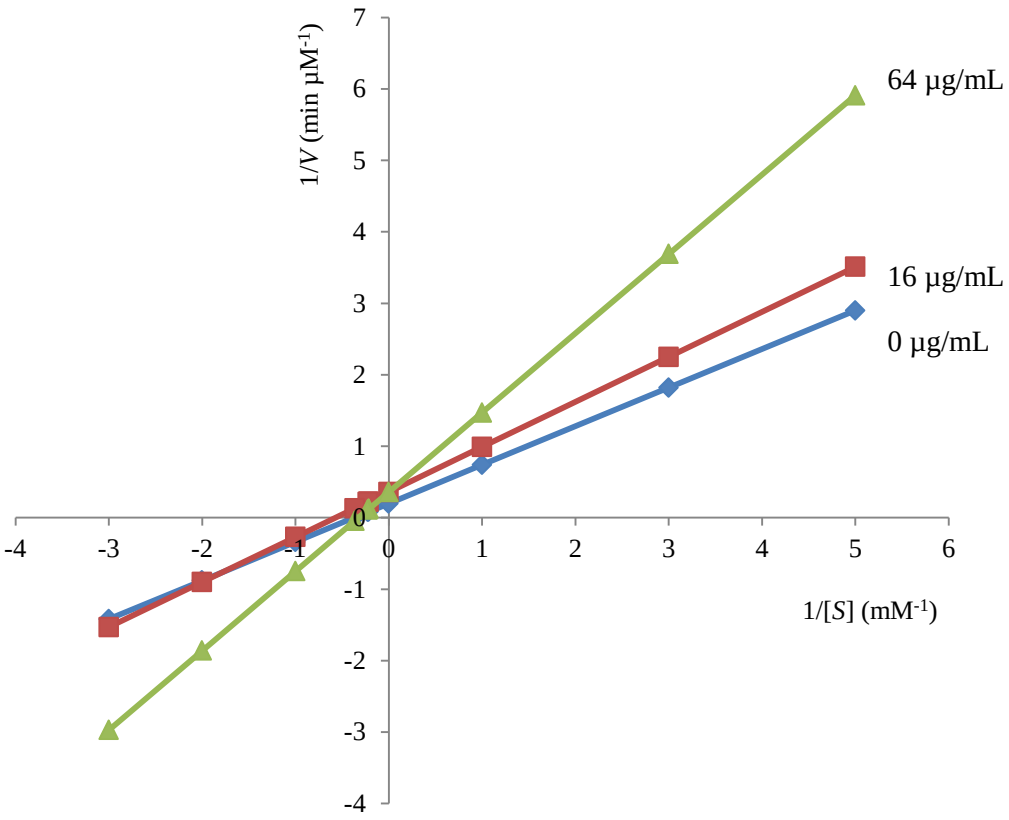


Figure 26. Lineweaver-Burk plot graph of QGlcA **7**.

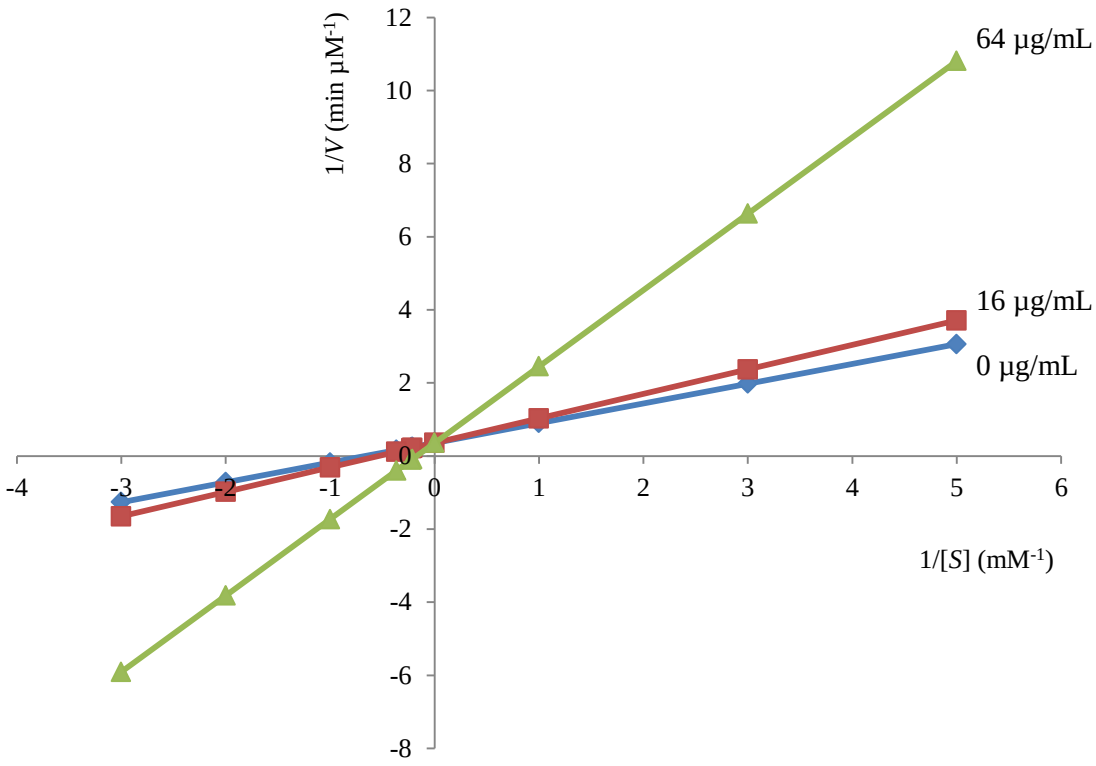


Figure 27. Lineweaver-Burk plot graph of QGlcA-Me **8**.

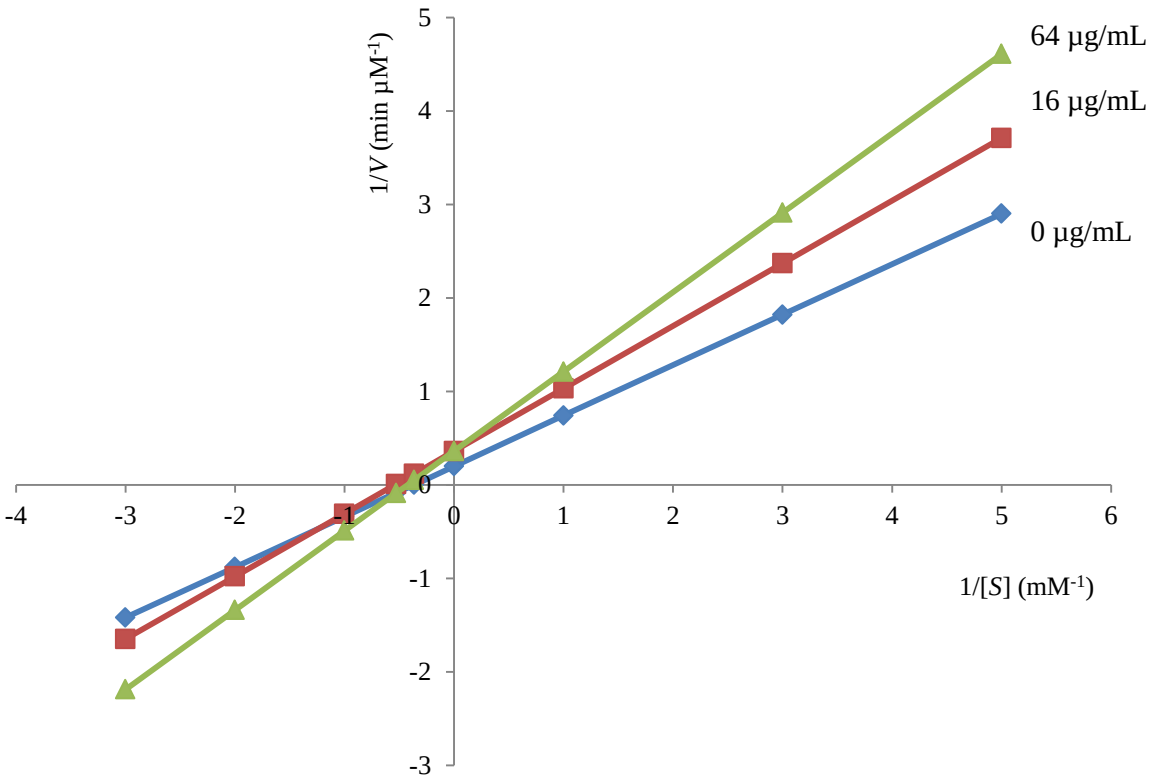


Figure 28. Lineweaver-Burk plot graph of KGlcA **9**.

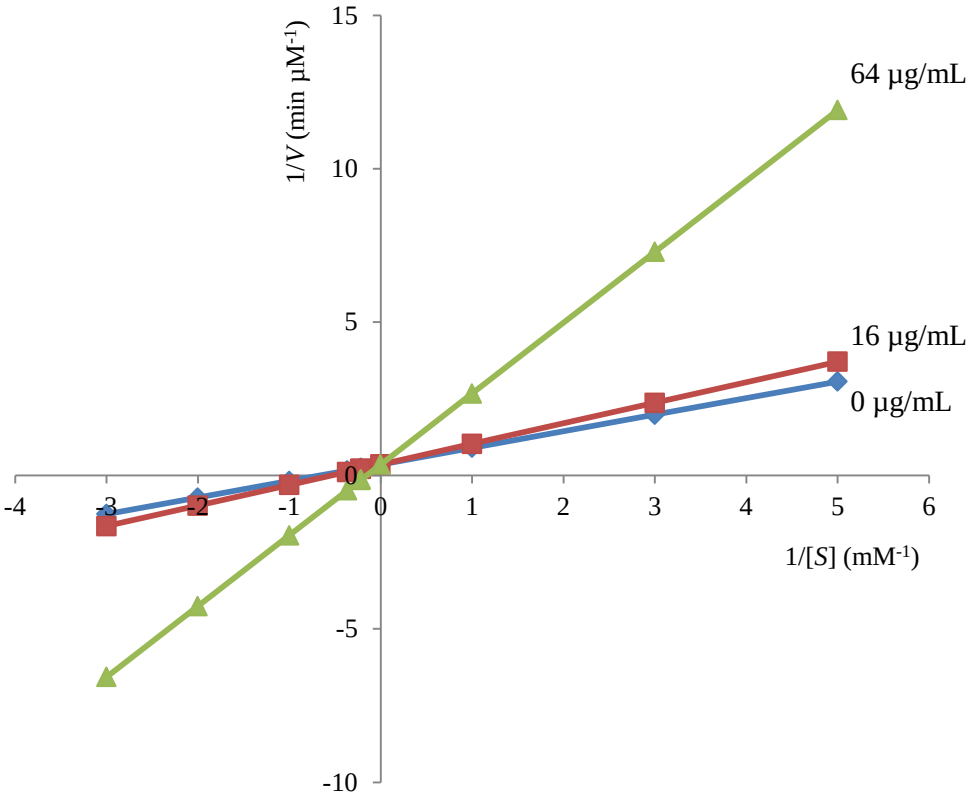


Figure 29. Lineweaver-Burk plot graph of KGlcA-Me **10**.

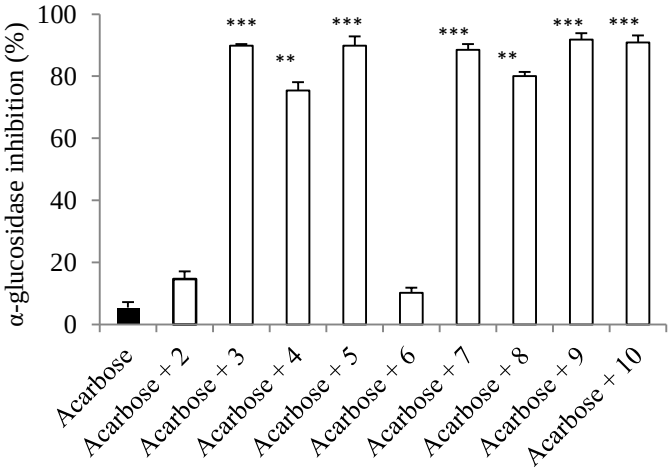


Figure 30. The combined effect of acarbose and flavonoids **2**-**10** on intestinal maltase inhibition; results expresses as means ± S.E.M.; n=3; *$p < 0.05$; ** $p < 0.01$; *** $p < 0.001$ compared with acarbose (0.5 μM).

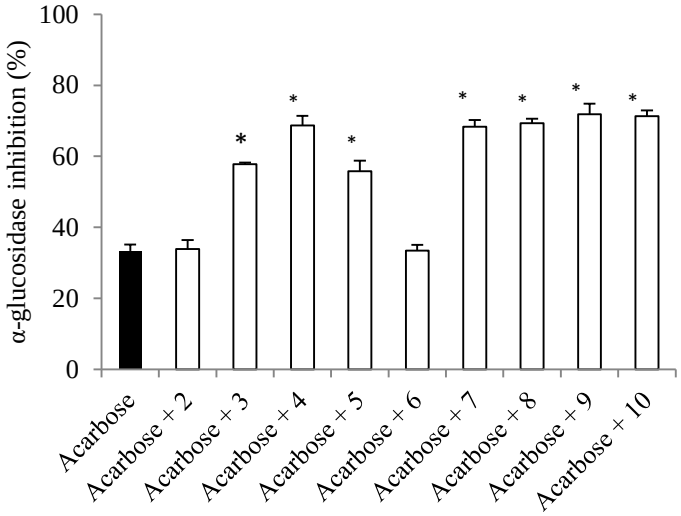


Figure 31. The combined effect of acarbose and flavonoids **2**-**10** on intestinal sucrase inhibition; results expresses as means ± S.E.M.; n=3. *$p < 0.05$; ** $p < 0.01$; *** $p < 0.001$ compared with acarbose (3.14 μM).

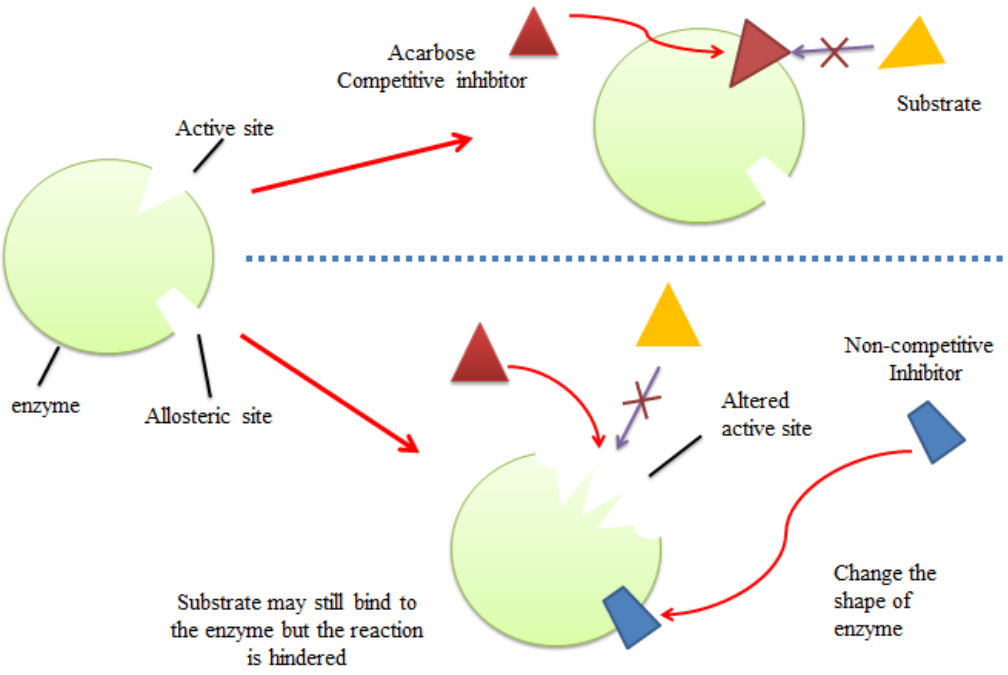


Figure 32. Proposed mechanism for the synergistic effect of flavonoids **7-10** (non-competitive inhibition).

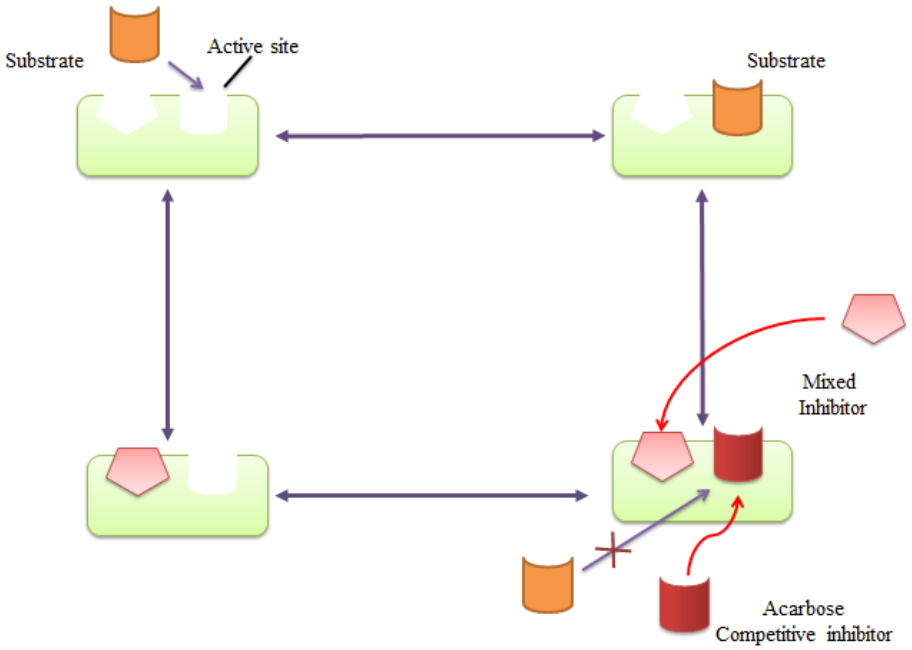


Figure 33. Proposed mechanism for the synergistic effect of flavonoids **3**-**5** (mixed inhibition)

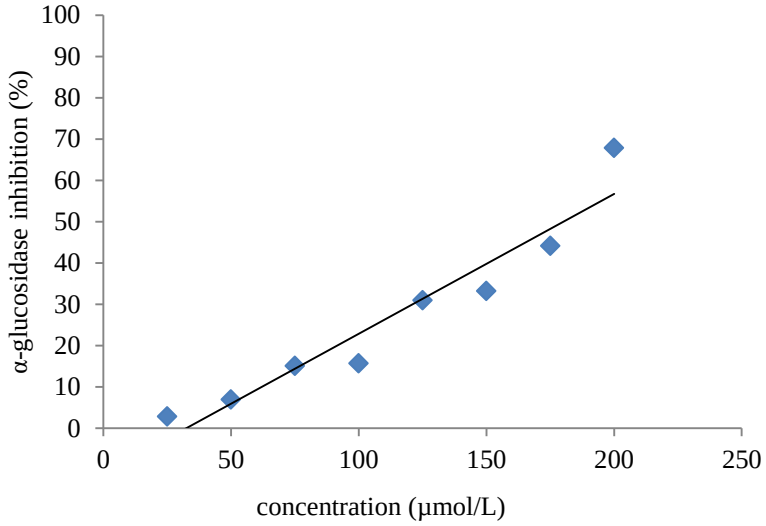


Tendency curve formula: Y = 0.338 X – 11.017

Figure 34. α-Glucosidase inhibition activity of naringenin (**1**).

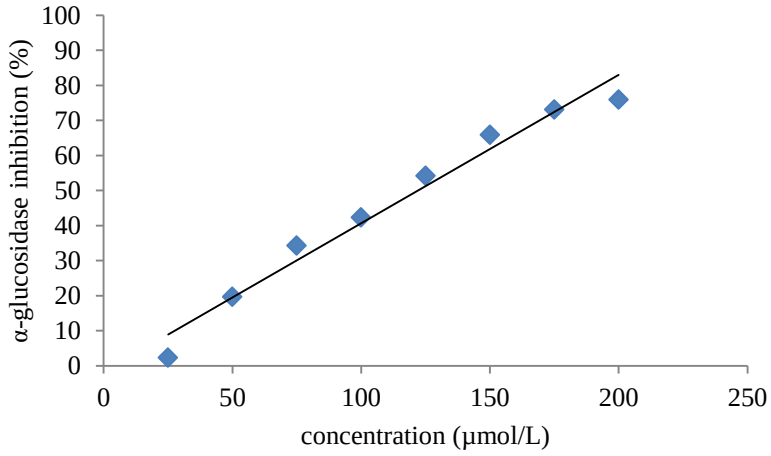


Tendency curve formula: Y = 0.424 X – 1.702

Figure 35. α-Glucosidase inhibition activity of kaempferol (**6**).

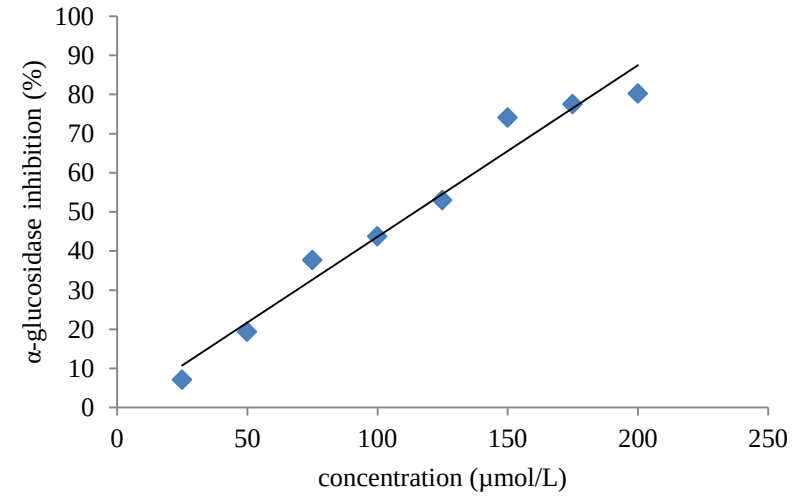


Tendency curve formula: Y = 0.438 X – 0.215

Figure 36. α-Glucosidase inhibition activity of quercetin (**2**).

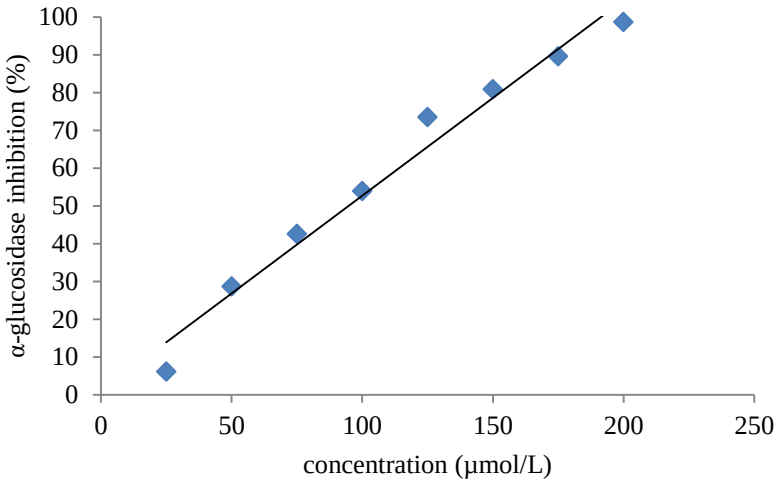


Tendency curve formula: Y = 0.517 X + 1.054

Figure 37. α-Glucosidase inhibition activity of rhamnetin (**3**).

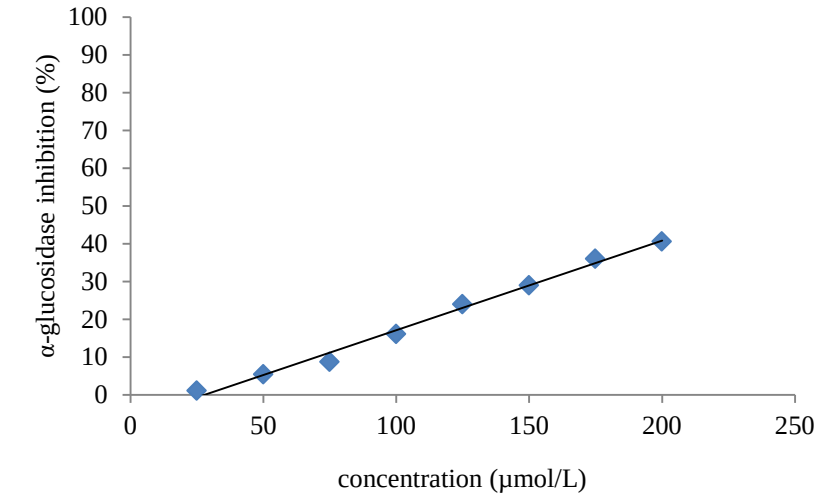


Tendency curve formula: Y = 0.2373 X – 6.594

Figure 38. α-Glucosidase inhibition activity of rhamnezin (**4**).

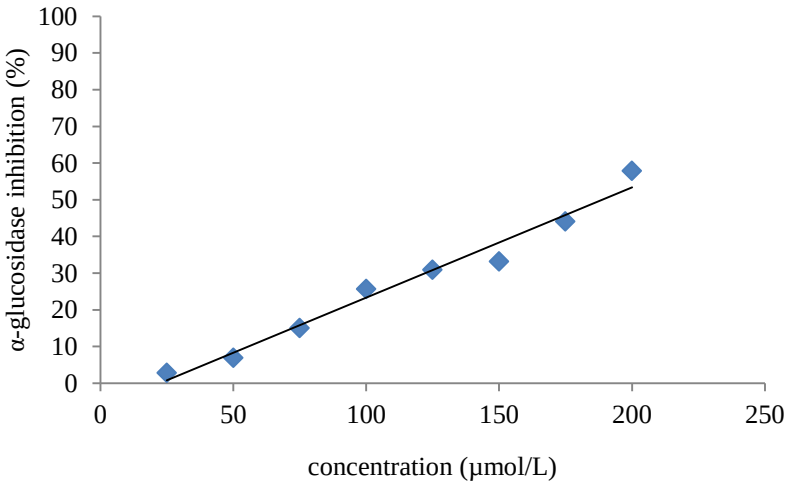


Tendency curve formula: Y = 0.301 X – 7.095

Figure 39. α-Glucosidase inhibition activity of tamarixetin (**5**).

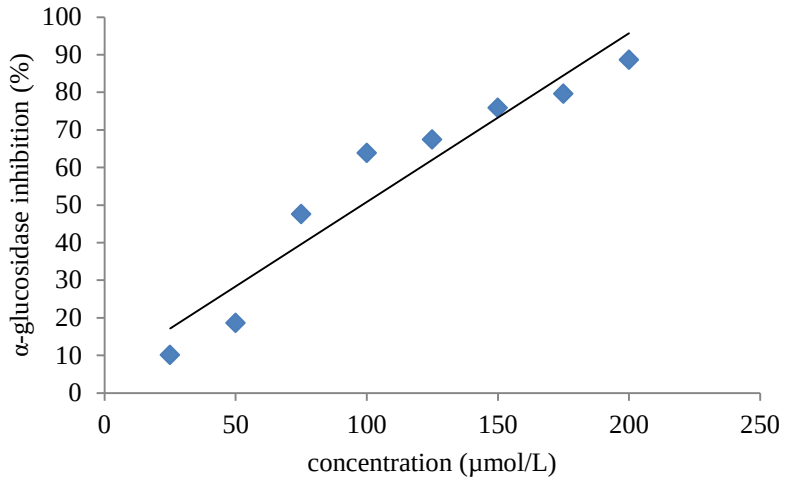


Tendency curve formula: Y = 0.517 X + 10.626

Figure 40. α-Glucosidase inhibition activity of QGlcA (**7**).

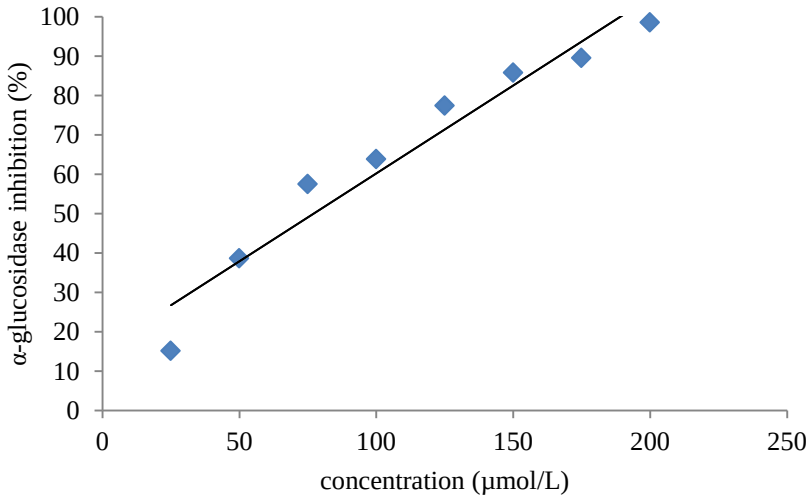


Tendency curve formula: Y = 0.446 X + 22.189

Figure 41. α-Glucosidase inhibition activity of QGlcA-Me (**8**).

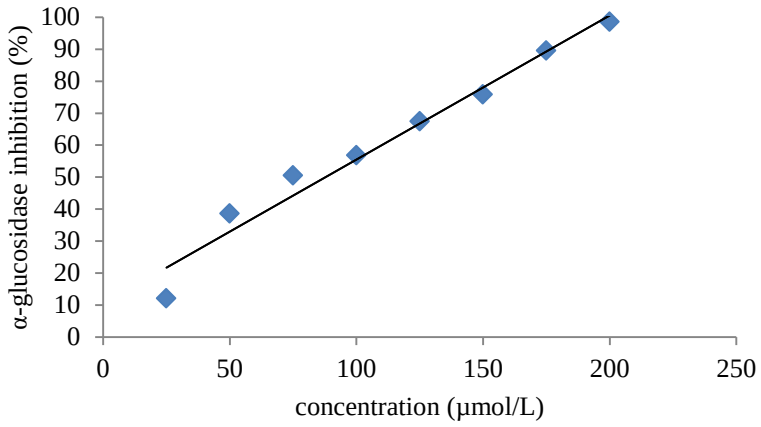


Tendency curve formula: Y = 0.451 X + 9.572

Figure 42. α-Glucosidase inhibition activity of KGlcA (**9**).

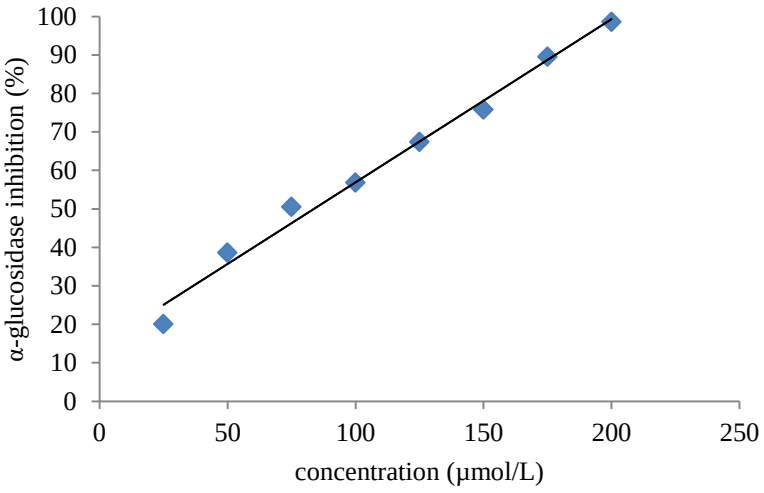


Tendency curve formula: Y = 0.424 X + 18.073

Figure 43. α-Glucosidase inhibition activity of KGlcA-Me (**10**).

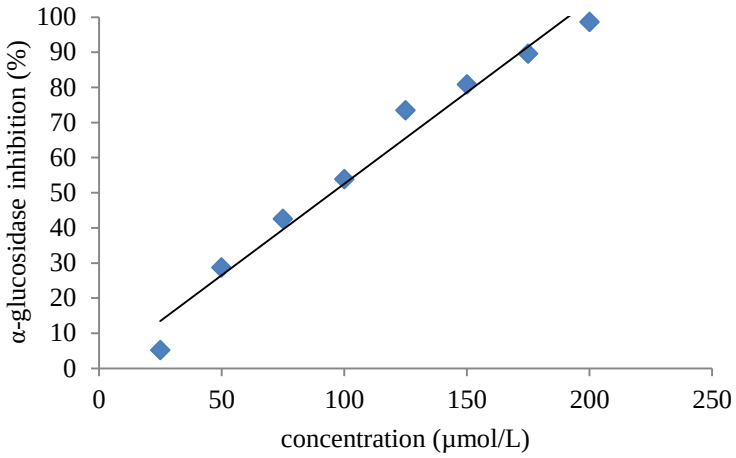


Tendency curve formula: Y = 0.5207 X + 0.48143

Figure 44. α-Glucosidase inhibition activity of acarbose (positive control).

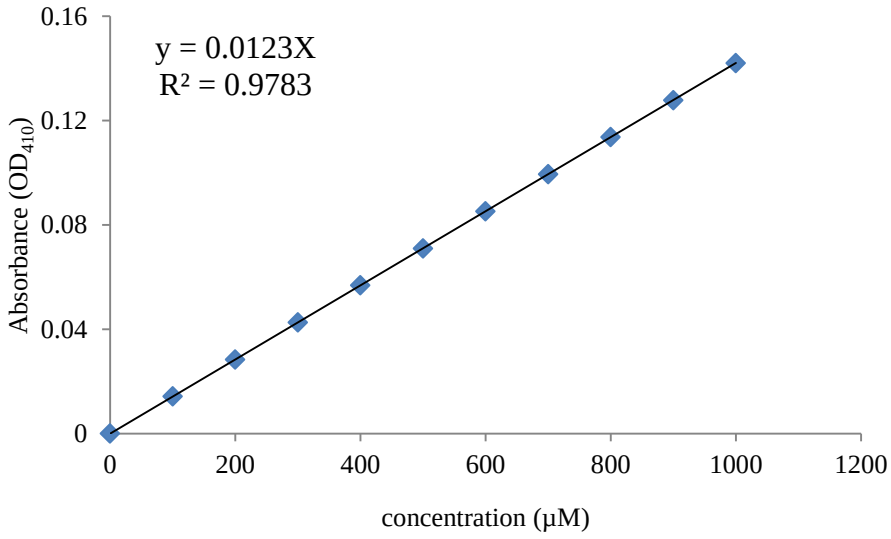


Figure 45. Standard curve of *p*-nitrophenol.

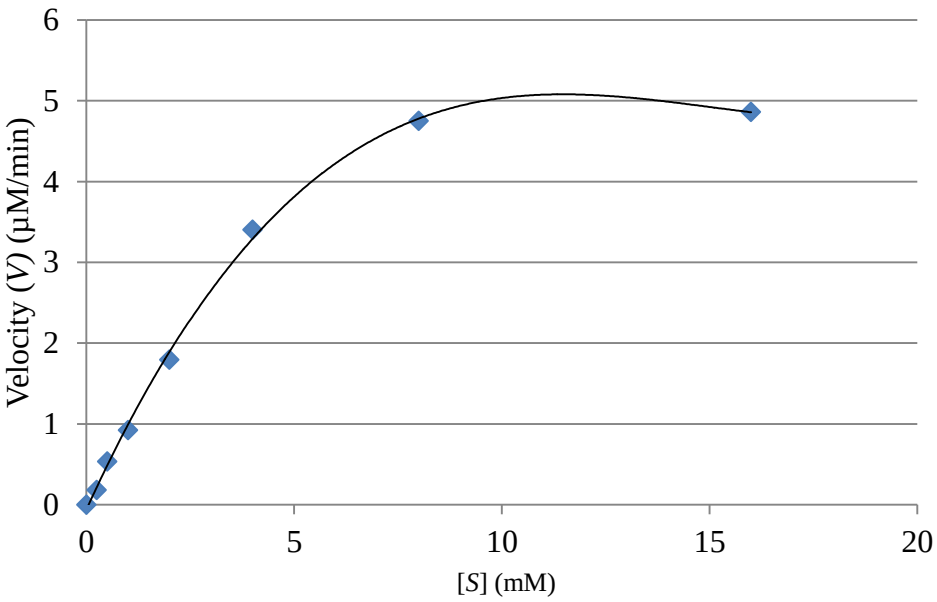


$$Y = 0.0018\ X^3 - 0.0796\ X^2 + 1.1288\ X - 0.0628$$

Figure 46. Velocity curve of substrate-enzyme reaction.

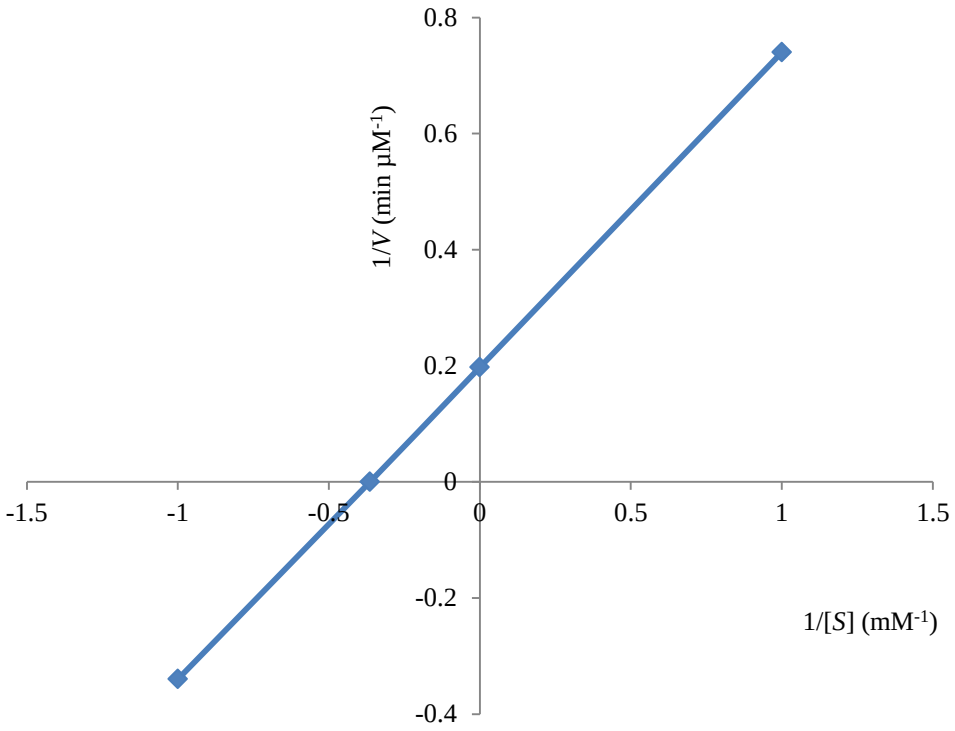


Figure 47. Lineweaver-Burk plot graph (reference graph).

*Chapter IV*

# Effect of flavonoids **1-10** towards amyloid aggregation related to diabetes and Alzheimer's diseases

## **IV-1.** Introduction

Amyloid aggregation has become the subject of rapidly increasing research activities across a wide range of scientific disciplines. Such activities have been stimulated by the association of amyloid deposition with a range of debilitating medical disorders, from T2D to AD, many of which are major threats to human health and welfare in the modern world[54].

The amyloid state of a protein is a highly ordered form of aggregate in which the polypeptide chains adopt a fibrillary structure, which is capable of self-replication, for example through secondary processes. Amyloid fibrils are rich in β-sheet structure and typically form from unfolded or partially unfolded conformations of proteins and peptides, some of which are fragments of larger proteins. The amyloid state is 'generic' in that its characteristic architecture is not encoded by specific amino acid sequences[55].

The aim of this chapter is to investigate the protective effect of flavonoids **1-10** from *T. gallica* towards hIAPP and Aβ aggregation inhibitors, as well as, their antioxidant effect.

Amyloid β (Aβ) is the components of the amyloid deposits in the AD brain, while the component of the amyloidogenic peptide deposit in the pancreatic islets of Langerhans is identified as islet amyloid polypeptide (IAPP).

## **IV- 2.** Thioflavin-T (Th-T) assay of flavonoids **1-10**

The Thioflavin-T (Th-T) assay showed that both catechol and non-catechol types suppressed the aggregation of amyloid, but at a different degree of inhibition on a dose dependent way (Figures 48-67).

In fact, flavonoids possessing a catechol moiety had a lower $IC_{50}$ than the non-catechol type (Table 20) indicating that the position and number of the hydroxyl group in the aromatic ring is important for the determination of aggregation inhibition potency.

This result is consistent with previous reports concerning Aβ[56-60)] and confirmed for hIAPP aggregation inhibition. This difference between the two substances types might be explained by the difference in the mechanisms of action[61)].

From Table 20, it was also deduced that *O*-methylation of the flavonoids reduced significantly the inhibition potential of the aglycone form since the activity of **2** considerably decreased when the hydroxyl group in the A-ring and B-ring were substituted with a methoxyl group in case of **3**, **4**, and **5**.

Among all the purified flavonoids **1**-**10**, QGlcA (**7**) showed the strongest effect with an $IC_{50}$ equal to 3.8 µM and 1.7 µM towards Aβ and hIAPP, respectively. Add at that it was observed that the glucuronide moiety increased the aggregation inhibitory activity of **2** and **6**.

Structure-activity relationship of flavonoids **1**-**10** (Table 20) suggest that, a part of the catechol moiety, carboxyl moiety, as well as, the presence or absence of double bond between C2 and C3 in C-ring, are important functional groups for amyloid aggregation inhibition.

**IV-3**. Transmission electronic microscopy (TEM) observation of flavonoids **1**-**10**

The Transmission electronic microscopy (TEM) images of Aβ and hIAPP fibrils, when applied with QGlcA (**7**), its aglycone form quercetin (**2**), and the methyl ester analogue QGlcA-Me (**8**), show that the fibril formation was strongly inhibited by **7** (Figures 69B and 73B) compared to **2** (Figures 69C and 73C) and **8** (Figures 69D and 73D).

*O*-Methyl group in the glucuronide moiety of **10** reduced the inhibitory potential of **9**, same as observed for kaempferol (**6**) analogs (Figures 68 and 72).

*O*-Methylated analogs **3**, **4**, and **5** of quercetin (**2**) didn't inhibit the fibril formation of amyloids (Figures 70 and 74).

Quercetin (**2**) is an antioxidant flavonoid widely distributed in the plant kingdom, including daily foods such as vegetables and fruits. This substance was reported to inhibit a wide variety of diseases and/or aging *in vivo*, such as, the generation of Aβ peptides, interfering with Aβ aggregation. However, the metabolic conversion of

quercetin (**2**) after oral intake is suggested to attenuate its biological activity since the aglycone form of QGlcA (**7**) is not bioavailable *in vivo*, particularly in the brain[62].

Ho *et al.,* reported that similar to quercetin, the glyconosylated brain-targeting quercetin metabolite, QGlcA (**7**), is capable of interfering with the assembly of Aβ peptides into neurotoxic oligomeric Aβ aggregates. QGlcA (**7**) at 1:1 molar ratio with $A\beta_{1-42}$ also significantly reduced the formation of higher-order $A\beta_{1-42}$ species[63] which is in consistence with the obtained results.

The present *in vitro* study reports for first time QGlcA (**7**) and KGlcA (**9**) as hIAPP aggregation inhibitors. And, it suggests that substances with catechol and glucuronide moieties, showing Aβ aggregation inhibition, can be used also in case of hIAPP aggregation prevention. Therefore, it would be also of interest to extend this study to other amyloidogenic diseases.

## **IV-4.** Experimental

### IV-4-1. General methods

Fort two-mer amyloid β-protein ($A\beta_{1-42}$) was synthesized by the standard protocol[64]. hIAPP (Amylin 1-37, human, purity > 95%) was purchased from Karebay Biochem Inc.

### IV-4-2. Th-T fluorescence assay

Aggregative ability of amyloid was evaluated at 37°C by Th-T using 42-mer amyloid β-protein ($A\beta_{1-42}$) for Alzheimer's disease and human islet amyloid polypeptide (hIAPP) which is a 37-residue peptide secreted by the pancreatic β –cells for T2D.

Briefly, $A\beta_{1-42}$ was dissolved in 0.1% $NH_4OH$ at 250 mM and hIAPP in hexafluoroisopropanol (HFIP). The amyloid solution was diluted 10-fold with 50 mM phosphate-buffered saline (PBS) (pH 7.4), and the solution incubated with or without samples.

A 2.5 μL volume of a peptide solution was added to 250 μL of 1mM Th-T in 50 mM Glycine-NaOH buffer (pH 8.5). The fluorescence intensity was measured at an excitation wavelength of 420 nm and an emission wavelength of 485 nm by a Multidetection Microplate Reader.

$A\beta_{1-42}$ was incubated alone for 2h, 6 h, 12 h, and 24 h, while hIAPP was incubated alone for 4 h, 8 h, and 24 h.

IV-4-3. Transmission electronic microscopy (TEM)

Effect of the flavonoids **1**-**10** on $A\beta_{1-42}$ and hIAPP fibrillogenesis was investigated by using TEM.

The incubating solution was the same as that used for preparing the samples in case of Th-T assay.

A 5.0 μL volume of each sample was spotted on to a glow-discharged, Formvar-carbon-coated grid and was incubated for 2 min and then washed twice with 5.0 μL of pure water (MiliQ).

The grid was finally negatively stained twice for 1 min each with 5.0 μL of 0.4% silicotungstic acid, and the solution was removed. After air drying for 5 min, each sample was examined with TEM (JEM-1400 electron microscope, JEOL, Japan).

Table 20. $IC_{50}$ of hIAPP and Aβ aggregation inhibitory activities of flavonoids **1-10.**

| Substance name | $IC_{50}$ (μM) | |
|---|---|---|
| | hIAPP | Aβ |
| naringenin (**1**) | 10.3 | 9.3 |
| quercetin (**2**) | 1.8 | 15.7 |
| rhamnetin (**3**) | 13.4 | 131.8 |
| rhamnezin (**4**) | > 100 | > 200 |
| tamarixetin (**5**) | 10.6 | 90.7 |
| kaempferol (**6**) | 25.4 | 51.6 |
| QGlcA (**7**) | 1.7 | 3.8 |
| QGlcA-Me (**8**) | 22.6 | 31.6 |
| KGlcA (**9**) | 18.5 | 19.4 |
| KGlcA-Me (**10**) | 28.2 | 22.4 |

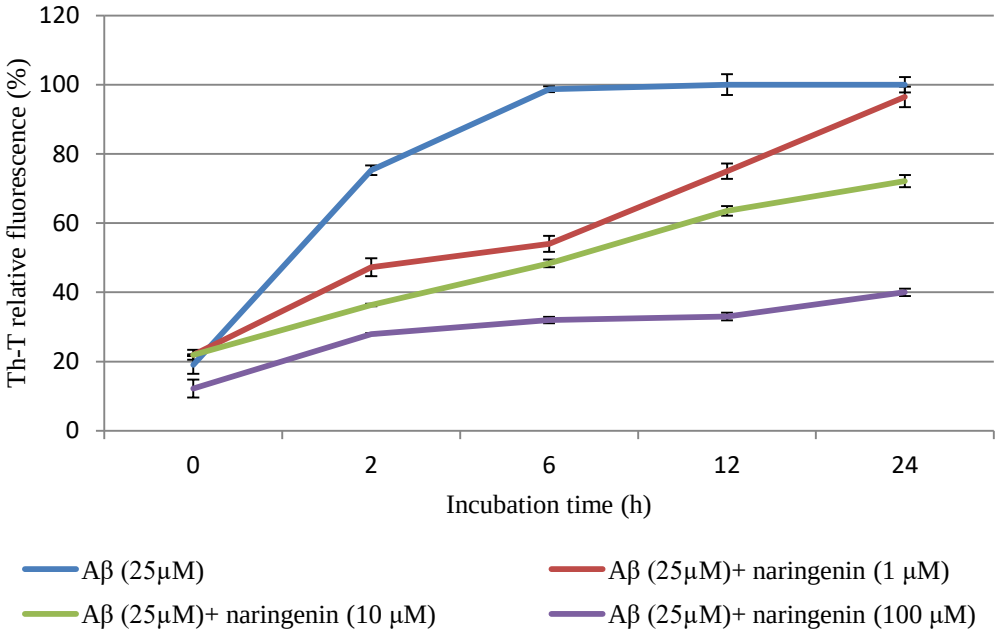


Figure 48. Amyloid β aggregation inhibition activity of naringenin (**1**).

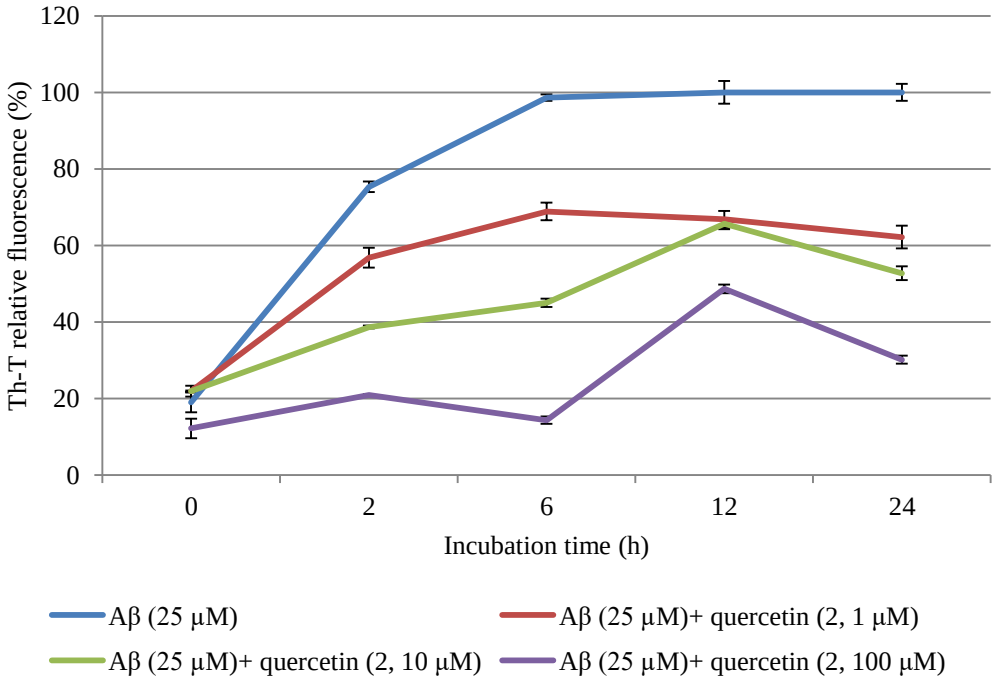


Figure 49. Amyloid β aggregation inhibition activity of quercetin (**2**).

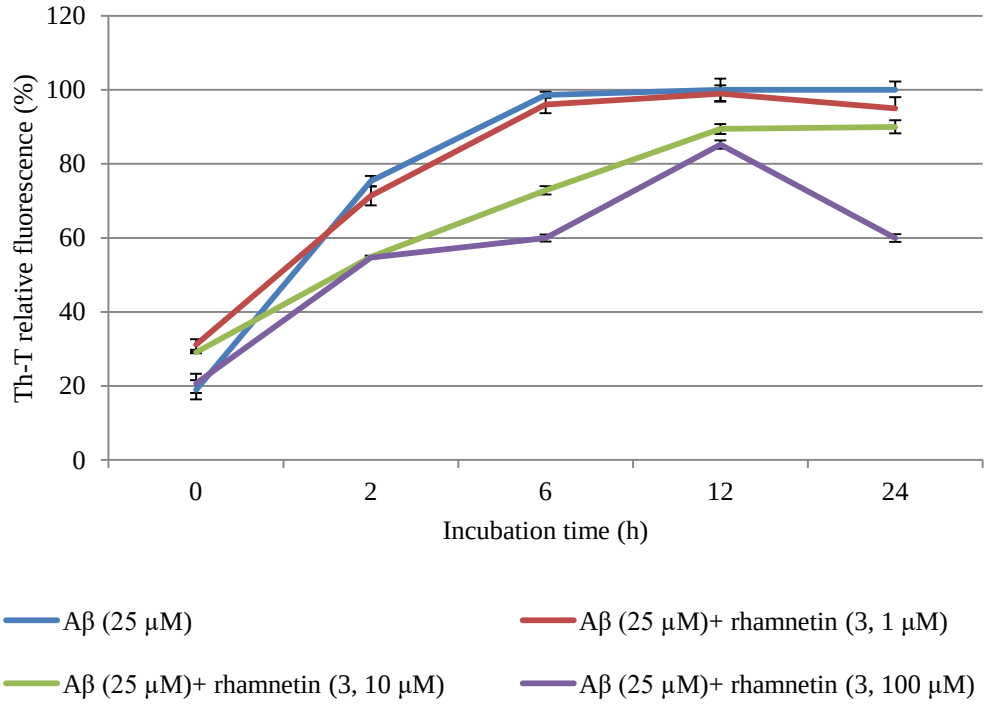


Figure 50. Amyloid β aggregation inhibition activity of rhamnetin (**3**).

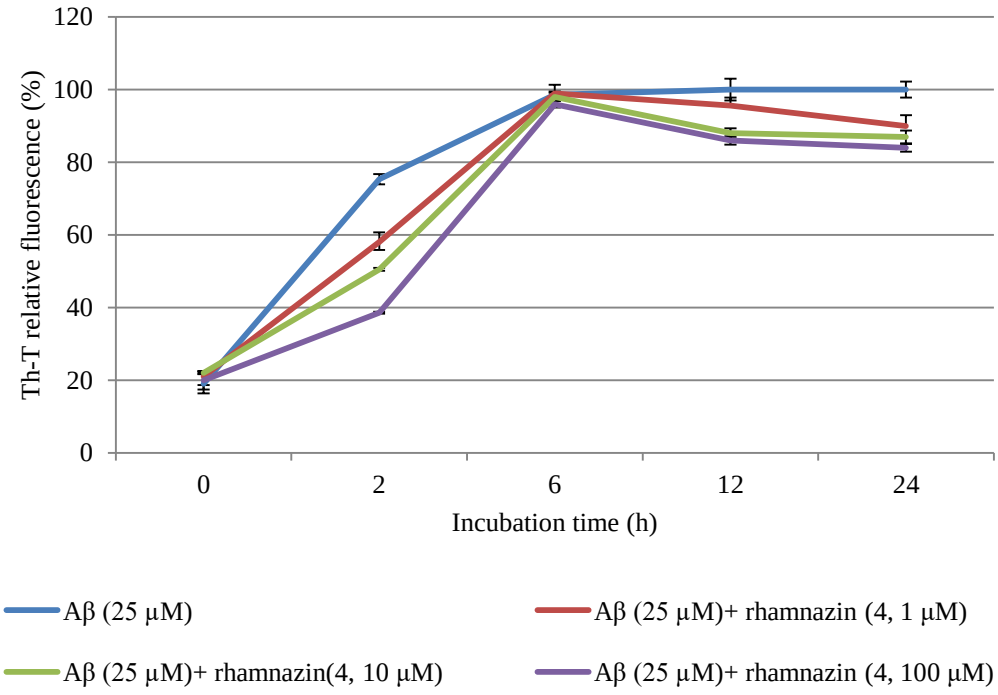


Figure 51. Amyloid β aggregation inhibition activity of rhamnazin (**4**).

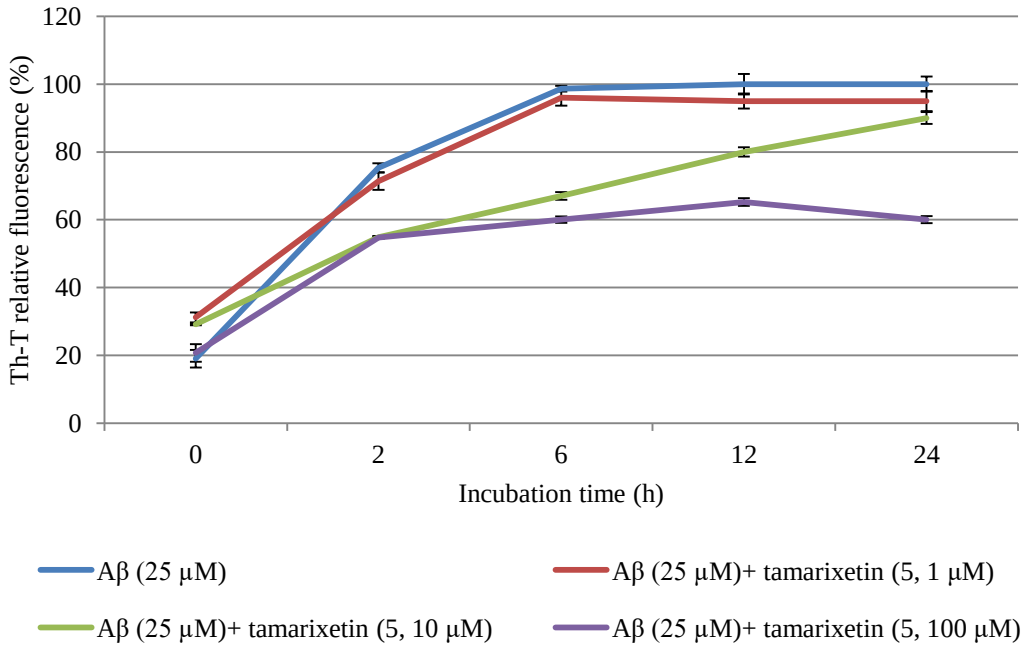


Figure 52. Amyloid β aggregation inhibition activity of tamarixetin (**5**).

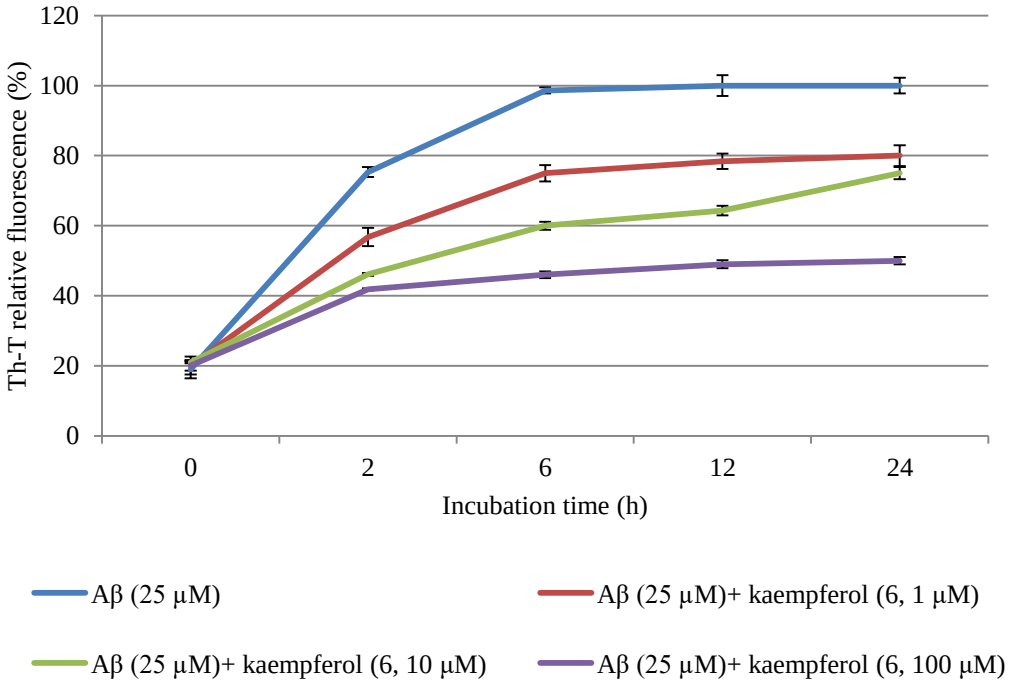


Figure 53. Amyloid β aggregation inhibition activity of kaempferol (**6**).

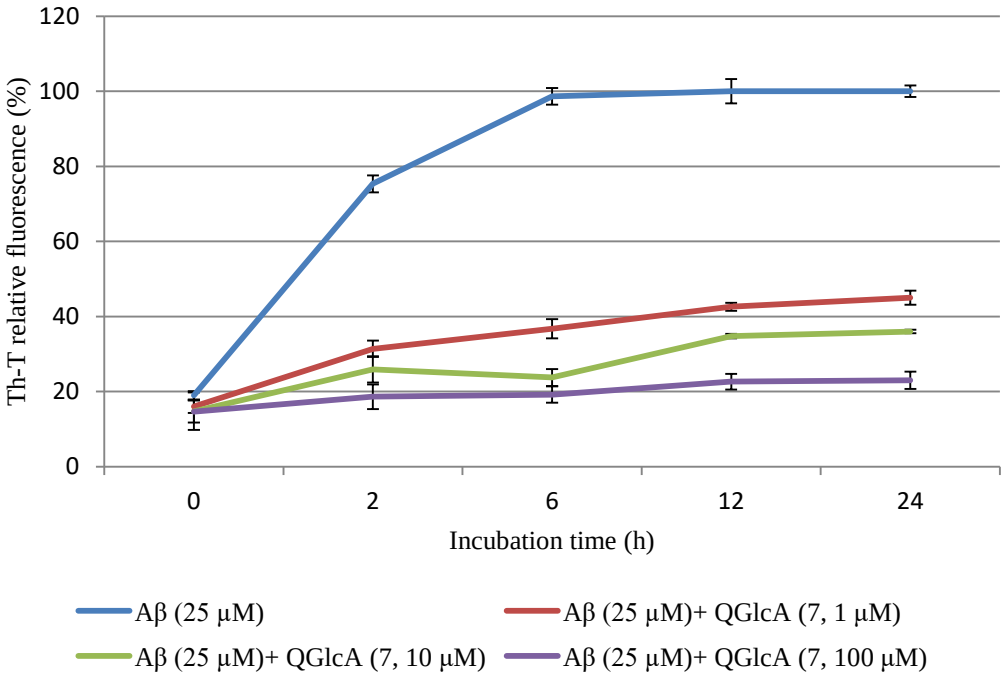


Figure 54. Amyloid β aggregation inhibition activity of QGlcA (**7**).

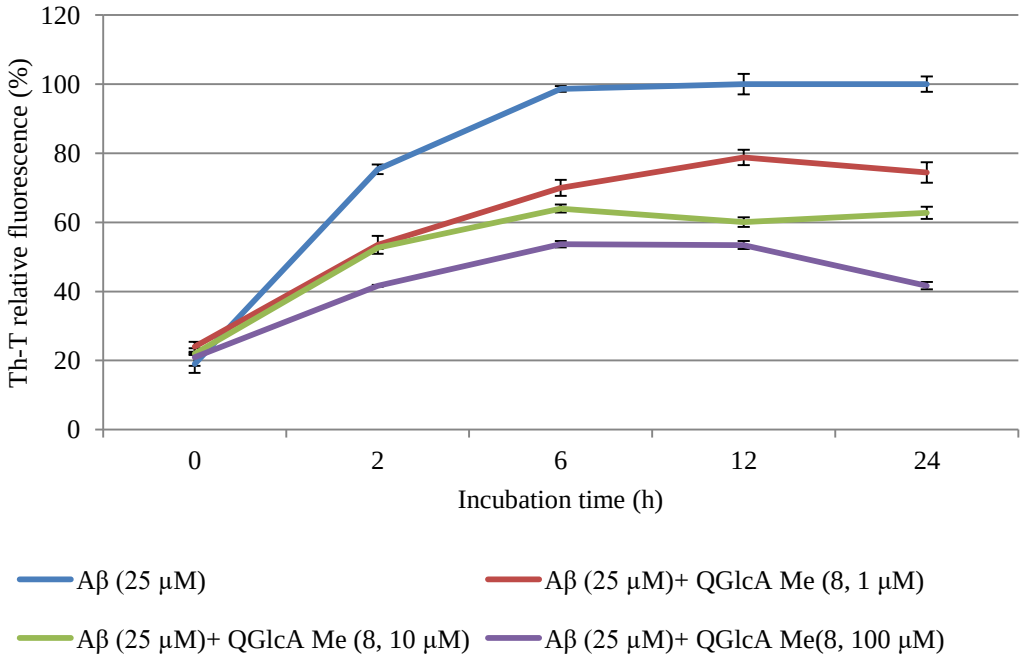


Figure 55. Amyloid β aggregation inhibition activity of QGlcA Me (**8**).

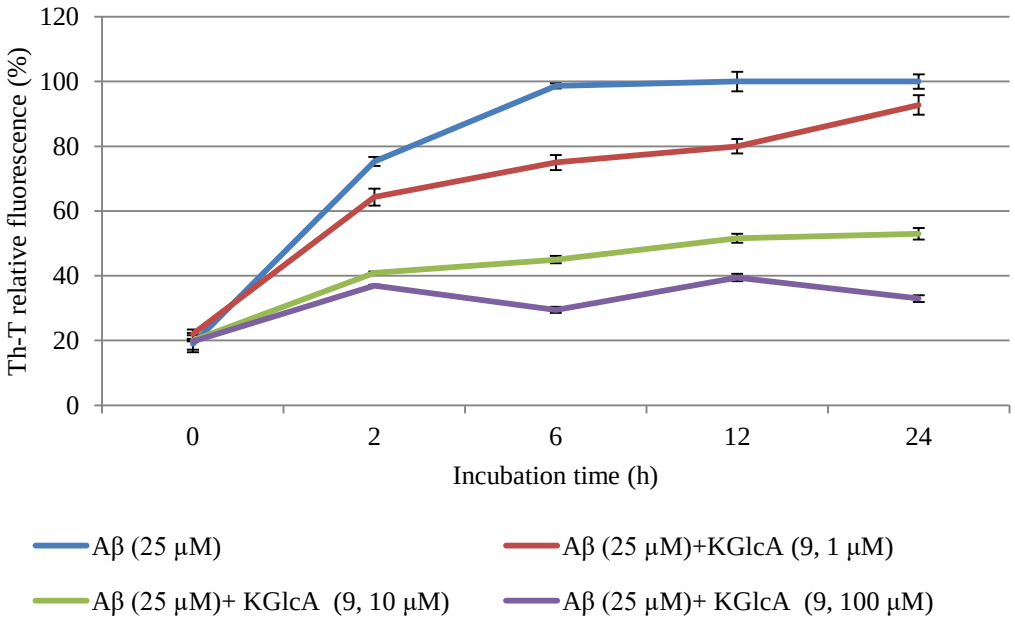


Figure 56. Amyloid β aggregation inhibition activity of KGlcA (**9**).

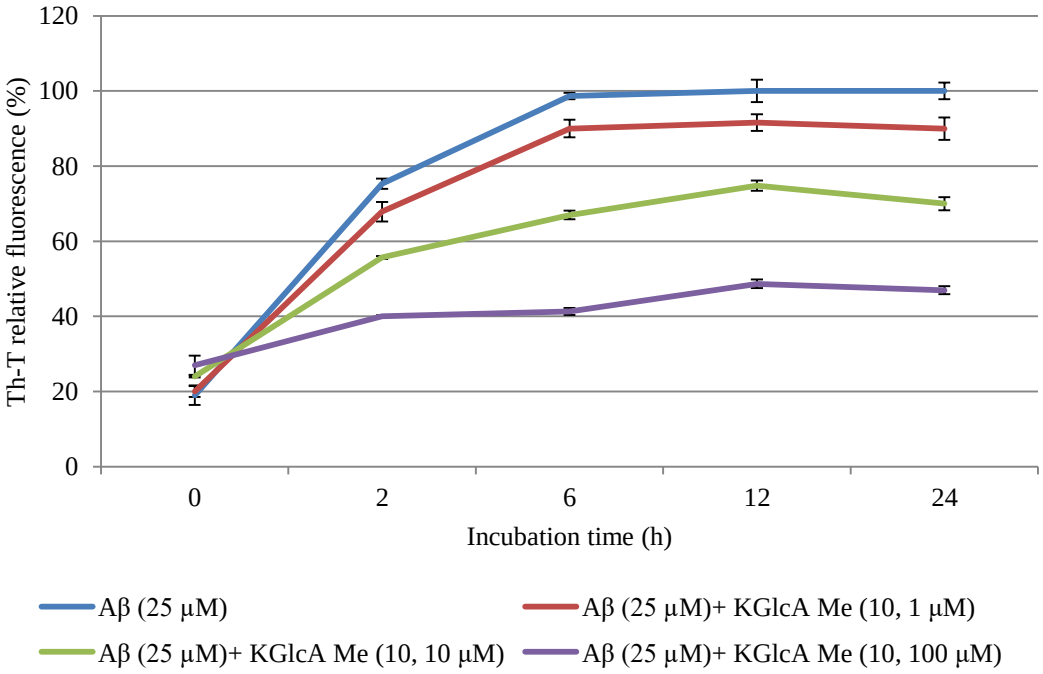


Figure 57. Amyloid β aggregation inhibition activity of KGlcA Me (**10**).

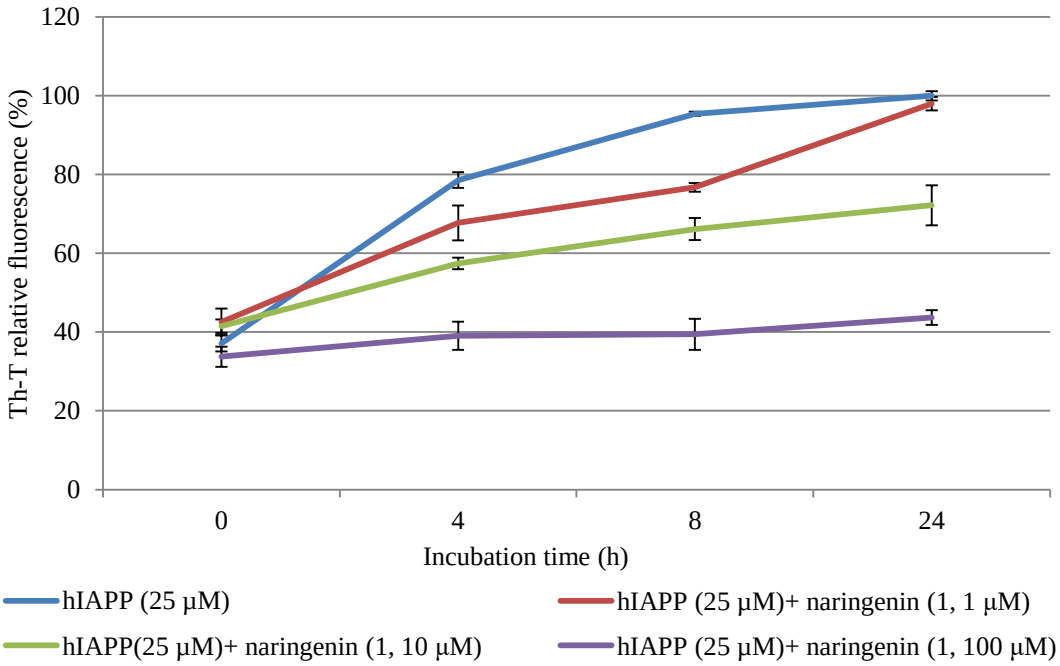


Figure 58. hIAPP aggregation inhibition activity of naringenin (**1**).

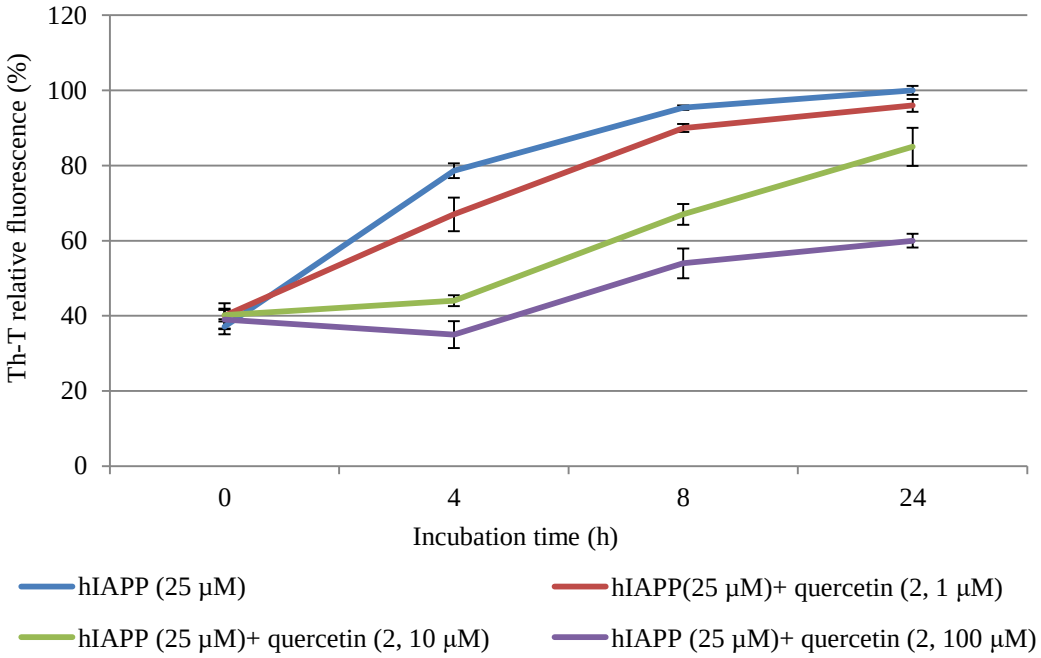


Figure 59. hIAPP aggregation inhibition activity of quercetin (**2**).

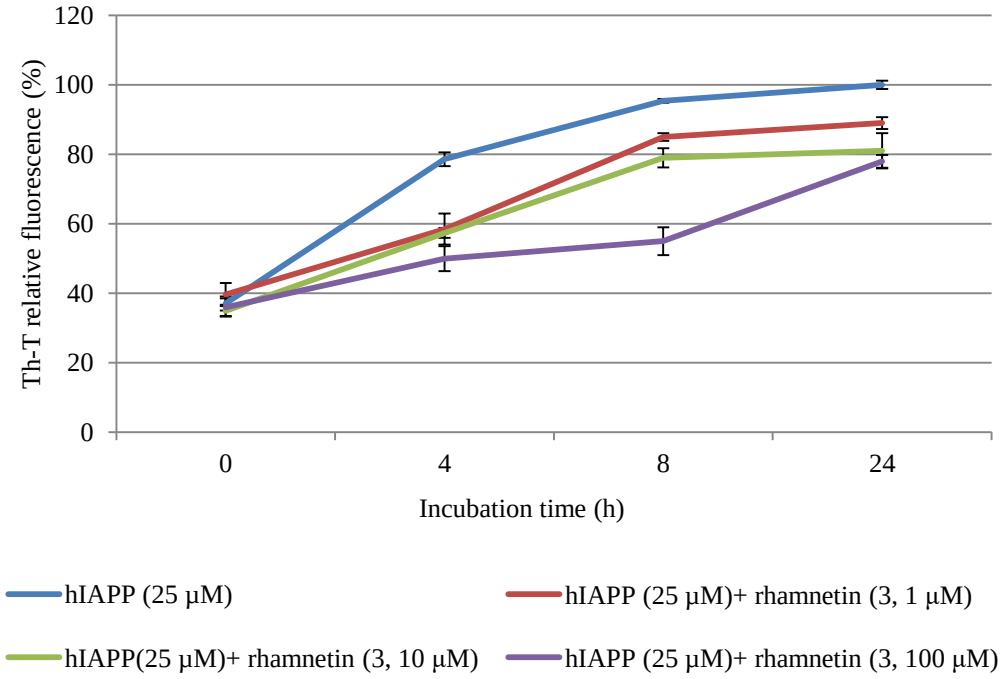


Figure 60. hIAPP aggregation inhibition activity of rhamnetin (**3**).

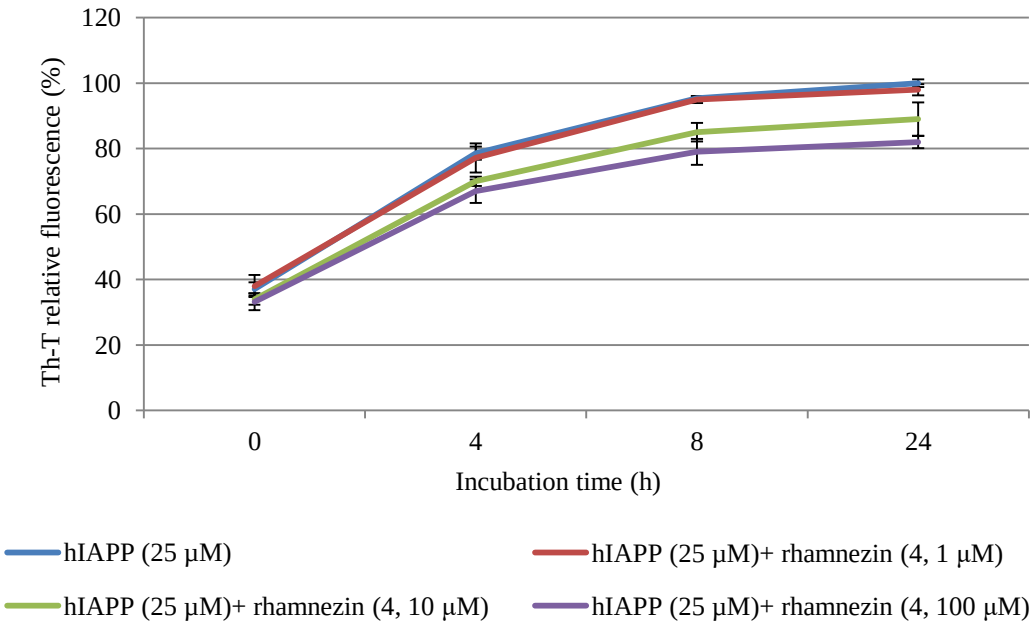


Figure 61. hIAPP aggregation inhibition activity of rhamnezin (**4**).

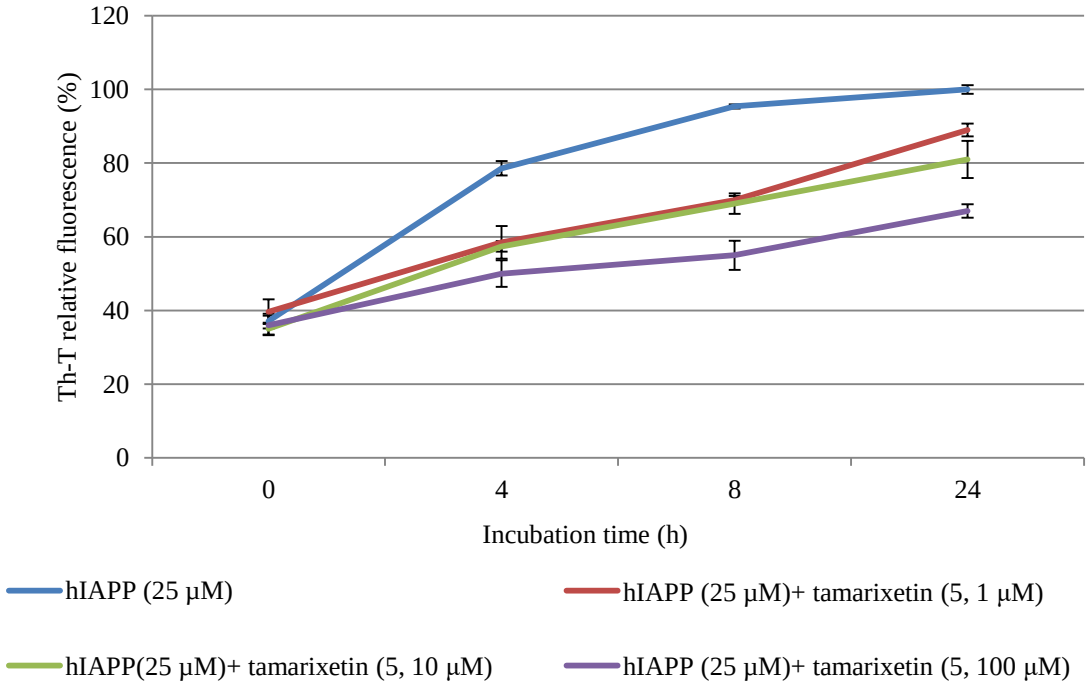


Figure 62. hIAPP aggregation inhibition activity of tamarixetin (**5**).

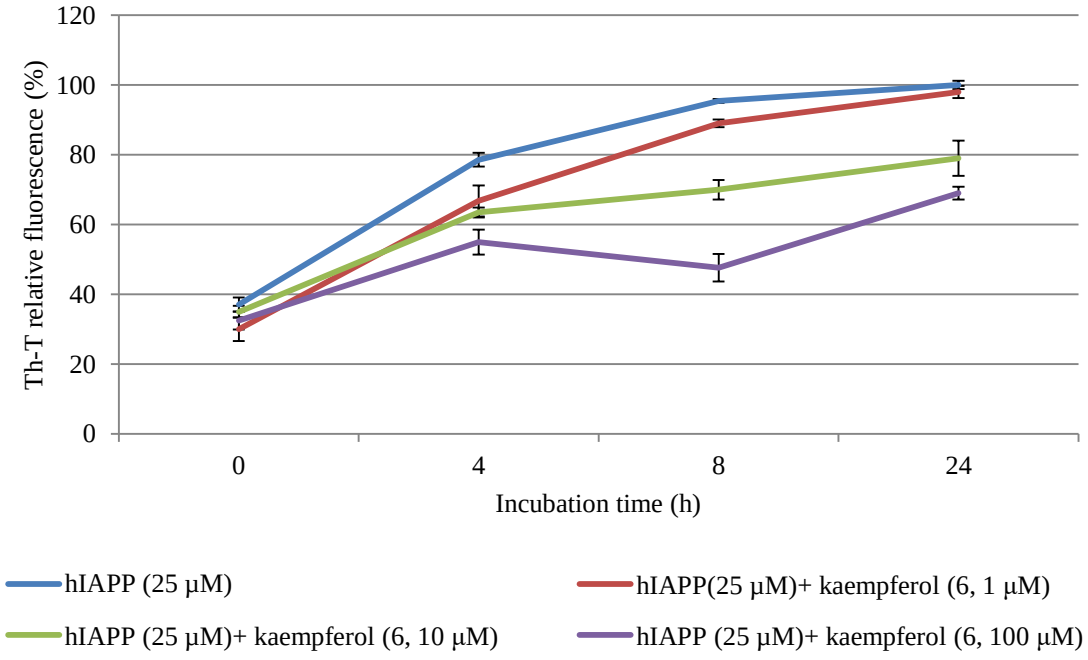


Figure 63. hIAPP aggregation inhibition activity of kaempferol (**6**).

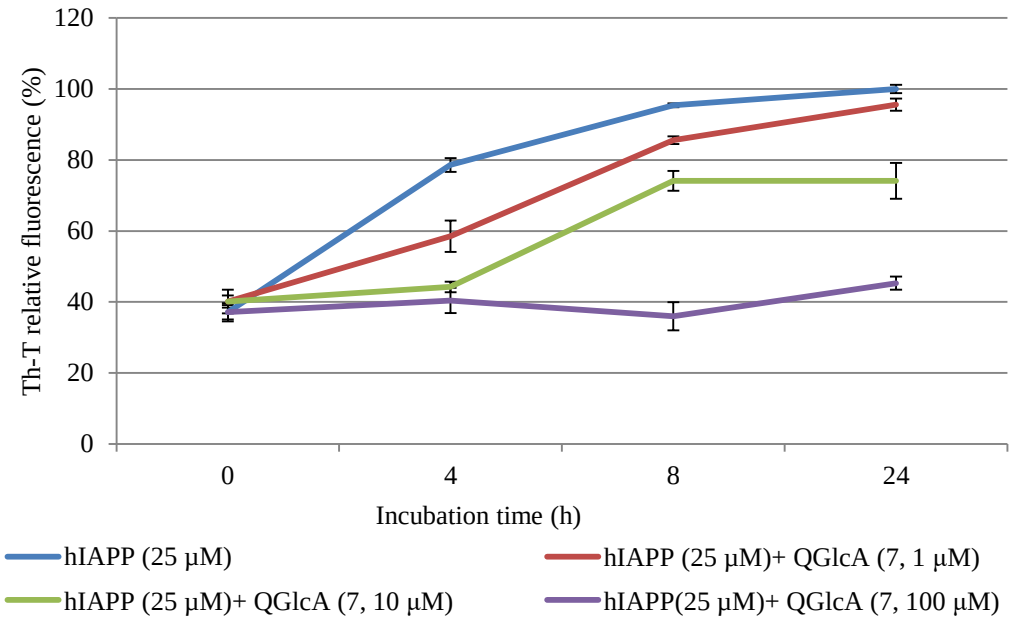


Figure 64. hIAPP aggregation inhibition activity of QGlcA (**7**).

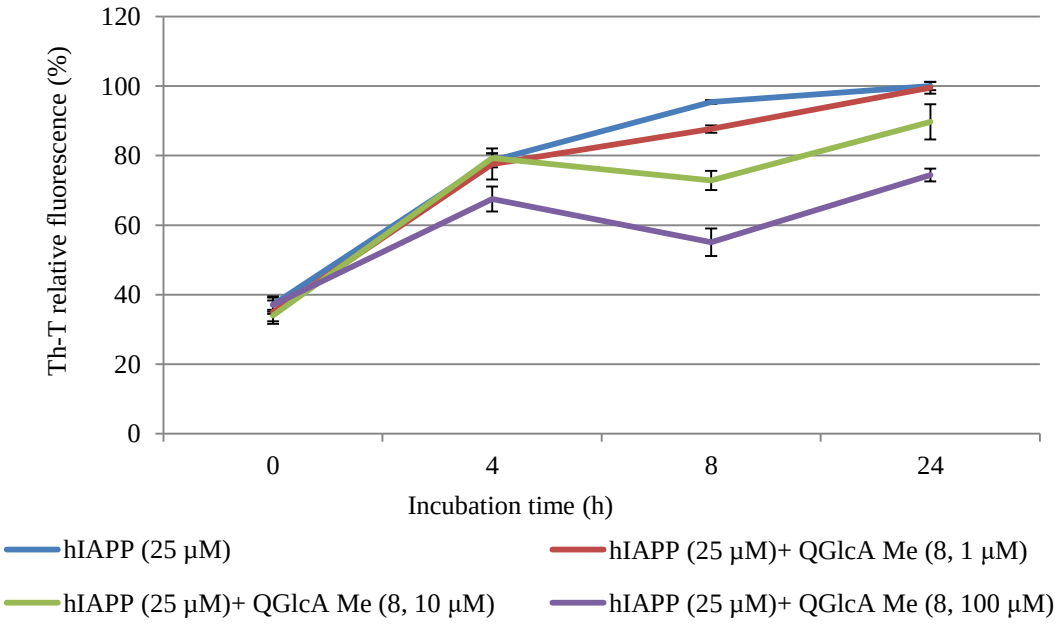


Figure 65. hIAPP aggregation inhibition activity of QGlcAMe (**8**).

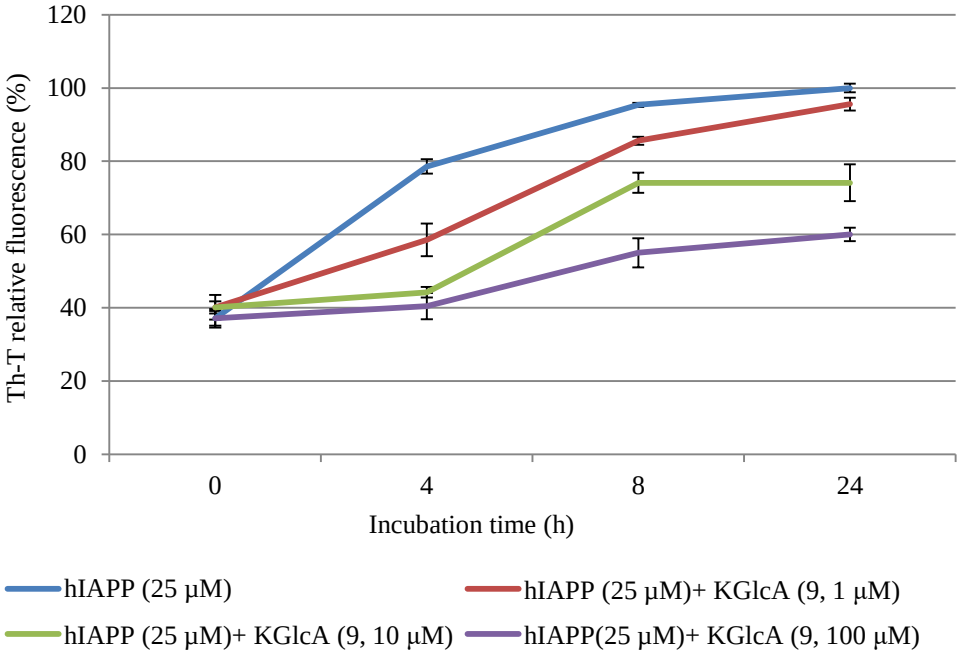


Figure 66. hIAPP aggregation inhibition activity of KGlcA (**9**).

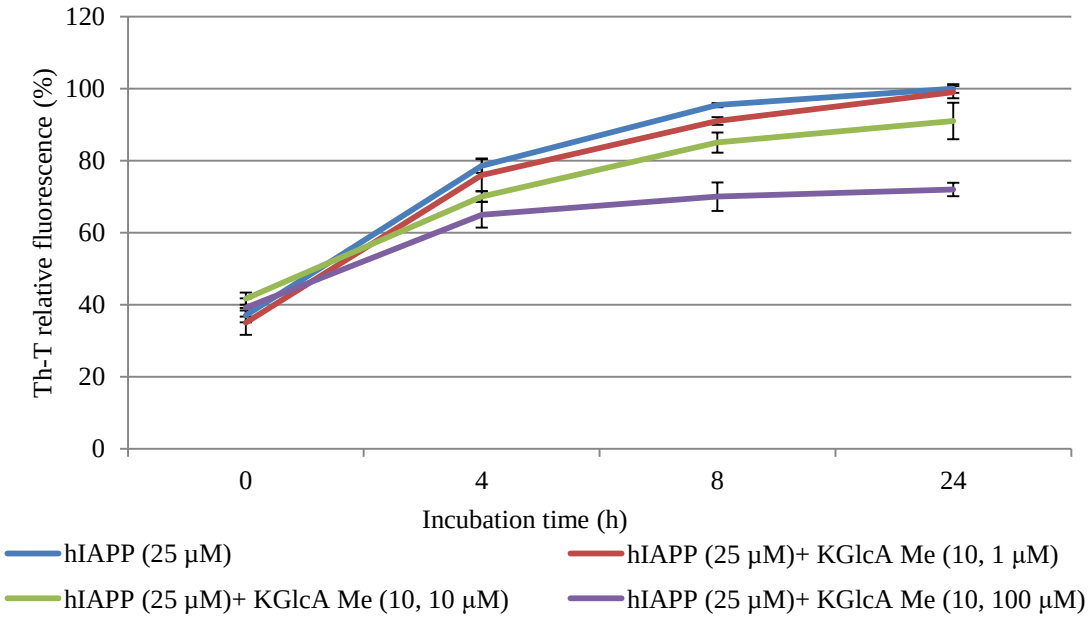


Figure 67. hIAPP aggregation inhibition activity of KGlcA Me (**10**).

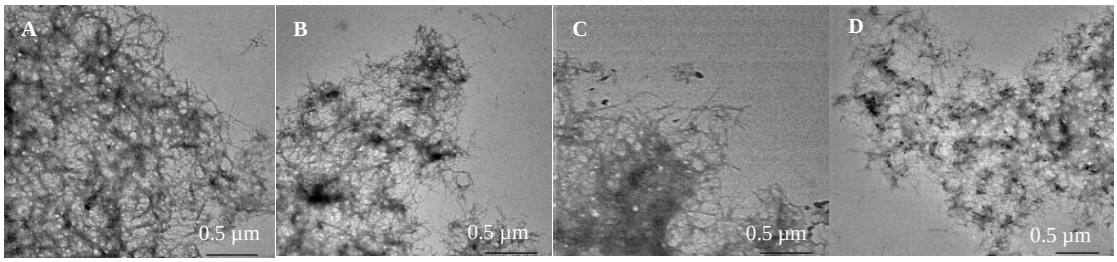


Figure 68. Transmission electron microscopy observation of Amyloid β aggregation inhibitory activity of 25 µM A β (A), 25 µM A β with 100 µM **9** (B), 25 µM A β with 100 µM **6** (C), and 25 µM A*β* with 100 µM **10** (D).

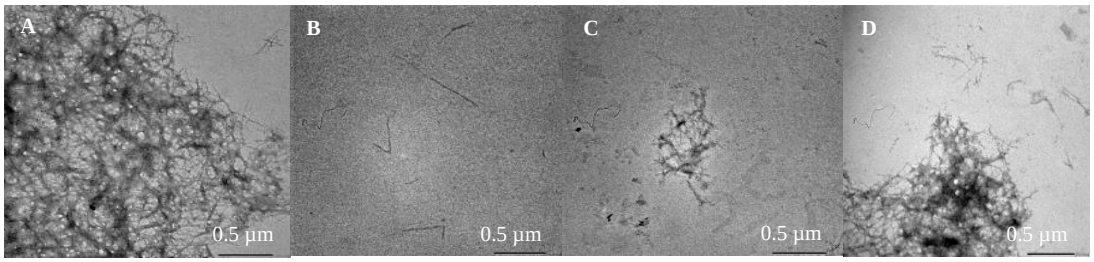


Figure 69. Transmission electron microscopy observation of Amyloid β aggregation inhibitory activity of 25 µM A β (A), 25 µM A β with 100 µM **7** (B), 25 µM A β with 100 µM **2** (C), and 25 µM A β with 100 µM **8** (D).

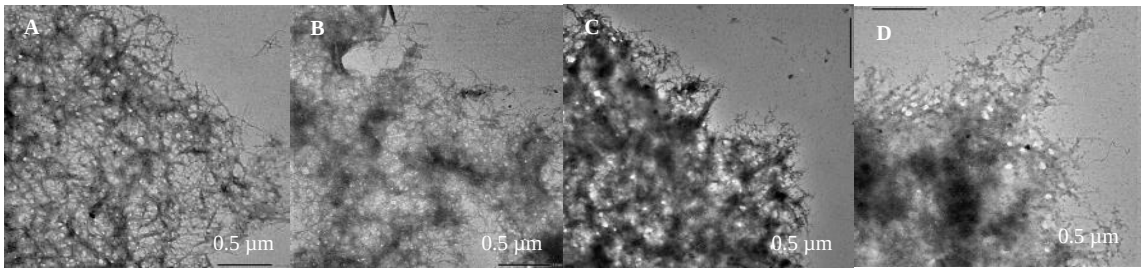


Figure 70. Transmission electron microscopy observation of Amyloid β aggregation inhibitory activity of 25 µM A β (A), 25 µM Aβ with 100 µM **3** (B), 25 µM Aβ with 100 µM **4** (C), and 25 µM Aβ with 100 µM **5** (D).

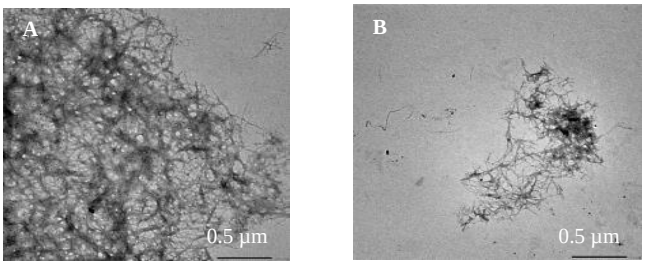


Figure 71. Transmission electron microscopy observation of Amyloid β aggregation inhibitory activity of 25 µM Aβ (A), 25 µM Aβ with 100 µM **1** (B).

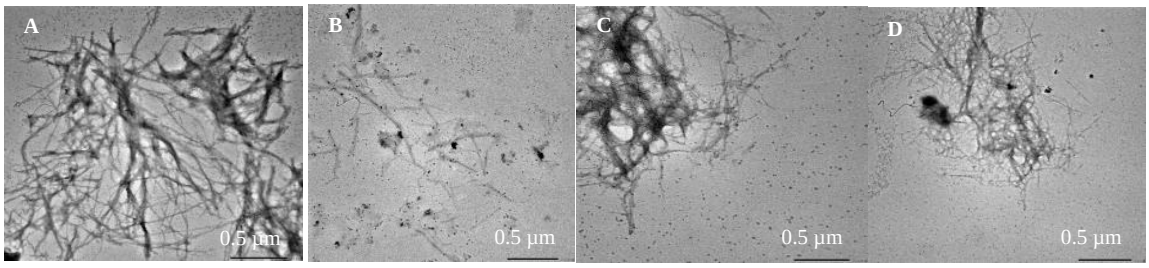


Figure 72. Transmission electron microscopy observation of hIAPP aggregation inhibitory activity of 25 µM hIAPP (A), 25 µM hIAPP with 100 µM **9** (B), 25 µM hIAPP with 100 µM **6** (C), and 25 µM hIAPP with 100 µM **10** (D).

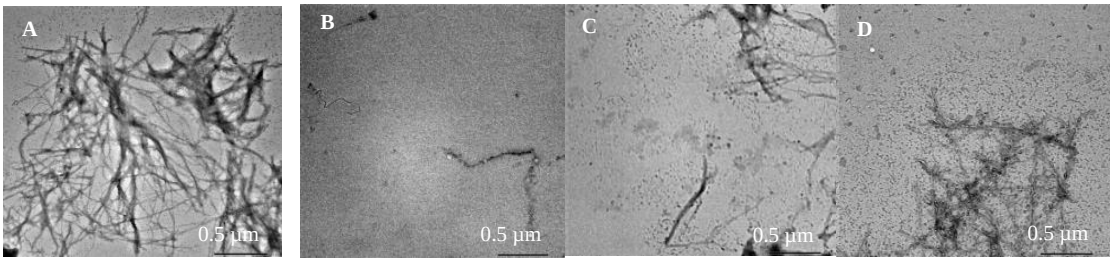


Figure 73. Transmission electron microscopy observation of hIAPP aggregation inhibitory activity of 25 µM hIAPP (A), 25 µM hIAPP with 100 µM **7** (B), 25 µM hIAPP with 100 µM **2** (C), and 25 µM hIAPP with 100 µM **8** (D).

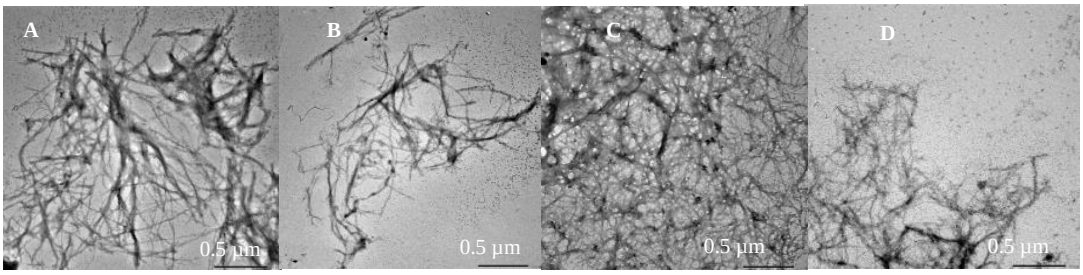


Figure 74. Transmission electron microscopy observation of hIAPP aggregation inhibitory activity of 25 µM hIAPP (A), 25 µM hIAPP with 100 µM **3** (B), 25 µM hIAPP with 100 µM **4** (C), 25 µM hIAPP with 100 µM **5** (D).

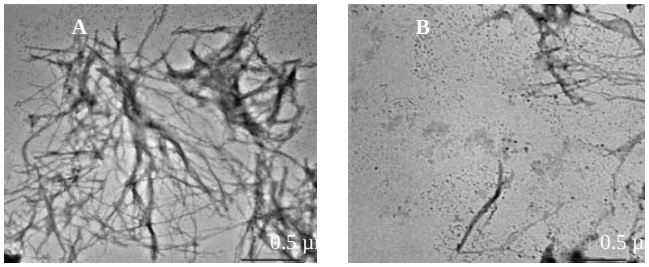


Figure 75. Transmission electron microscopy observation of hIAPP aggregation inhibitory activity of 25 µM hIAPP (A), 25 µM hIAPP with 100 µM **1** (B).

# *Chapter V*

# General conclusion

Ten flavonoids **1**-**10** were isolated and identified from the medicinal halophyte *T. gallica* as α-glucosidase inhibitors towards both yeast and mammalian enzymes: naringenin (**1**), quercetin (**2**), rhamnetin (**3**), rhamnezin (**4**), tamarixetin (**5**), kaempferol (**6**), QGlcA (**7**), QGlcA-Me (**8**), KGlcA (**9**), and KGlcA-Me (**10**).

The flavonoids were also proved to exhibit an antioxidant activity and inhibition potential for Aβ and hIAPP aggregation.

QGlcA-Me (**8**) showed the strongest α-glucosidase inhibition among all the purified flavonoids **1**-**10** with an $IC_{50}$ equal to 62.3 µM, while QGlcA (**7**) have the most potent amyloid aggregation inhibition activity ($IC_{50}$ 1.7 µM in case of hIAPP and $IC_{50}$ 3.8 µM in case of Aβ).

The structure-activity relationship study of α-glucosidase inhibitory activity shows that the presence of *O*-methyl moiety in the flavonoid increases its inhibitory potential, when substituted in the A-ring of the aglycone and in the glucuronide moiety. However, the substitution of OH group in the catechol of B-ring with OMe reduced considerably the inhibition potential.

The substitution of OH group at C-3 position with glucuronide moiety also increased also the activity of quercetin (**2**) and kaempferol (**6**).

The same result was also observed in case of amyloid aggregation inhibition. But, the methylation of the aglycone forms and the glucuronide moiety decreased their potential to inhibit the aggregation of Aβ and hIAPP.

Glucuronosylated flavonoids are reported for the first time as α-glucosidase and hIAPP aggregation inhibitors. Consequently, advanced studies were conducted on those substances and compared with their aglycone and methylated analogs.

The study of the mechanism of action for α-glucosidase inhibition activity suggested that, *O*-methylated and aglycone flavonoids have a mixed inhibition, while the glucuronosylated flavonoids have a non-competitive inhibition.

Furthermore, *O*-Methylated and glucuronosylated flavonoids showed also a synergistic effect when applied with acarbose, suggesting that they can be used to

reduce the side effect of commercially available α-glucosidase inhibitors. The synergistic effect of those flavonoids can be related to their inhibition mode which is different from acarbose. In fact, acarbose is known to exhibit a competitive inhibition targeting the enzyme active site, yet the tested flavonoids target is different from that site and as a result, two different α-glucosidase inhibitors may bind simultaneously.

In case of amyloid aggregation, QGlcA (**7**), KGlcA (**9**), and naringenin (**1**) showed inhibition potentials for the fibril formation.

The obtained results provided a better understand about the structural moieties potentially important for the inhibition of α-glucosidase and amyloid aggregation.

Add at that, it was find that *O*-methylated and glucuronosylated flavonoids, able to inhibit Aβ responsible of the neuronal cell death in AD, exhibit also aggregation inhibitory activity towards hIAPP, which are the cause of the cell destruction and insulin secretion disturbance in the pancreas of diabetic patients.

It was proved also that the antioxidant potential of QGlC-A (**7**) was in correlation with its amyloid aggregation inhibition potential and α-glucosidase inhibition activity. However, the antioxidant potential of O-Methylated flavonoids **3─5** was in correlation with the α-glucosidase inhibition activity but not with their amyloid aggregation inhibition potential

The conducted experiments may also be proposed to valorize the use of the invasive halophyte *T. gallica* (homeopathic drug) as a multi-model treatment that target diabetes and Alzheimer's diseases common pathophysiological features.

# References


1) Centers for Disease Control and Prevention. Estimates of Diabetes and Its Burden in the United States. National Diabetes Statistics Report. Atlanta, GA: US Department of Health and Human Services; **2014**. Available from: http: //www.cdc.gov/diabetes/pubs/statsreport14.htm.

2) Kukull, W. A.; Higdon, R.; Bowen, J. D.; McCormick, W. C.; Teri, L.; Schellenberg, G.D.; Van Belle, G.; Jolley, L.; Larson, E.B. Dementia and Alzheimer's disease incidence: a prospective cohort study. *Arch. Neurol.* **2002**, *59*, 1737–1746.

3) Hu, F.B. Globalization of Diabetes: The role of diet, lifestyle, and genes. *Diabetes Care*. **2011**, *34*, 1249–1257.

4) Adeghate, E.; Donáth, T.; Adem, A. Alzheimer's disease and diabetes mellitus: do they have anything in common? *Curr. Alzheimer Res.* **2013**, *10*, 609-17.

5) De la Monte, S.M.; Neusner, A.; Chu, J.; Lawton, M. Epidemilogical trends strongly suggest exposures as etiologic agents in the pathogenesis of sporadic Alzheimer's disease, diabetes mellitus, and non-alcoholic steatohepatitis. *J. Alzheimer's. Dis*. **2009**, *17*, 519–529.

6) Akter, K.; Lanza, E. A.; Martin, S. A.; Myronyuk, N.; Rua, M.; Raffa, R. B. Diabetes mellitus and Alzheimer's disease: Shared pathology and treatment? *Br. J. Clin. Pharmacol.* **2011**, *71*, 365–376.

7) Hoyer, S. Glucose metabolism and insulin receptor signal transduction in Alzheimer's disease. *Eur. J. Pharmacol*. **2004**, *490*,115–125.

8) Rivera, E. J.; Goldin, A.; Fulmer, N.; Tavares, R.; Wands, J. R.; De la Monte, S. M. Insulin and insulin-like growth factor expression and function deteriorate with progression of Alzheimer's disease: Link to brain reductions in acetylcholine. *J. Alzheimer's Dis*. **2005**, *8*, 247–268.

9) De la Monte S. M. Brain insulin resistance and deficiency as therapeutic targets in Alzheimer's disease. *Curr. Alzheimer Res*. **2012**, *9*, 35–66.

10) Barbagallo, M.; Dominguez, L. Type 2 diabetes mellitus and Alzheimer's diseases. *World J. Diabetes*. **2014**, *5*, 889-893.

11) Blázquez, E.; Velázquez, E.; Hurtado-Carneiro, V.; Ruiz-Albusac, J. M. Insulin in the brain: Its pathophysiological implications for states related with central insulin resistance, type 2 diabetes and Alzheimer's disease. *Front. Endocrin.* **2014**, *5*, 161.

12) Takeda, S.; Sato, N.; Rakugi, H.; Morishita, R. Molecular mechanisms linking diabetes mellitus and Alzheimer's disease: β-amyloid peptide, insulin signaling, and neuronal function. *Mol. Biosyst.* **2011**, *7*, 1822-1827.

13) Zhao, W. Q.; Townsend, M. Insulin resistance and amyloidogenesis as common molecular foundation for type 2 diabetes and Alzheimer's disease. *Biochi. Bioph. Acta*, **2009**, *1792*, 482-496.

14) Adolfsson, R.; Bucht, G.; Lithner, F.; Winblad, B. Hypoglycemia in Alzheimer's disease. *Acta. Med. Scand.* **1980**, *208*, 387-388.

15) Haass, C.; Koo, E. H.; Mellon, A.; Hung, A. Y.; Selkoe, D. J. Targeting of cell-surface β-amyloid precursor protein to lysosomes: alternative processing into amyloid-bearing fragments. *Nature* **1992**, *357*, 500-503.

16) Cooper, G. J.; Willis, A. C.; Clark, A.; Turner, R. C.; Sim, R. B.; Reid, K. B. Purification and characterization of a peptide from amyloid-rich pancreases of type 2 diabetic patients. *Proc. Natl. Acad. Sci. U. S. A.* **1987**, *84*, 8628-8632.

17) Janson, J.; Laedtke, T.; Parisi, J. E.; O'Brien, P.; Petersen, R. C.; Butler, P. C. Increased risk of type 2 diabetes in Alzheimer's disease. *Diabetes* **2004**, *53*, 474–481.

18) Toyama, B. H.; Weissman, J. S. Amyloid Structure: Conformational diversity and consequences. *Annu. Rev. Biochem*. **2011**, *80*, 557.

19) Porat, Y.; Kolusheva, S.; Jelinek, R.; Gazit, E. The human islet amyloid polypeptide forms transient membrane-active prefibrillar assemblies. *Biochemistry* **2003**, *42*, 10971-10977.

20) Green, J. D.; Goldsbury, C.; Kistler, J.; Cooper, G. J.; Aebi, U. Human amylin oligomer growth and fibril elongation define two distinct phases in amyloid formation. *J. Biol. Chem*. **2004**, *279*, 12206-12212.

21) Kayed, R.; Head, E.; Thompson, J. L.; McIntire, T. M.; Milton. S. C.; Cotman, C. W.; Glabe, C. G. Common structure of soluble amyloid oligomers implies common mechanism of pathogenesis. *Science*. **2003**, *300*, 486- 489.

22) Sandhir, R.; Gupta, S. Molecular and biochemical trajectories from diabetes to Alzheimer's disease: A critical appraisal. *World J. Diabetes* **2015**, *6*, 1223-1242.

23) Xueping, C.; Chunyan, G.; Jiming, K. Oxidative stress in neurodegenerative diseases. *Neural Regen. Res.* **2012**, *7*, 376–385.

24) De la Monte, S. M. Therapeutic targets of brain insulin resistance in sporadic Alzheimer's disease. *Front. Biosci.* (Elite Ed) **2012**, *4*, 1582-1605.

25) Orfali, R. S.; Ebada, S. S.; El-Shafae, A. M.; Al-Taweel, A. M.; Lin, W. H.; Wray, V.; Proksch, P. 3-*O*-*trans*-caffeoylisomyricadiol: a new triterpenoid from *Tamrix nilocita* growing in Saudia Arabia. *Z. Naturforsch.* **2009**, *64*, 637-643.

26) Whitcraft, C. R.; Talley, D. M.; Crooks, J. A.; Boland, J.; Gaskin, J. Invasion of tamarisk (*Tamarix* spp.) in a southern California salt marsh. *Biol. Invasions*. **2007**, *9*, 875.

27) Tabassum, N.; Chatturvedi, S.; Agrawal, S. S. Effect of *Tamarix gallica* leaves on experimental liver cell injury. *JK-Practitioner*. **2016**, *13*, 43-44.

28) Ksouri, R.; Falleh, H.; Megdiche, W.; Trabelsi, N.; Mhamdi, B.; Chaieb, K.; Bakrouf, A.; Magné, C.; Abdelly, C. Antioxidant and antimicrobial activities of the edible medicinal halophyte *Tamarix gallica* L. and related polyphenolic constituents. *Food Chem. Toxicol*. **2009**, *47*, 2083–2091.

29) Mayuresh, R.; Andrzej, P.; Patrycja, L. K.; Wojciech, Z.; Rafal, F. Herbal medicine for treatment and prevention of liver diseases. *J. Pre-clin. Clin. Rese*. **2014**, *8*, 55–60.

30) Drabu, S.; Chaturvedi. S.; Sharma. M. *Tamarix gallica*-An overview. *Asian J. Pharm. Clinical Res*. **2012**, *5*, 17-19.

31) Lefahal, M.; Benahmed, M.; Louaar, S.; Zallagui, A.; Duddeck, H.; Medjroubi, K.; Akkal, S. Antimicrobial activity of *Tamarix gallica* L. extracts and isolated flavonoids. *Adv. Nat. Appl. Sci*. **2010**, *4*, 289-292.

32) Pandey, D. P.; Karnatak, K. B.; Singh, R. P.; Rather, M. A.; Bachheti, R. K.; Chand, S. Phytochemical analysis of *Tamrix gallica*. *Int. J. Pharm. Tech. Res*. **2010**, *2*, 2340-2342.

33) Kimmel, B.; Inzucchi, S. Oral agents for type 2 diabetes: an update. *Clin. Diab*. **2005**, *23*, 64-76.

34) Woerle, H. J.; Pimenta, W. P.; Meyer, C.; Gosmanov, N. R.; Szoke, E.; Szombathy, T.; Mitrakou, A.; Gerich, J. E. Diagnostic and therapeutic implications of relationships between fasting, 2-hour postchallenge plasma glucose and hemoglobin a1c values. *Arch. Intern. Med.* **2004**, *164*, 1627-1632.

35) Casirola, D. M.; Ferraris, R. P. Alpha-glucosidase inhibitors prevent diet-induced increases in intestinal sugar transport in diabetic mice. *Metabolism*. **2006**, *55*, 832–841.

36) Zhang, L.; Hogan, S.; Li, J. R.; Sun, S.; Canning, C.; Zheng, S. J. Grape skin extract inhibits mammalian intestinal α-glucosidase activity and suppresses postprandial glycemic response in streptozocin-treated mice. *Food Chem.* **2011**,*126*, 466–471.

37) Madar, Z. The effect of acarbose and miglitol (BAY-M-1099) on postprandial glucose levels following ingestion of various sources of starch by non-diabetic and streptozotocin-induced diabetic rats. *J. Nutr.* **1989**,*119*, 2023–2029.

38) Murai, A.; Iwamura, K.; Takada, M.; Ogawa, K.; Usui, T.; Okumura, J. Control of postprandial hyperglycaemia by galactosyl maltobionolactone and its novel anti-amylase effect in mice. *Life Sci*. **2002**, *71*, 1405–1415.

39) Fujisawa, T.; Ikegami, H.; Inoue, K.; Kawabata, Y.; Ogihara, T. Effect of two alpha-glucosidase inhibitors, voglibose and acarbose, on postprandial hyperglycemia correlates with subjective abdominal symptoms. *Metabolism* **2005**, *54*, 387–390.

40) Ceriello, A.; Esposito, K.; Piconi, L.; Ihnat, M. A.; Thorpe, J. E.; Testa, R.; Boemi, M.; Giugliano, D. Oscillating glucose is more deleterious to endothelial function and oxidative stress than mean glucose in normal and type 2 diabetic patients. *Diabetes.* **2008**, *56*, 2806-2821.

41) Saewan, N.; Koysomboom, S.; Chantrapromma, K. Anti-tyrosinase and anti-cancer activities of flavonoids from *Blumea balsamifera* DC. *J. Med. Plants Res*. **2011**, *18*, 1018-1025.

42) Paya, M.; Manez, S.; Villar, A. Flavonoid constituents of *Rhamnus lycioides* L. *Z. Naturforsch*. **1986**, *41c*, 976-978.

43) Nawwar, M. A. M.; Souleman, A. M. A.; Buddrus, J.; Linscheid, M. Flavonoids of the flowers of *Tamarix nilotica*. *Phytochemistry*. **1984**, *23*, 2347-2349.

44) Maltese, F.; Erkelens, C.; van der Kooy, F.; Choi, Y. H.; Verpoorte, R. Identification of natural epimeric flavanone glycosides by NMR spectroscopy. *Food Chem*. **2009**, *116*, 575–579.

45) O'Leary, K. A.; Day, A. J.; Needs, P. W.; Sly, W. S.; O'Brien, N. M.; Williamson, G. Flavonoid glucuronides are substrates for human liver β-glucuronidase. *FEBS Lett.* **2001**, *503*, 103-106.

46) Cheng, Y.; Prusoff, W. H. Relationship between the inhibition constant (Ki) and the concentration of inhibitor which causes 50 per cent inhibition ($IC_{50}$) of an enzymatic reaction. *Biochem. Pharmacol.* **1973**, *22*, 3099–3108.

47) Mullen, W.; Edwards, C. A.; Crozier, A. Absorption, excretion and metabolite profiling of methyl-, glucuronyl-, glucosyl- and sulpho-conjugates of quercetin in human plasma and urine after ingestion of onions. *Br. J. Nutr*. **2006**, *96*, 107–116.

48) Thilakarathna, S. H.; Rupasinghe, H. P. V. Flavonoid bioavailability and attempts for bioavailability enhancement. *Nutrients*. **2013**, *5*, 3367-3387.

49) Tadera, K.; Minami, Y.; Takamatsu, K..; Matsuoka, T. Inhibition of α-glucosidase and α - amylase by flavonoids. *J. Nutr. Sci. Vitaminol.* **2006**, *52*, 149–153.

50) Li, Y. Q.; Zhou, F. C.; Gao, F.; Bian, J. S.; Shan, F. Comparative evaluation of quercetin, isoquercetin and rutin as inhibitiors of α-glucosidase. *J. Agric. Food Chem.* **2009**, *57*, 11463-11468.

51) Rodier, M.; Richard, J. L.; Monnier, L.; Mirauze, J. Effect of long term acarbose (Bay g 5421) therapy on metabolic control on non-insulin-dependent (type II) diabetes mellitus. *Diabetes Met.* **1988**,*14*, 12–14.

52) Santeusanio, F.; Ventura, M. M.; Contadinbi, S. Efficacy and safety of two different dosages of acarbose in non-insulin dependent diabetic patients treated by diet alone. *Diabetes Nutr. Metab.* **1993**, *6*, 147–154.

53) Breitinger H. G. Drug synergy-mechanisms and methods of Analysis. *Toxicity and DrugTtesting*. **2012**, 528 p.

54) Knowles, T. P. J.; Vendruscolo, M.; Dobson, C. M. The amyloid state and its association with protein misfolding diseases. *Nature Rev. Mol.Cell Biol*. **2014**, *15*, 384–396.

55) Chiti, F.; Dobson, C. M. Protein misfolding, functional amyloid, and human disease. *Annu. Rev. Bioch.* **2006**, *75*, 333–366.

56) Sato, M.; Murakami, K.; Uno, M.; Nakagawa, Y.; Katayama, S.; Akagi, K.; Masuda, Y.; Takegoshi, K.; Irie, K. Site-specific inhibitory mechanism for amyloid β42 aggregation by catechol-type flavonoids targeting the Lys residues. *J. Biol. Chem.* **2013**, *288*, 23212-23224.

57) Sato, M.; Murakami, K.; Uno, M.; Ikubo, H.; Nakagawa, Y.; Katayama, S.; Akagi, K.; Irie, K. Structure-activity relationship for (+)-taxifolin isolated from silymarin as an inhibitor of amyloid β aggregation. *Biosci. Biotechnol. Biochem*. **2013**, *77*, 1100-1103.

58) Miyamae, Y.; Han, J.; Sasaki, K.; Terakawa, M.; Isoda, H.; Shigemori, H. 3,4,5-Tri-*O*-caffeoylquinic acid inhibits amyloid β-mediated cellular toxicity on SH-SY5Y cells through the upregulation of PGAM1 and G3PDH. *Cytotechnology*. **2011**, *63*, 191–200.

59) Miyamae, Y.; Kurisu, M.; Murakami, K.; Han, J.; Isoda, H.; Irie, K.; Shigemori, H. Protective effects of caffeoylquinic acids on the aggregation and neurotoxicity of the 42-residue amyloid β-protein. *Bioorg. Med. Chem.* **2012**, *20*, 5844–5849.

60) Kurisu, M.; Miyamae, Y.; Murakami, K.; Han, J.; Isoda, H.; Irie, K.; Shigemori, H. Acteoside, a phenylethanoid glycoside, inhibits amyloid β aggregation. *Biosci. Biotechnol. Biochem*. **2013**, *77*, 1329–1332.

61) Hanaki, M.; Murakami, K.; Akagi, K.; Irie, K. Structural insights into mechanisms for inhibiting amyloid β42 aggregation by non-catechol-type flavonoids. *Bioorg. Med. Chem*. **2016**, *24*, 304–313.

62) Day, A. J.; Mellon, F.; Barron, D.; Sarrazin, G.; Morgan, M. R.; Williamson, G. Human metabolism of dietary flavonoids: identification of plasma metabolites of quercetin. *Free Radical Res.* **2001**, *35*, 941–952.

63) Ho, L.; Ferruzzi, M. G.; Janle, E. M.; Wang, J.; Gong, B.; Chen, T. Y.; Lobo, J.; Cooper, B.; Wu, Q. L.; Talcott, S. T.; Percival, S. S.; Simon, J. E.; Pasinetti, G. M. Identification of brain-targeted bioactive dietary quercetin 3-*O*-glucuronide as a novel intervention for Alzheimer's disease. *FASEB J.* **2013**, *27*, 769–781.

64) Murakami, K.; Irie, K.; Ohigashi, H.; Hara, H.; Nagao, M.; Shimizu, T.; Shirasawa, T. Formation and stabilization model of the 42-mer Abeta radical: implications for the long-lasting oxidative stress in Alzheimer's disease. *J. Am. Chem. Soc.* **2005**, *127*, 15168-15174.

65) Park, J.; Ryu, J.; Jin, L. H.; Bahn, J. H.; Kim, J. A.; Yoon, C. S.; Kim, D. W.; Han, K. H.; Eum, W. S.; Kwon, H. Y.; Kang, T. C.; Won, M. H.; Kang, J. H.; Cho, S. W.; Choi, S. Y. 9-Polylysine protein transduction domain: Enhanced penetration efficiency of superoxide dismutase into mammalian cells and skin. *Mol. Cells*. **2002**, *13*, 202-208.

# Acknowledgements

I thank all who in one way or another contributed in the completion of this thesis.

My special and heartily thanks to my supervisor, Professor Hideyuki SHIGEMORI (University of Tsukuba) who encouraged and directed me. His challenges and inspiring suggestions brought this work towards a completion. I would like to express my deepest appreciation for allowing me to conduct my research on Tunisian plants under his supervision.

I am thankful to Associate Professor Kosumi YAMADA (University of Tsukuba) for his kind guidance and productive critics during seminars.

A thank to the committee members Professor Hiroko ISODA (University of Tsukuba) and Associate Professor Motoo UTSUMI (University of Tsukuba) for accepting the evaluation of my research.

I am grateful to Prof. Abderrazak Smaoui and Prof. Chedly Abdelly (Center of Biotechnology of Borj Cedria, Tunisia) for collecting the plant materials.

Thanks are due to my lab-mates in the laboratory of Natural Product Chemistry for their help. I would like also to thank all the faculty members and professors.

My deepest heartfelt appreciation goes to my beloved family. Words cannot express how grateful I am to them for all the sacrifices that they have made on my behalf. Although the long distance between us, their prayer for me was what sustained me thus far.

And finally, I want to thank all my friends, from all of over the world that I had the chance to meet in Japan, who incented me to strive towards my goal and with whom I spent so many wonderful moments.

This work was partially supported by the JST-JICA's Science and Technology Research Partnership for Sustainable Development (SATREPS) and Grants-in-Aid for Scientific Research (C) (Grant No. 24580156) of Japan Society for the Promotion of Science (JSPS).